

UNIVERSITY OF BELGRADE

FACULTY OF TECHNOLOGY AND METALLURGY

Ayad Abdelsalam Musa Salem

**CORROSION OF STEEL WITH  
POLYANILINE BASED COMPOSITE  
COATINGS**

Doctoral Dissertation

Belgrade, 2018

UNIVERZITET U BEOGRADU

TEHNOLOŠKO-METALURŠKI FAKULTET

Ayad Abdelsalam Musa Salem

**KOROZIJA ČELIKA SA KOMPOZITNIM  
PREVLAKAMA NA BAZI POLIANILINA**

doktorska disertacija

Beograd, 2018

**Mentor:**

**Dr Branimir Grgur, redovni profesor,**

Univerzitet u Beogradu, Tehnološko-metalurški fakultet

**Članovi komisije:**

**Dr Milica Gvozdrenović, vanredni profesor,**

Univerzitet u Beogradu, Tehnološko-metalurški fakultet

**Dr Branimir Jugović, naučni savetnik,**

Institut tehničkih nauka – SANU, Beograd

Datum odbrane: \_\_\_\_ \_\_\_\_ \_\_\_\_\_ god.

## **ACKNOWLEDGEMENT**

**I would like to express this appreciation to Professor Branimir Grgur, for his supervision, guidance, encouragements, and advice throughout the duration of study and experimental work.**

**I would also to thanks sincere appreciation to my Mentor Professor Branimir Grgur, Professor Milica Gvozdenović and Dr. Branimir Jugović, for guideless during the work on this doctoral dissertation.**

**Finally deep thanks to the Libyan Government, and my family, for their patent, and encouragements during my Ph.D study at Belgrade University.**

**Thank you.**

## **CORROSION OF STEEL WITH POLYANILINE BASED COMPOSITE COATINGS**

### **ABSTRACT**

The chemically synthesized polyaniline in the powdered form by the procedure recommended by IUPAC is reprotonated using sulfamic, citric, succinic and acetic acid. Typical procedures for corrosion protection investigations based on UV-vis characterization, linear polarization measurements and optical microscopy investigations are developed with composite coatings based on well-characterized polyaniline doped with benzoate. The UV-vis spectroscopy is applied to estimate doping degree of the reprotonated samples. The estimated doping degrees are as follows: the polyaniline doped with sulfamic acid 0.28, with succinic acid 0.18, with citric acid 0.15 and with acetic acid 0.13. The composite coatings are prepared by mixing the alkyd based commercial paint with 5 wt.% of the reprotonated samples and painted on mild steel. Using linear polarization method, the polarization resistances of the composite and base coatings are determined in 3% NaCl over time. It is shown that initial oxidation state of the polyaniline, determined the values of polarization resistance which decrease in the following order:  $R_p(\text{sulfamic}) > R_p(\text{succinic}) > R_p(\text{citric}) > R_p(\text{acetic}) \sim R_p(\text{base coating})$ . For all composite coatings, increases in the corrosion potentials are observed during the time, while for the base coating decrease.

The higher area steel samples with base and composite coatings are also immersed in 3% NaCl. The corrosion current density is determined after 100 h in site using ASTM 1,10-phenanthroline method. The samples are also visually inspected, and by the optical microscope. It is shown that composite coatings reduce the possibility of blister formations and delamination. The corrosion current density and the appearance of the corrosion products closely follow the initial oxidation state of the polyaniline.

The role of the initial state of the polyaniline is discussed. It is suggested that such behavior could be connected with the oxygen reduction mechanism that proceed mainly

via two electron path on the polyaniline particles, releasing a much smaller amount of hydroxyl ions, responsible for the delamination and blister formations of the commercial coatings.

**Keywords:** Reprotonation, Organic acids, Doping degree, Delamination, Alkyd paints

**Scientific field:** Technological engineering

**Specific scientific field:** Chemical engineering

# KOROZIJA ČELIKA SA KOMPOZITNIM PREVLAKAMA NA BAZI POLIANILINA

## REZIME

Hemijski sintetisani polianilin u praškastoj formi postupkom preporučenim od strane IUPAC-a je reprotoniran pomoću sulfaminske, limunske, ćilibarne i sirćetne kiseline. Procedura za ispitivanje zaštite od korozije čelika zasnovana na UV-vis karakterizaciji, merenju linearne polarizacione otpornosti i ispitivanju optičkom mikroskopijom je razvijena na kompozitnom premazu zasnovanom na okarakterisanom polianilinu dopovanom benzoatom. UV-vis spektroskopija je primenjena za procenu stepena dopovanja reprotonovanih uzorka. Procenjeni stepeni dopovanja su bili sledeći: polianilin dopovan sa sulfaminskom kiselinom 0,28, sa ćilibarnom kiselinom 0,18, sa limunskom kiselinom 0,15 i sa sirćetnom kiselinom 0,13. Kompozitni premazi su pripremljeni mešanjem komercijalnog premaznog sredstva na bazi alkidne smole sa 5 mas.% reprotoniranih uzoraka polianilina i naneti na čelik. Koristeći metodu linearne polarizacije, određene su vrednosti polarizacione otpornosti kompozitnih i osnovnog premaza u 3% NaCl tokom vremena. Pokazano je da početno stanje oksidacije polianilina određuje vrednosti polarizacione otpornosti koja se smanjuje u sledećem redosledu:  $R_p$  (sulfaminska) >  $R_p$  (ćilibarna) >  $R_p$  (limunska) >  $R_p$  (sirćetna) ~  $R_p$  (osnovni premaz). Kod svih kompozitnih premaza, tokom vremena je uočeno povećanje korozionog potencijala, dok je kod osnovnog premaza uočeno smanjuje.

Uzorci čelika veće površine sa osnovnim i kompozitnim premazima su takođe ispitani u 3% NaCl. Gustina struje korozije je određena nakon 100 h, određivanjem koncentracije jona gvožđa u rastvoru, koristeći ASTM 1,10-fenantrolin metod. Uzorci su takođe vizuelno pregledani i ispitani optičkim mikroskopom. Pokazano je da kompozitni premazi smanjuju mogućnost formiranja plikova i delaminacije. Gustina struje korozije i pojava korozionih produkata blisko prate početno oksidaciono stanje polianilina.

Uloga početnog oksidacionog stanja polianilina na koroziono ponašanje je razmatrana. Predloženo je da se poboljšanje korozionog ponašanja može povezati sa mehanizmom reakcije redukcije kiseonika koji se uglavnom odigrava dvo-elektronskom razmenom na česticama polianilina, oslobađajući mnogo manju količinu hidroksilnih jona, odgovornih za formiranje plikova i delaminacije kod komercijalnih premaza.

**Ključne reči:** Reprotonacija, Organske kiseline, Stepen dopovanja, Delaminacija,

Alkidni premaz

**Naučna oblast:** Tehnološko inženjerstvo

**Uža naučna oblast:** Hemijsko inženjerstvo



## CONTENTS

<b>1. INTRODUCTION</b>	<b>1</b>
<b>2. THEORETICAL PART</b>	<b>3</b>
2.1. The intrinsically conducting polymers-polyaniline	3
2.2. Corrosion of the mild steel with composite polyaniline coatings	13
2.3. Possible mechanisms of the mild steel corrosion protection with polyaniline composite coatings	25
2.3.1. <i>Barrier properties</i>	25
2.3.2. <i>Corrosion inhibition</i>	26
2.3.3. <i>Anodic protection</i>	26
2.3.4. <i>Complex formation effect</i>	29
2.3.5. <i>Other mechanisms and factors</i>	30
2.4. Methods for polyaniline characterization and corrosion determination	32
2.4.1. <i>UV visible spectroscopy study of polyaniline</i>	32
2.4.2. <i>The determination of the corrosion current densities by the electrochemical measurements</i>	39
2.4.3. <i>The 1,10-phenanthroline spectroscopic determination of the iron</i>	43
<b>3. EXPERIMENTAL</b>	<b>47</b>
3.1. Preparation and characterization of the polyaniline powders	47
3.2. Sample preparations and corrosion investigations	48
3.3. 1,10-phenanthroline standard method for iron concentration determination	51
<b>4. RESULTS AND DISCUSSION</b>	<b>53</b>
4.1. Characterization of the polyaniline-benzoate powder	53
4.1.1. <i>Corrosion investigations</i>	55
4.2. The influence of the initial oxidation state of polyaniline on the corrosion of steel with composite coatings	63

<i>4.2.1. Characterization of the polyaniline powder</i>	63
<i>4.2.2. Corrosion behavior</i>	66
<i>4.2.3. The 1,10-phenanthroline spectroscopic determination of the iron corrosion</i>	73
<b>4.3. Possible mechanism of the corrosion behavior</b>	78
<b>5. CONCLUSIONS</b>	83
<b>REFERENCES</b>	85
<b>BIOGRAPHY</b>	96
<b>Prilog 1.</b>	98
<b>Prolog 2.</b>	99
<b>Prilog 3.</b>	100

## 1. INTRODUCTION

Conducting polymers or *intrinsically conducting polymers (ICP's)*, has been recognized as a frontier area of research and potential materials for technological applications since last decades [1, 2, 3, 4, 5]. The significance of the conducting polymer was distinguished in the form of Nobel Prize in chemistry received by MacDiarmid, Heeger and Shirakawa [6, 7, 8]. The polymerization kinetics and mechanism [9], processability [10], and ion transport mechanism [11] are the points of academic and scientific attractions. There is a huge area of the technological applications including biosensors [12], gas sensors [13], electrochromic devices [14], electromagnetic shielding [15], light emitting devices and organic electronics [16] photovoltaic applications [17], energy conversion and storage [18], etc. The class of conducting polymers consisting of various polymers such as polythiophene [19], polypyrrole [20], polyparaphenylene, [21 22] poly(3,4-ethylenedioxythiophene), PEDOT, [23] etc. The polyaniline (PANI) is one of the most extensively studied polymers because of its relatively high electrical conductivity, oxidative properties, environmental stability and ease preparation [24].

Among above-mentioned application, corrosion protection of different metals, and especially steel, is one of the well-studied field [25]. Many researchers groups [26, 27, 28, 29, 30, 31, 32, 33, 34, 35] reported various views about the corrosion protection by polyaniline coatings and composite polyaniline based coatings, and hence various mechanisms were suggested to explain anticorrosion properties. These include anodic protection, controlled inhibitor release as well as barrier protection mechanisms. Different approaches have been developed for the use of polyaniline in protective coatings (dopants, composites, blends). A careful choice of synthesis parameters could lead to an

improvement in the anticorrosion properties of the coatings prepared using ICP's for metals and their alloys.

Due to the extreme differences of experimental results, it is still not clear how the dopant anion (conductivity of the polyaniline) influenced corrosion behavior. Also, many different mechanisms were proposed for systems mild steel - polyaniline composite coatings. Hence the aim of this work will be to investigate corrosion protection of mild steel with composite base coating- polyaniline in the form of powder as anticorrosion additives, for which polyaniline will be prepared according to recommended IUPAC procedure [36] and reprotonated with different dopant anions which possess a wide range of initial conductivity. The main goal will be to determine does the initial conductivity or doping degree of the polyaniline influenced the corrosion behavior and based on these results to propose the most likely mechanism of the corrosion protection.

In addition, the goal will be to eventually suggest the procedures to investigate corrosion protection of mild steel with composite base coating-polyaniline using different techniques and methods.

## 2. THEORETICAL PART

### 2.1. The intrinsically conducting polymers-polyaniline

Polyaniline is a class of intrinsically conducting polymers (ICP's) consisted of four repeated monomer units in a polymer chain, as shown in a Fig. 2.1 [37]. For the simplicity, the polyaniline is often ideally represented as four repeat monomer units in which the leucoemeraldine ( $y=1$ ) oxidation state consists of the fully reduced polymer, the emeraldine ( $y=0.5$ ) oxidation state consists of a 3:1 ratio of benzenoid and quinoneimine moieties linking the nitrogen atoms of the backbone, and the pernigraniline ( $y=0$ ) is the fully oxidized form of the polymer.

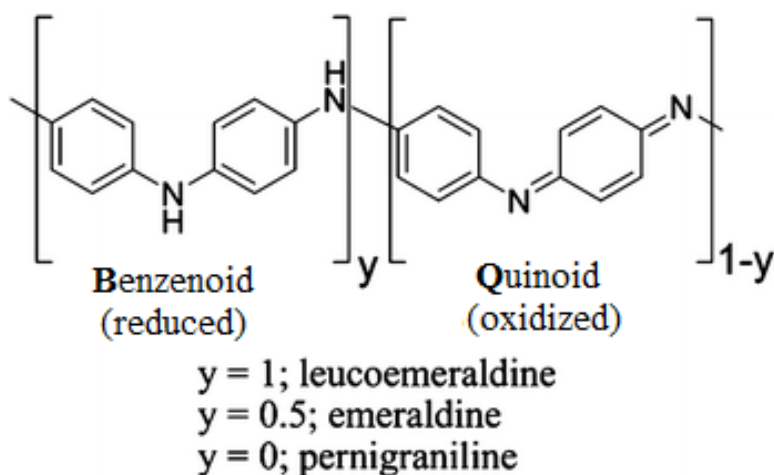
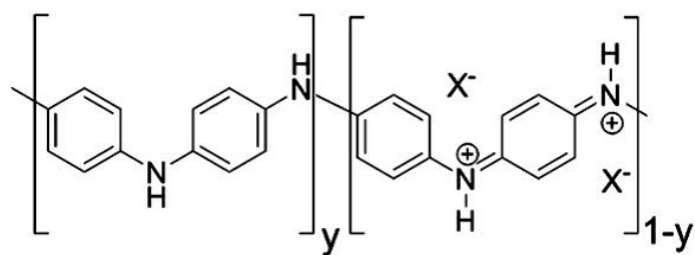


**Figure 2.1.** The idealized oxidation states of polyaniline in the base forms (top).

Leucoemeraldine ( $y = 1$ ) is the most reduced oxidation state, pernigraniline ( $y = 0$ ) is the most oxidized state, and emeraldine ( $y = 0.5$ ) is an intermediate oxidation state. [37]

The emeraldine base form can be doped with a strong protonic acid to generate the conducting emeraldine salt form of polyaniline, Fig. 2.2



$X^- = \text{anion}$

**Figure 2.2.** Emeraldine salt form [37]

Polyaniline (PANI) exists in a variety of forms that differ in chemical and physical properties [36]. The most common green protonated emeraldine has conductivity on a semiconductor level of the order of  $10^0 \text{ S cm}^{-1}$ , many orders of magnitude higher than that of common polymers ( $<10^{-9} \text{ S cm}^{-1}$ ) but lower than that of typical metals ( $>10^4 \text{ S cm}^{-1}$ ). Protonated PANI, (e.g., PANI hydrochloride) converts to a non-conducting blue emeraldine base when treated with the base, for example, ammonium hydroxide (Fig. 2.3).

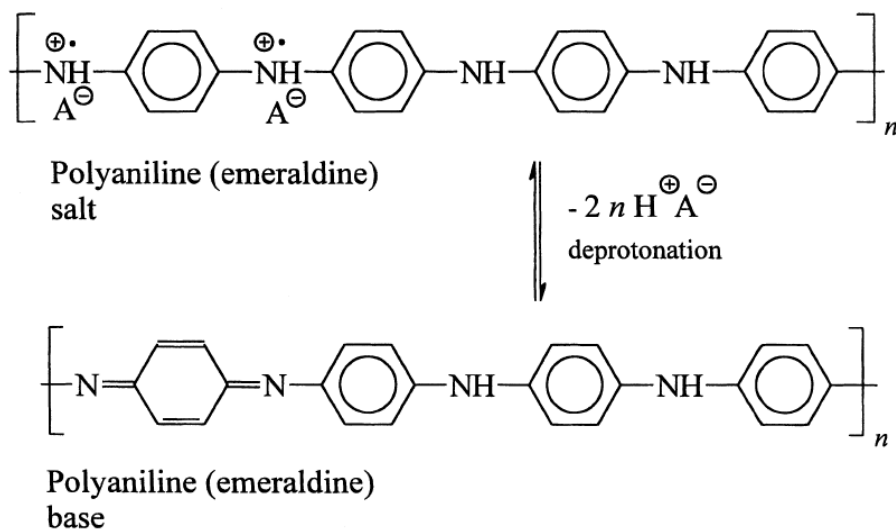


**Figure 2.3.** Polyaniline (emeraldine) salt form can be deprotonated in the alkaline medium to polyaniline (emeraldine) base form. A<sup>-</sup> is an arbitrary anion, e.g., chloride [36].

Interconversion of the different forms of polyaniline is strongly pH and potential dependent. The influence of pH leads to the formation of different salt-base equilibrium of three different polyaniline fundamental forms as shown in Fig. 2.4 [38]. In aqueous electrolytes, the extent of protonation depends on the solution pH (increasing left to right). For leucoemeraldine, the  $pK_a$  is between 0 and 1: protonation begins at approximately pH 2 and is completed at pH  $\sim 1$ . The pH at which the polymer protonates/deprotonates depends on the acid, however. In naphthalene sulfonic acid, for example, leucoemeraldine is fully protonated even at pH 2. The  $pK_a$  of the emeraldine state is approximately 3, while that of pernigraniline is below 0. Fully protonated chains consist only of segments labeled  $x$  in Fig. 2.4, but in most acids, the chains are mixtures of  $x$  and  $y$  units, the ratio depending on pH. Only the fully protonated form of emeraldine salt is shown in the left column of Fig. 2.4; this is the lone state of the six that is electrically conducting [38]. The two structures shown for this salt are chemically equivalent resonance structures called polarons.

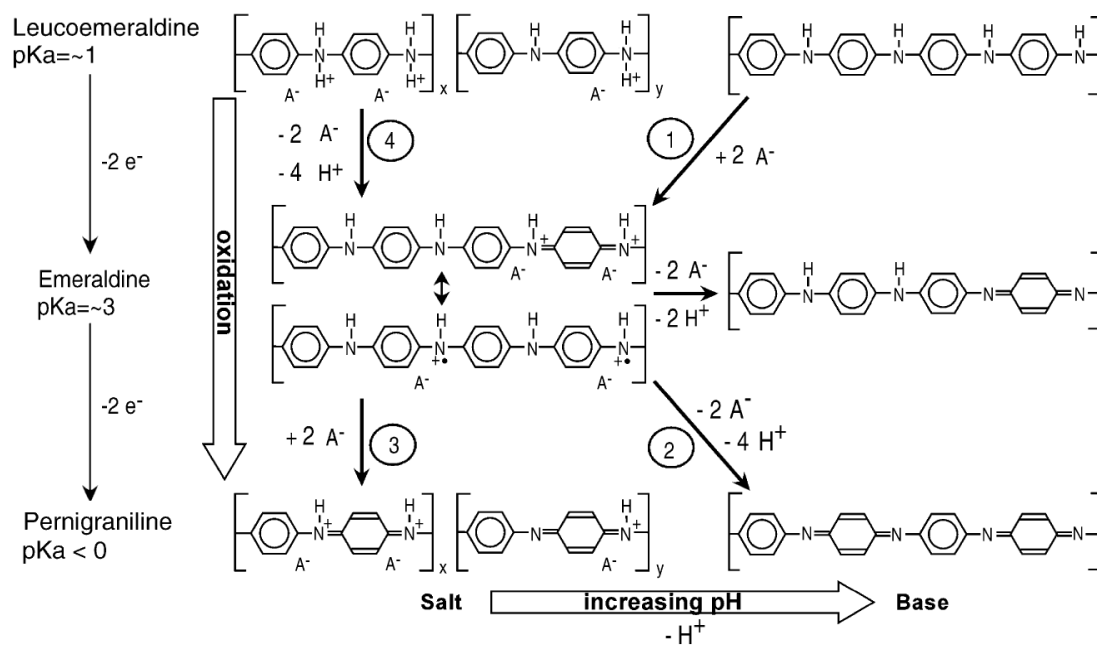


**Figure 2.4.** Oxidation states of polyaniline. In the fully protonated states (left), the polymer comprises only  $x$  units, but in most acids, the chains are mixtures of  $x$  and  $y$  units, the ratio depending on pH. During electrochemical oxidation in aqueous electrolytes, the gain or loss of anions and protons, and the strain depends on solution pH [38].

The pH changes also provoke changes on the electrical conductivity of emeraldine as shown in Fig. 5 [39]. These changes are mainly connected with salt-base equilibrium, as shown in Fig. 2.5.

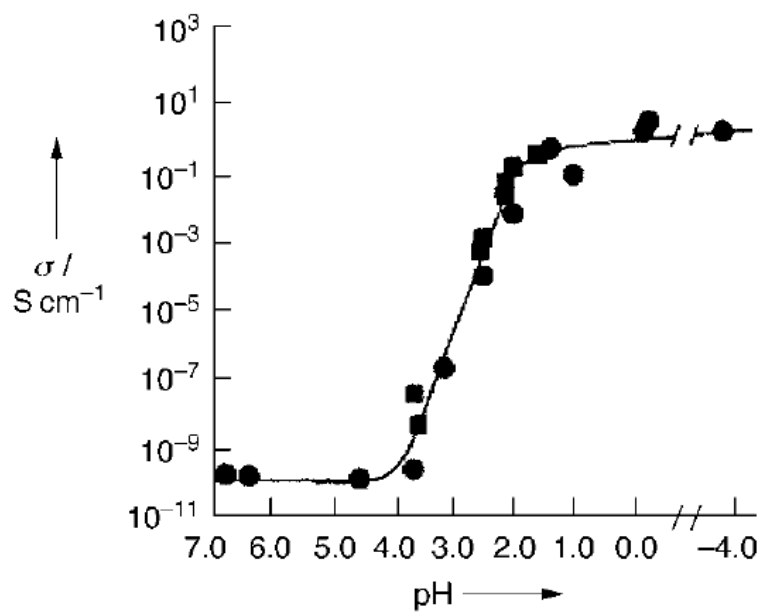


**Figure 2.5.** The conductivity of emeraldine form of polyaniline as a function of the pH of the HCl dopant solutions as it undergoes protonic acid doping [39].

Polyaniline is usually synthesized by the chemical methods. The common chemical synthesis of the polyaniline is the oxidative polymerization of the aniline monomer with ammonium peroxodisulfate  $[(\text{NH}_4)_2\text{S}_2\text{O}_7]$ , as an oxidant [36, 40]. During polymerization, the first product is blue protonated pernigraniline intermediate, which is further oxidized to green protonated emeraldine, as shown in Fig. 2.6. The problem of using ammonium peroxodisulfate is that protonated emeraldine salt, even some other acid anions are present, will be doped with sulfate anions. Consequently, the claim of some authors that under this conditions the polyaniline will be doped with used acid are very problematic [41, 42, 43, 44].



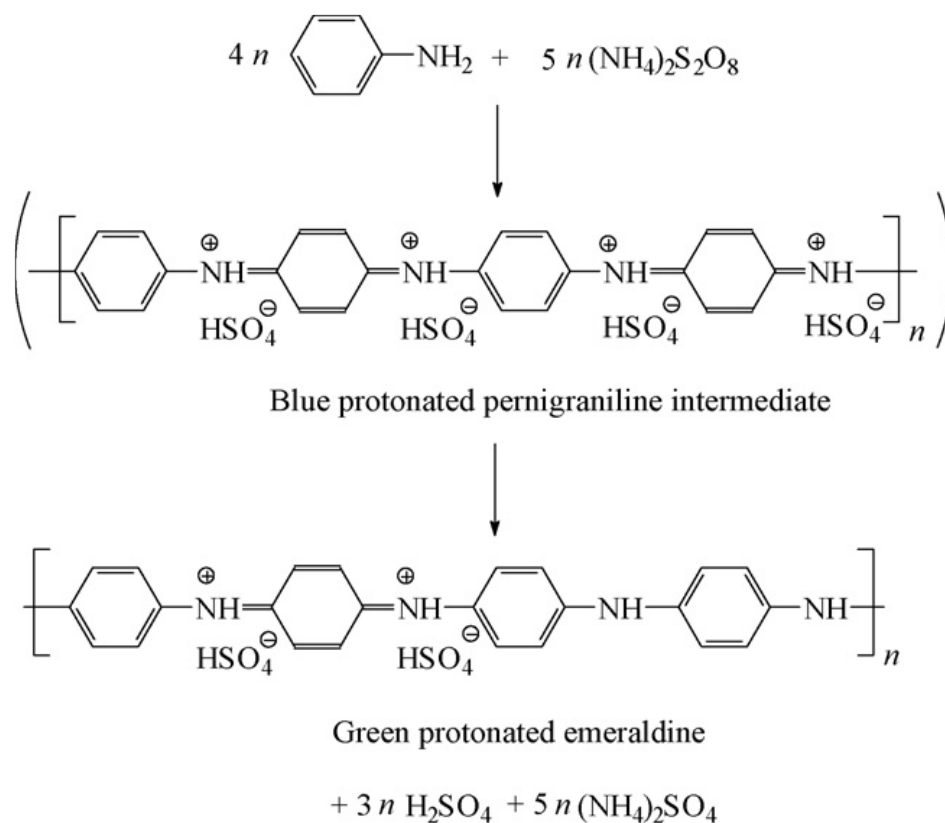


**Figure 2.6.** Schematic presentation of the oxidation of aniline with ammonium peroxydisulfate in acidic medium [36, 40].

The most generalized polymerization mechanism of aniline was suggested by Wei et al. [45, 46] which schematic representation is shown in Fig. 2.7. According to the authors, the rate determining step in the polymerization of the aniline is the oxidation of aniline monomer to form dimeric species (*i.e.* *p*-aminodiphenylamine, PADPA, *N*-*N*'-diphenylhydrazine and benzidine), because the oxidation potential of the aniline is higher than those of dimers, subsequently formed oligomers and polymer. After formation, the dimers are immediately oxidized and then react with an aniline monomer via an electrophilic aromatic substitution, followed by further oxidation and deprotonation to afford the trimers. This process is repeated, leading to the formation of polyaniline.

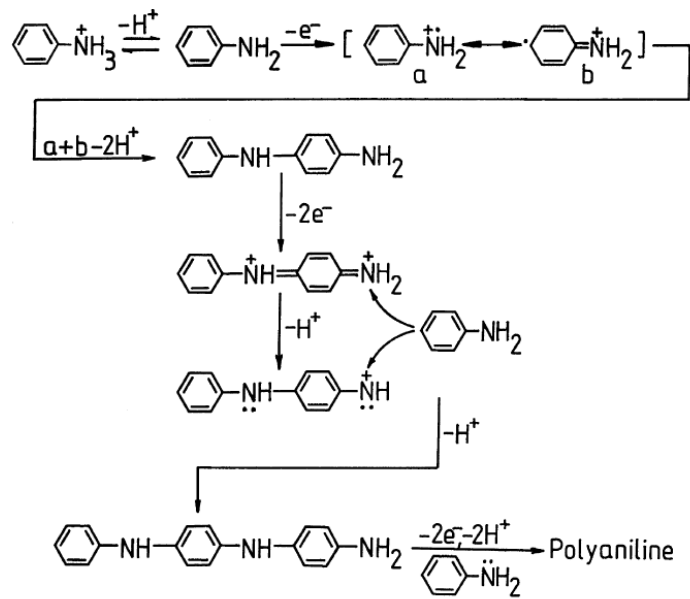


**Figure 2.7.** Mechanism of the aniline polymerization, proposed by Wei et al. [45, 46].

One of the astonishing observations given by Prof. A.G. MacDiarmid that "there are as many different types of PANI as there are people who synthesize it." [47]. Therefore, the way of synthesis decides the conductivity, band gap, chemical structure, polymerization mechanism and ease of attachment and detachment of different functional groups. Synthesis route also strongly affects corrosion behavior of polyaniline composite coatings [48]. Whether the conductive or non-conductive forms of PANI provide better corrosion protection remains unknown [49]. For example, Araujo et al. [50] reported that dedoped PANI, emeraldine base, did not have required properties for use in anti-corrosive coatings. After comparing emeraldine salt and emeraldine base coatings, Spinks et al. [51] decided that the emeraldine base coating provided improved protection from corrosion for steel. Talo et al. [52] and Dominis et al. [53] found that emeraldine base coatings offered improved corrosion protection than those based on a conductive, emeraldine salt, PANI form. In addition, Dominis et al. [53] described that the corrosion protection provided by emeraldine salt primers is strongly influenced by the type of the anion dopant. Meanwhile, Gasparac and Martin [54] found that the protective properties of PANI against corrosion remained independent of the doping level, and a completely undoped emeraldine base coating is equally capable of maintaining the potential of the

stainless steel substrate within the passive region. Armelin et al. [55, 56], first reported that a coating consisting of an epoxy paint modified with polyaniline salt dispersed in xylene provided the best protection against corrosion, even at very low polymer concentrations (0.3 wt%). After 1 year, the steel panels coated with the epoxy/emeraldine base formulation were better protected than those coated with emeraldine salts. These differences could be partially attributed to different conditions used for polyaniline synthesis.

Hence, for the further studies, the standard procedure based on IUPAC recommendation should be applied [36].

#### ***“Standard” preparation of polyaniline according to the IUPAC recommendation***

In this IUPAC project [36], participants followed the same instructions to oxidize 0.2 M aniline hydrochloride with 0.25 M ammonium peroxydisulfate in an aqueous medium. Aniline hydrochloride (purum; 2.59 g, 20 mmol) was dissolved in distilled water in a volumetric flask to 50 mL of solution. Ammonium peroxydisulfate (purum; 5.71 g, 25 mmol) was dissolved in water also to 50 mL of solution. Both solutions were kept for 1 h at room temperature (~18–24 °C), then mixed in a beaker, briefly stirred, and left at rest to polymerize. Next day, the PANI precipitate was collected on a filter, washed with three 100-mL portions of 0.2 M HCl, and similarly with acetone. Polyaniline (emeraldine) hydrochloride powder was dried in air and then in vacuum at 60 °C. Polyanilines prepared under these reaction and processing conditions are further referred to as “standard” samples. Under this synthesis conditions samples shows very reproducible characteristics like conductivity, UV-visible and FTIR positions of the peaks.

According to this procedure, Stejskal et al. [57] investigated conductivity of different reprotonated polyaniline. They used protonated PANI obtained after the polymerization which was converted to a PANI base in excess of 1 mol L<sup>-1</sup> ammonium hydroxide, and dried. The obtained conductivity of PANI base was 3 x 10<sup>-9</sup> S cm<sup>-1</sup>. The portions of PANI base (1.81 g, 5 mmol based on the four constitutional units) were suspended in 40 mL of 1 mol L<sup>-1</sup> aqueous acid solution (40 mmol of an acid), or in more concentrated acid when specified, for 24 h. The resulting product was collected on a filter, rinsed with acetone, and dried at room temperature in air and later in a desiccator. The acid concentrations used, and the pH of the acid solutions before the addition of PANI

base are listed in Table 2.1. The primary experimental results are represented by the conductivity of the reprotonated PANI, its density, water contact angle, and increase in mass after the reaction with an acid.

**Table 2.1.** Acids used in the reprotonation of PANI base. The acid concentration in aqueous solution (molar concentration unless specified otherwise. S = saturated solution), , the corresponding pH, the conductivity of the resulting PANI,  $\sigma$ , the relative change in mass of the PANI,  $\Delta g/g$ , the density of the PANI,  $d$ , the water contact angle,  $\theta$ , and derived quantities, such as the degree of protonation,  $x$ , and the relative volume change,  $\Delta V/V$ . [57]

Acid	$C_A$ mol L <sup>-1</sup>	pH	$\sigma$ S cm <sup>-1</sup>	$\Delta g/g$ wt. %	$d$ g cm <sup>-3</sup>	$\theta$ °	$x$ %	$\Delta V/V$ %
Tetrafluoroboric	50%	–	1.22	18	1.418	44	37	4
Tetrafluoroboric	1	–	0.80	12	1.374	46	25	2
Sulfuric	5	<0	0.53	34	1.509	36	63	13
Phosphoric	5	-0.86	0.50	50	1.557	43	92	25
Methanesulfonic	5	<0	0.48	37	1.414	32	70	23
Hydriodic	1	1.47	0.40	54	2.056	95	77	-11
Hydrochloric	5	<0	0.39	16	1.340	42	80	8
Sulfamic <sup>a</sup>	5	0.35	0.38	24	1.387	34	45	13
Hydrobromic	1	-0.09	0.34	25	1.478	72	56	6
Hydrochloric	1	<0	0.33	15	1.337	52	75	8
Sulfuric	1	<0	0.32	27	1.438	40	50	11
Methanesulfonic	1	0.28	0.27	27	1.377	41	51	16
Nitric	1	<0	0.23	18	1.380	48	52	7
Hydriodic	5	0.90	0.14	50	2.046	87	71	-14
Phosphoric	1	1.02	0.13	31	1.428	50	57	16
Sulfamic <sup>a</sup>	1	0.57	0.11	13	1.333	39	24	6
Hydrobromic	5	-1.24	$9.0 \times 10^{-2}$	24	1.544	52	54	0
Hydrofluoric	1	<0	$3.9 \times 10^{-2}$	-3	1.389	70	-27	-15
Perfluorooctanesulfonic	40%	0.18	$3.3 \times 10^{-2}$	54	1.509	95	20	33
Toluenesulfonic	1	0.50	$3.0 \times 10^{-2}$	27	1.275	54	28	25
Dodecylbenzenesulfonic	S	–	$1.2 \times 10^{-2}$	30	1.224	76	17	32
Camphorsulfonic	1	0.46	$1.1 \times 10^{-2}$	35	1.281	54	27	7
Tartaric	1	1.62	$1.1 \times 10^{-2}$	27	1.352	61	33	18
Picric <sup>b</sup>	S	1.31	$9.6 \times 10^{-3}$	28	1.403	73	22	15

Acid	$C_A$ mol L <sup>-1</sup>	pH	$\sigma$ S cm <sup>-1</sup>	$\Delta g/g$ wt. %	$d$ g cm <sup>-3</sup>	$\theta$ °	$x$ %	$\Delta V/V$ %
Perfluorooctanesulfonic	5%	1.41	$7.3 \times 10^{-3}$	36	1.448	102	13	20
Malic	1	1.60	$6.8 \times 10^{-3}$	7	1.279	47	9	4
Phenylphosphonic	1	0.81	$4.9 \times 10^{-3}$	37	1.339	60	42	29
Citric	1	1.51	$4.4 \times 10^{-3}$	26	1.301	54	22	21
Acetic	99%	-0.54	$3.8 \times 10^{-3}$	11	1.238	42	33	11
Acrylic	100%	-0.24	$2.8 \times 10^{-3}$	20	1.237	35	50	21
Formic	100%	-	$2.8 \times 10^{-3}$	(-6)	1.285	62	-24	-9
Orthanilic <sup>c</sup>	S	1.45	$2.5 \times 10^{-3}$	-	1.401	47	-	-
Hydrofluoric	5	<0	$1.6 \times 10^{-3}$	1	1.281	39	9	-2
3,5-Dinitrosalicylic	S	0.95	$1.5 \times 10^{-3}$	-	1.357	43	-	-
5-Sulfosalicylic	1	0.20	$7.3 \times 10^{-4}$	37	1.388	33	26	25
Aminomethanesulfonic	S	1.65	$6.2 \times 10^{-5}$	-	1.521	44	-	-
Tungstosilicic	5%	1.12	$5.1 \times 10^{-5}$	12	1.464	49	-	-
Sulfanilic <sup>d</sup>	S	2.12	$4.8 \times 10^{-5}$	-	1.420	34	-	-
Formic	5	1.38	$6.7 \times 10^{-6}$	4	1.252	63	16	3
Succinic	S	2.48	$5.9 \times 10^{-6}$	-	1.266	65	-	-
Ascorbic	1	2.05	$5.9 \times 10^{-6}$	6	1.271	82	6	4
Methacrylic	98%	-	$2.5 \times 10^{-6}$	5	1.194	40	11	9
Acetic	5	1.90	$5.4 \times 10^{-7}$	7	1.241	53	21	7
Acrylic	1	2.17	$1.9 \times 10^{-7}$	(-3)	1.272	44	-	0
Aspartic	S	3.00	$1.5 \times 10^{-7}$	-	1.210	49	-	-
Formic	1	2.03	$6.2 \times 10^{-8}$	1	1.230	60	4	2
Salicylic	S	2.25	$3.7 \times 10^{-8}$	-	1.274	50	-	-
Barbituric <sup>e</sup>	S	2.31	$2.9 \times 10^{-8}$	-	1.369	29	13	-
Nafion 117 solution	5%	1.80	$1.8 \times 10^{-8}$	5	1.262	124	-	3
Boric	S	2.87	$1.3 \times 10^{-8}$	-	1.258	46	0	-
<i>o</i> -Aminobenzoic	S	3.61	$8.2 \times 10^{-9}$	-	1.278	40	8	-
Oxalic	1	0.80	$7.6 \times 10^{-9}$	(-2)	1.252	74	-	-3
Acetic	1	2.51	$7.1 \times 10^{-9}$	0	1.228	59	0	1
Benzoic	S	2.59	$4.6 \times 10^{-9}$	-	1.238	41	-	-
Alanine	1	7.28	$1.3 \times 10^{-9}$	(-4)	1.221	47	-	-2
Glycine	S	7.61	$9.8 \times 10^{-10}$		1.212	46	-	-

Acid	$C_A$ mol L <sup>-1</sup>	pH	$\sigma$ S cm <sup>-1</sup>	$\Delta g/g$ wt. %	$d$ g cm <sup>-3</sup>	$\theta$ °	$x$ %	$\Delta V/V$ %
Methacrylic	1	2.22	$9.3 \times 10^{-10}$	(-4)	1.232	45	-	-1
Phenylboronic <sup>f</sup>	1	-	$4.8 \times 10^{-10}$	(-1)	1.206	62	-	-
Taurine <sup>g</sup>	S	4.78	$3.6 \times 10^{-10}$	-	1.366	46	-	-
(Water, no acid)	-	6.50	$1.8 \times 10^{-10}$	-	1.206	55	-	-

<sup>a</sup> Aminosulfonic acid.

<sup>b</sup> 2,4,6-Trinitrophenol.

<sup>c</sup> o-Aminobenzenesulfonic acid.

<sup>d</sup> p-Aminobenzenesulfonic acid.

<sup>e</sup> 2,4,6-Trihydroxypyrimidine.

The authors clearly connected pH of acid solutions used for reprotonation of polyaniline base with a conductivity of polyaniline as shown in Fig. 2.8 [57].

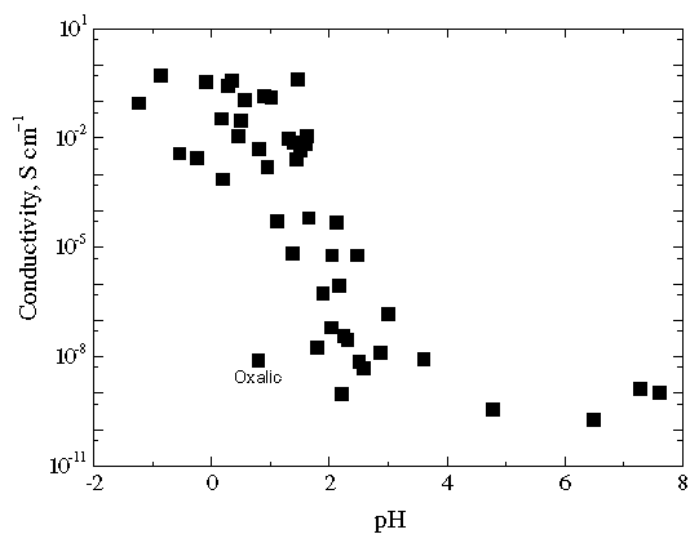


**Figure 2.8.** The dependence of the conductivity of reprotonated PANI bases on the pH of acid solutions [57].

## 2.2. Corrosion of the mild steel with composite polyaniline coatings

Polyaniline blend or composite coatings are usually considered to be the best choice for the application in corrosion protection of the steel. Explicitly, in such coatings, polyaniline is highly dispersed in some classical polymer [58]. Such system can provide many advantages in the application as anticorrosion coatings on steel.

Talo et al. [52] investigated emeraldine base polyaniline/epoxy blend coatings on steel in 0.1 M HCl, 0.6 M NaCl and 0.1 M NaOH solutions, and found efficient protection in the latter two media even when a hole was drilled in the coating. These findings indicate that EB offered more than simple barrier protection. X-ray photoelectron spectroscopy (XPS) revealed a passive film of  $\text{Fe}_2\text{O}_3/\text{Fe}_3\text{O}_4$  is formed on the metal surfaces, suggesting the protection was anodic.

Corrosion protection of the mild steel by PANI-HCl containing paint (0.1-20 wt.%) was studied by Samui et al. [59]. Corrosion protection studies were conducted under both atmospheric and saline water conditions. The paints have shown appreciable corrosion protection properties at a relatively low thickness ( $80 \pm 5 \mu\text{m}$ ). In accelerated weathering test, painted mild steel panels did not undergo any corrosion after 1200 h of exposure. Humidity cabinet, salt spray and saline water exposure studies revealed that lower PANI-HCl containing paint protected mild steel better compared to that containing higher PANI-HCl. Potentiodynamic measurement in 3.5% sodium chloride solution has also shown more noble characteristics of lower PANI-HCl loaded paint. Water vapor permeability of lower PANI-HCl containing paint was very low which indicates its superior barrier properties. The barrier property contributes appreciably towards corrosion resistance of the PANI-HCl containing paint films. The paint system has shown appreciable corrosion resistance without any top barrier coat. Adhesion strength of paint on mild steel surface was found to be fairly good during the exposure and remains unaffected even after the onset of corrosion compared to that containing higher PANI-HCl.

Anticorrosion performances of polyaniline emeraldine base/epoxy resin (EB/ER) coating on mild steel in 3.5% NaCl solutions of various pH values were investigated by

electrochemical impedance spectroscopy (EIS) for 150 days by Chen et al. [60]. They found that in neutral solution (pH 6.1), EB/ER coating of 20  $\mu\text{m}$  offered very efficient corrosion protection with respect to pure ER coating, especially when EB content was 5–10%. The impedance at 0.1 Hz of the coating increased in the first 1–40 immersion days and then remained constant above  $10^9 \Omega \text{ cm}^2$  until 150 days, Fig 2.9, which in combination with the observation of a  $\text{Fe}_2\text{O}_3/\text{Fe}_3\text{O}_4$  passive film formed on steel confirmed that the protection of EB was mainly anodic. In acidic or basic solution (pH 1 or 13), EB/ER coating also performed much better than pure ER coating. However, these media weakened the corrosion resistance due to the breakdown of the passive film or deterioration of the ER binder.

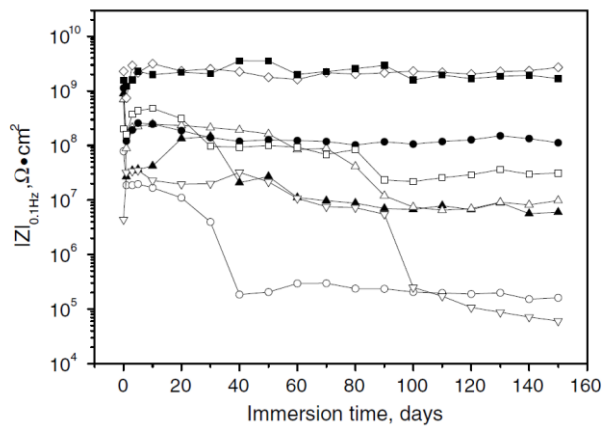


**Figure 2.9.** Evolution of  $|Z|_{0.1 \text{ Hz}}$  with immersion time in 3.5% NaCl solution for steel coated with ER coating ( $\circ$ ), EB/ER coatings with EB contents of 1% ( $\blacktriangle$ ), 3% ( $\triangle$ ), 5% ( $\bullet$ ), 7% ( $\diamond$ ), 10% ( $\blacksquare$ ), 13% ( $\square$ ) and 15% ( $\nabla$ ) [60].

Incorporation of polyaniline (PANI) in epoxy type powder coating formulations was investigated by Radhakrishnan et al. [61]. Using the specific grade of PANI with low doping degree, it can be incorporated in the epoxy powder coating formulations by twin screw extrusion process. The powder formulations were deposited on steel substrates by electrostatic spray coating at 60 kV and baked at 140  $^{\circ}\text{C}$  for 20 min. These samples were extensively tested for corrosion resistance by exposure to hot saline conditions, Fig. 2.10, followed by electrochemical impedance spectroscopy and also salt spray testing.



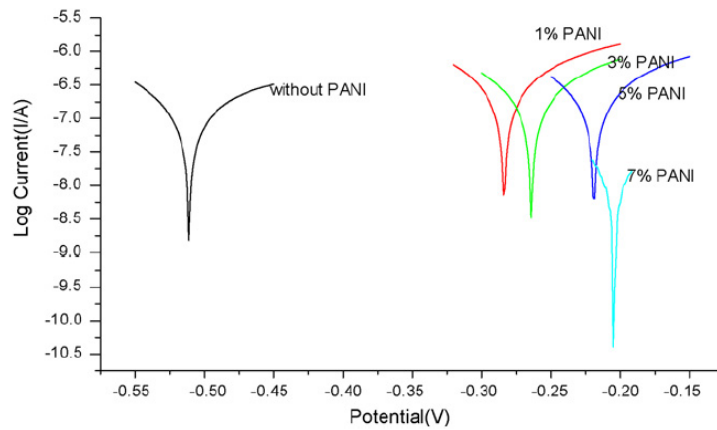


**Figure 2.10.** Tafel plots for intentionally scratched epoxy powder coating and exposed to hot saline conditions [61].

PANI incorporated coatings showed no deterioration even after 1400 h of hot (65 °C) saline treatment [61]. The coatings intentionally scratched also exhibited self-healing properties and no rust formation was observed even after prolonged exposure to hot saline conditions, Fig. 2.11. These results could be explained on the basis of additional crosslinking due to PANI, as confirmed by DSC results, which gave rise to improved barrier property and self-healing was associated with the scavenging of ions by PANI which prevented corrosion of the underlying substrate.

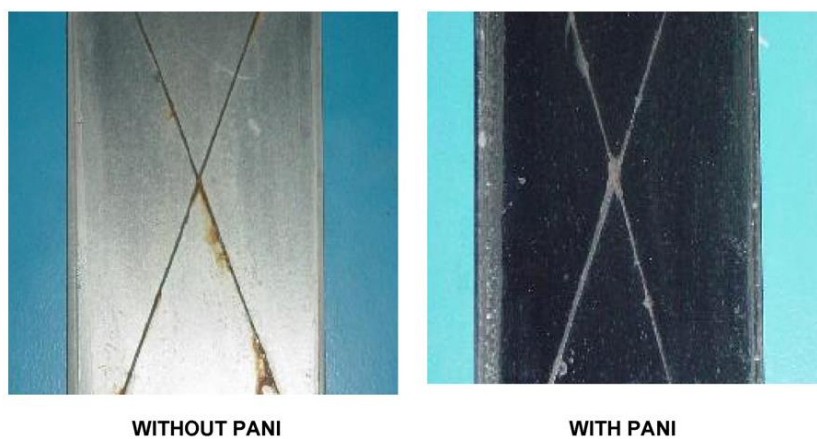


**Figure 2.11.** Photographs of the surface of epoxy coatings (left) and PANI modified epoxy coating subjected to salt spray tests after 700 h [61].

The epoxy coating with the phosphate doped polyaniline (1%) was able to offer protection in saline and acid media [62]. Phosphate doped polyaniline has been prepared by a chemical oxidative method using ammonium persulphate as the oxidant. FTIR study has shown that phosphate dopant is present as  $\text{H}_2\text{PO}_4^-$  ion in polyaniline. Conductivity measurements indicated that the polymer has got good conductivity. The coating on steel has been found to be more protective in 3% NaCl and 0.1 M  $\text{H}_3\text{PO}_4$  than in 0.1 M HCl.

Armelin et al [55, 56] investigated the influences of PANI emeraldine base (EB) and salt (ES) in an epoxy paint. In 2008 they reported that “The coating constituted by the epoxy paint modified with Pani-ES dispersed in xylene provided the best corrosion protection, even under very low conducting polymer concentration (0.3 wt%)” Fig. 2.12. [55].

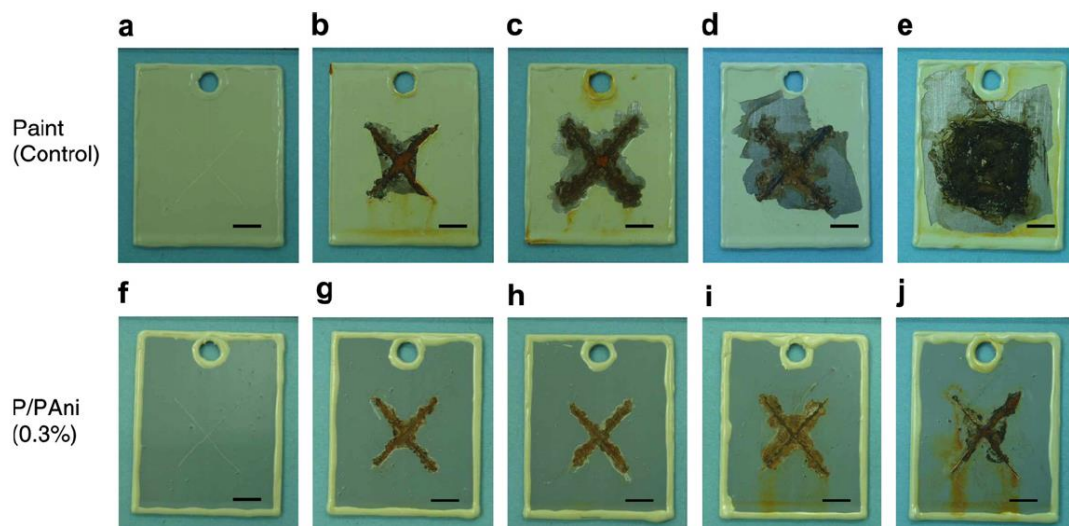


**Figure 2.12.** Test panels of epoxy paint without conducting polymer (control) and paint modified with PANi-ES (0.3%) before (a, f) and after 120 h (b, g), 240 h (c, h), 480 h (d, i), and 720 h (e, j) of exposure in 3.5% NaCl solution. Scale bar: 9 mm [55].

After one year, the same authors [56] concluded the following “*Accelerated assays using an aggressive saline solution reveals that the panels coated with the epoxy + PANi-EB formulation are significantly more resistant against corrosion than those*

*protected with the unmodified epoxy paint*". Thus, results in evidence that PANi-EB is very effective in inhibiting corrosion. Furthermore, the epoxy + PANi-EB formulation provides more protection than the epoxy + PANi-ES and the epoxy +  $Zn_3(PO_4)_2$ , Figs. 2.13 and 2.14. These results combined with those obtained for other epoxy coatings containing conducting and electroactive polymers as anticorrosive additives indicate that the protection mechanism of PANi-EB is based on the ability of this polymer to store charge (molecular condenser). Moreover, as the highest protection was imparted by epoxy + PANi-EB paint, we concluded that the mechanism based on the electroactivity of partially oxidized polymers is more effective than that based on the interception and transport of electrons. Finally, the comparison between the performance of the epoxy + PANi-EB and epoxy +  $Zn_3(PO_4)_2$  suggests the replacement of the conventional inorganic corrosion inhibitors by a small concentration of PANi-EB".

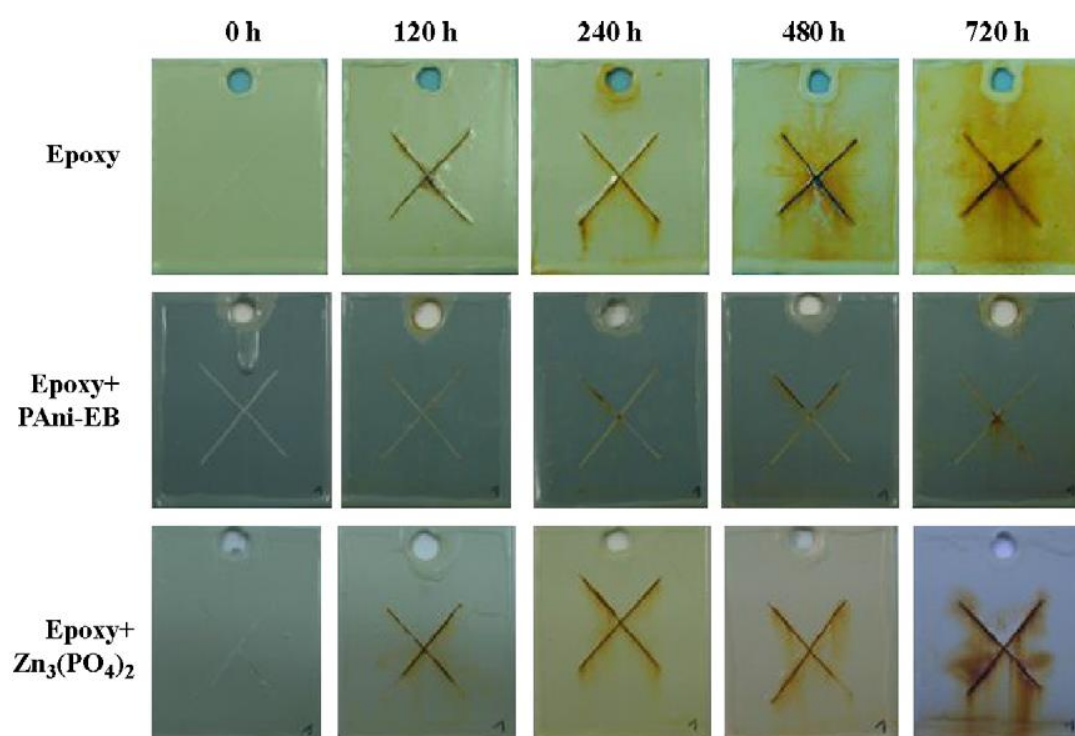


**Figure 2.13.** Test panels of epoxy, epoxy + PANi-EB and epoxy +  $Zn_3(PO_4)_2$  before and after 120, 240, 480 and 720 corrosion cycles [56].



**Figure 2.14.** Scrapped test panels of epoxy, epoxy + PAni-ES, epoxy + PAni-EB and epoxy +  $Zn_3(PO_4)_2$  after 720 corrosion cycles [56].

Diniz et al. [63] investigated organic coatings based on the epoxy and polyurethane matrices containing polyaniline doped with dodecyl benzene sulfonic acid. Pani-DBSA were prepared and applied to steel plates (SAE 1020). The plates were submitted to salt spray chamber for up to 30 days in order to evaluate the corrosion protection of these coatings. The properties of the coated plates were analyzed as a function of time by electrochemical impedance spectroscopy, open circuit potential, optical microscopy, and Raman spectroscopy. In general, results indicate a decrease in the electrical resistance, increase in capacitance and decrease in open circuit potential. Epoxy based coatings have improved performance when Pani-DBSA is used as a pigment, Fig. 2.15, whereas for the polyurethane coatings, Pani-DBSA seems to play an adverse effect. Raman spectroscopy indicates a possible chlorination of the epoxy matrix after 30 days exposure to salt spray chamber.

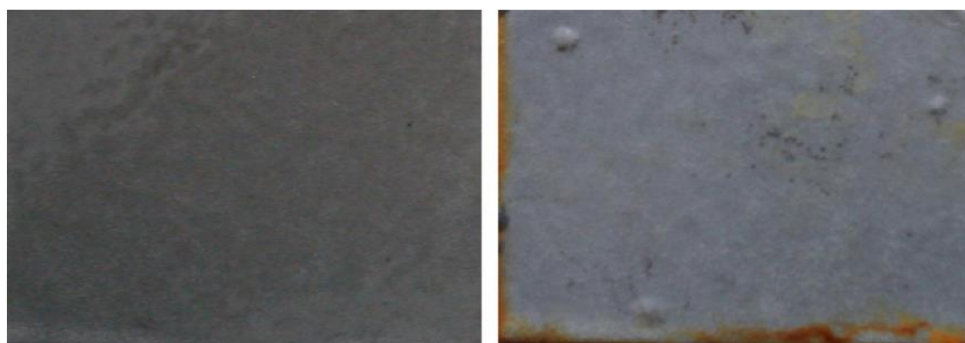


**Figure 2.15.** Photograph of a plate coated with a polyurethane containing 0.1% Pani-DBSA. Left-fresh plate, right-plate after 30 days of salt spray chamber accelerated corrosion essay [63].

Sakhri et al. [64] investigated the corrosion protection behavior of mild steel in neutral saline conditions (salt spray/immersion) by using coatings based on chlorinated rubber and benzene-sulfonate (BS) or lignosulfonate (LS)-doped polyaniline (PANI). Standardized accelerated (salt spray) and immersion tests were performed to assess the protective performance of the coatings. Analysis and interpretation of the experimental data (i.e., EIS, potentiodynamic data and visual observations) showed that both PANI-BS and PANI-LS inhibit corrosion of painted steel exposed to a 3.5% NaCl solution, Fig. 2.16.

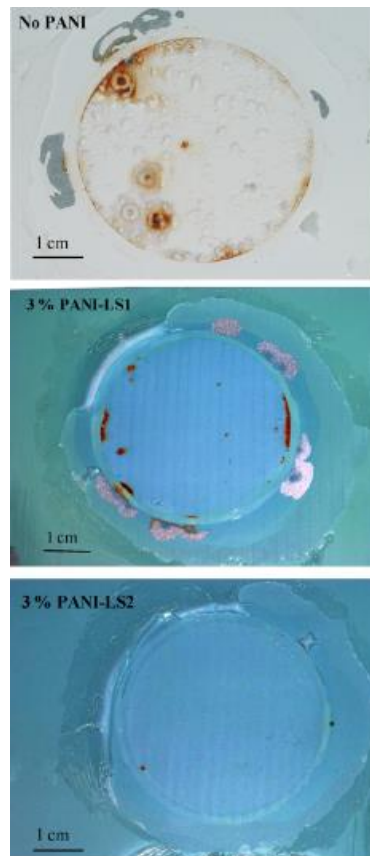


**Figure 2.16.** Photograph of the painted steel panels with no PANI with 3% PANI-LS1 and with 3% PANI-LS2 pigment after 80 days of exposure in 3.5% NaCl solution [64].

Among the tested concentrations (0.5, 1.5 and 3 wt.%), the greatest inhibition was observed at a low concentration of PANI-BS (0.5%). Samples with higher PANI-BS loadings (1.5 and 3%) appear severely corroded after 560 h of salt spray exposure, which was related to the release of corrosive benzene sulfonic acid. On the contrary, the coatings with lignosulfonate doped PANI performed well both in the salt spray and immersion

tests, especially at the highest PANI concentrations (1.5 or 3%). With regard to the healing properties, PANI-LS with the lowest conductivity ( $1 \text{ S cm}^{-1}$ ) showed the best characteristics.

Ge et al. [65] prepared PANI nanofibers using four kinds of different dopant acids by the quickly mixed reaction. The best morphology with a uniform diameter and several microns length was observed, especially in  $\text{H}_2\text{SO}_4$ . The study also found that the curing time of epoxy resin could be delayed by adding PANI. Morphology and counter-anion would impact the anticorrosion effect of the doped PANI. It was observed that  $\text{H}_3\text{PO}_4$ -doped PANI showed the best protective effect 0.5 wt.%, followed by  $\text{H}_2\text{SO}_4$ -doped PANI, and then by  $\text{HNO}_3$ -doped PANI and  $\text{HCl}$ -doped PANI, as can be clearly seen from the EIS and polarization data in 3.5% sodium chloride solution, shown in Fig. 2.17 and extrapolated corrosion parameters are shown in Table 2.1.

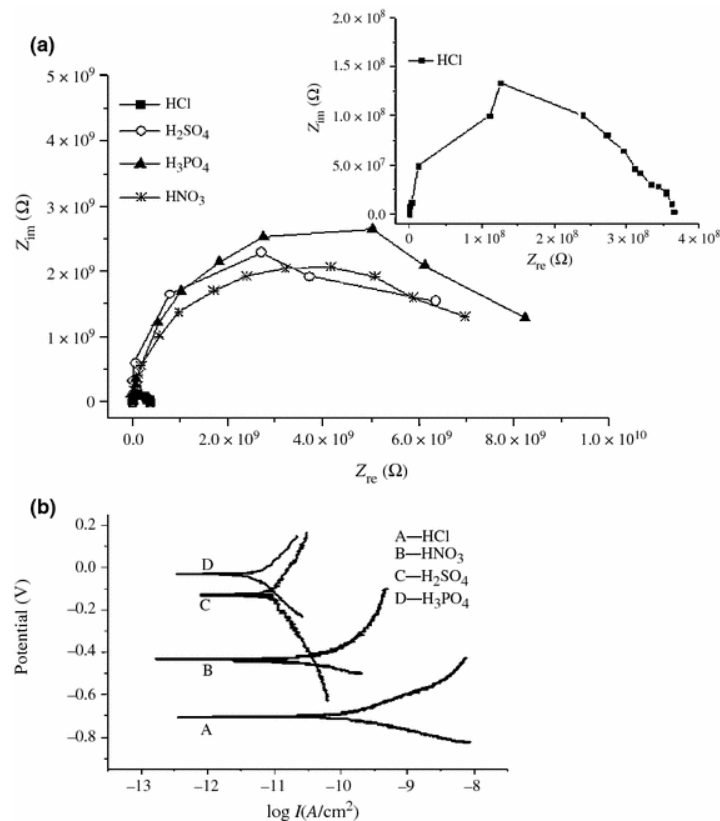


**Figure 2.17.** EIS plots (a) and Tafel polarization curve (b) of epoxy coating mixed with different PANI 0.5 wt.% after being immersed for 3 months in 3.5% sodium chloride solution [65].

**Table 2.2.** Fitting values of Tafel curve of different composite coatings after being immersed for 3 months in 3.5% sodium chloride solution [65].

Acid kinds	HCl	HNO <sub>3</sub>	H <sub>2</sub> SO <sub>4</sub>	H <sub>3</sub> PO <sub>4</sub>
$E_{\text{corr}}$ (mV)	-652	-437	-127	-31
$I_{\text{corr}}$ (A/cm <sup>2</sup> )	$1.175 \times 10^{-4}$	$8.532 \times 10^{-5}$	$9.090 \times 10^{-6}$	$8.830 \times 10^{-6}$

Alkyd-based coatings are described to exhibit good adhesion, durability, flexibility, and high resistance [66] Oil-based alkyds are one of the most widely used industrial protective coating materials due to their color stability, low cost, and exceptional weatherability in most environmental situations [67].

Bhanvase et al. [68] dispersed PANI and PANI–CaCO<sub>3</sub> nano-composite in alkyd resin in different percentages. The structure and morphology effect of adding PANI and PANI–CaCO<sub>3</sub> nano-composite on the anticorrosion and mechanical properties of alkyd resin were discussed. The results showed that PANI–CaCO<sub>3</sub> resulted in an enhanced adhesion of alkyd resin to the metal substrate, an improvement in the impact strength of composite alkyd coatings, and a decreased corrosion rate of PANI–CaCO<sub>3</sub> alkyd resin. These results were attributed to the synergistic effects of PANI and nano-size CaCO<sub>3</sub>.

Marti et al. [69] examined the performance of four anticorrosive pigments used in alkyd primer. Very small weight percentages of PANI showed good dispersion in organic solvents such as xylene and organochloride and provided greater protection to the matrix than other conducting polymers or zinc phosphate. Specifically, the four corrosion inhibitors used in this work were: zinc phosphate (10 wt.%), PANi-EB (0.3 wt.%), PANi-ES (1.0 wt.%) or PTE-a partially oxidized polythiophene (1.0 wt.%). Among the three CP-containing formulations, the Alkyd-PET was found to impart the highest protection against corrosion, as can be seen in Fig. 2.18. This has been attributed to the fact that the PTE eco-friendly additive shows better miscibility properties with the alkyd formation than PANi-ES and PANi-EB. Therefore, it is suggested that PANI-ES and PTE could be a satisfactory substitute for classical zinc-containing corrosion inhibitors.

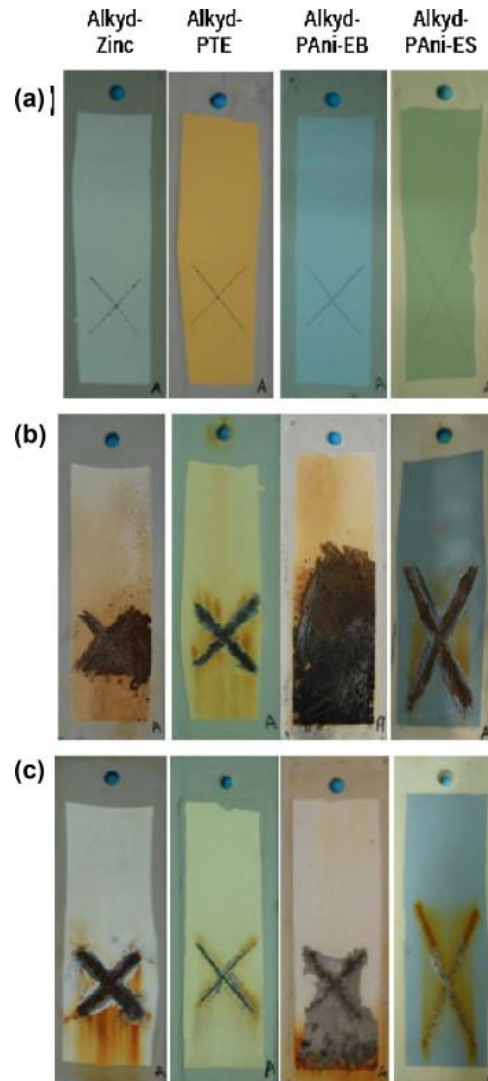


**Figure 2.18.** Scrapped test panels of the alkyd panels after (a) 120, (b) 240 and (c) 480 corrosion cycles in  $\text{NaHSO}_3$  aqueous solution [69].

Bagherzadeh et al. [70] investigated the anticorrosion performance of a two components water-based epoxy coating system is improved by using the nanopolyaniline (nanoPAni) particles. The purchased nanopolyaniline which was dispersed in water was mixed mechanically with the water-based polyamidoamine hardener of the epoxy system using ultrasonic homogenizer. The average particle size of the polyaniline in hardener was determined using dynamic light scattering technique (DLS). Results revealed that the particles were in the range of 50–57 nm. After combining the prepared sample with the DGEBA epoxy resin, the finished coating was applied on steel substrates. Anticorrosion performance and adhesion properties of coating which contained nanoPAni were compared to the model water-based epoxy coating with the help of salt spray and adhesion



tests. Results showed that anticorrosive performance of the model water-based epoxy system improved dramatically by adding only 0.02 wt.% nanoPAni. However in contrast to model coating, adherence of PAni-epoxy coating to steel plates was remained constant after their exposure to the corrosive media. The surfaces of steel samples coated with the model water-based epoxy coating and the coatings containing nanoPAni after 650 h exposure to the salt spray medium are shown in Fig. 2.19.

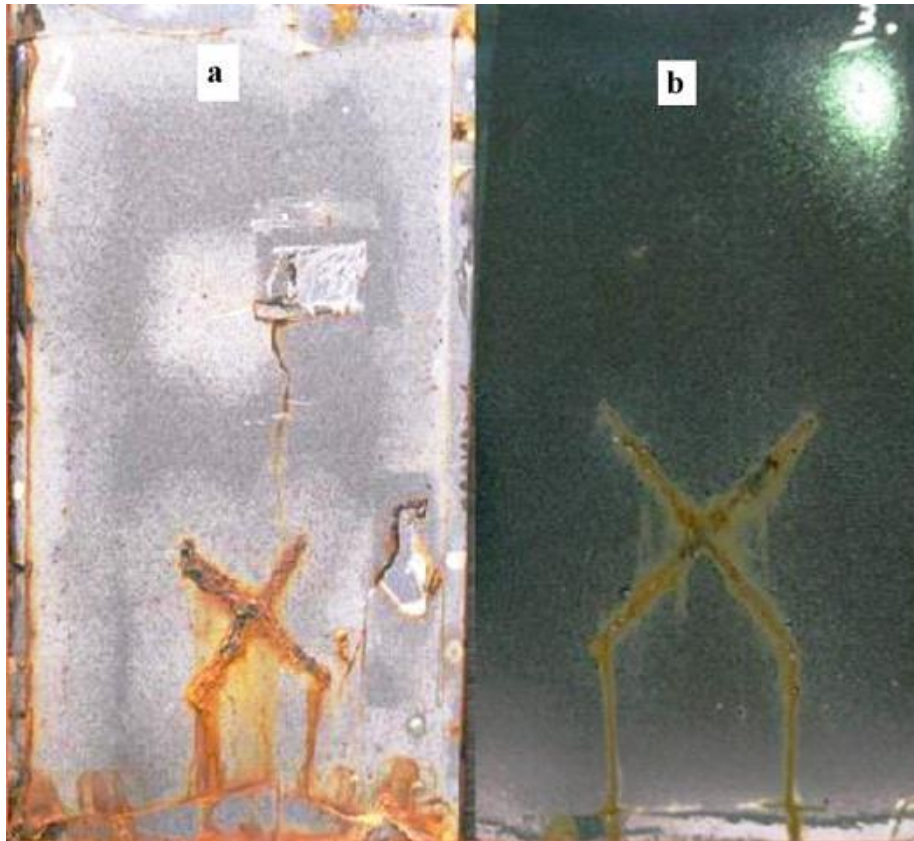


**Figure 2.19.** The surfaces of steel samples coated with the model water-based epoxy coating and the coatings containing nanoPAni after 650 h exposure to the salt spray medium [70].

The anticorrosion performance of plasticized chlorinated rubber coated mild steel sheets incorporating polyaniline emeraldine salt or zinc phosphate as active pigments were compared using salt spray and immersion in 3.5% NaCl solution was investigated by Sakhri et al. [71]. The results obtained by different electrochemical methods indicate the superiority of polyaniline in comparison with zinc phosphate in terms of corrosion protection. The time of the emergence of the first rust spot in 3.5% NaCl solution for the film containing 1.5 wt% polyaniline reach 960 h, which is six times higher than that of

the film without polyaniline. The effect of the amount of PANI was also studied comparing the corrosion behavior of CR coatings with different loadings of PANI (CR-H1 0.5 wt%, CR-H2 1.5 wt%, and CR-H3 3 wt%). The polarization curves in 3.5 % NaCl are shown in Fig. 2.20., while the photograph of the painted steel panels after 80 days of exposure in 3.5% NaCl solution (scale bar: 1 cm) is shown in Fig. 2.21.

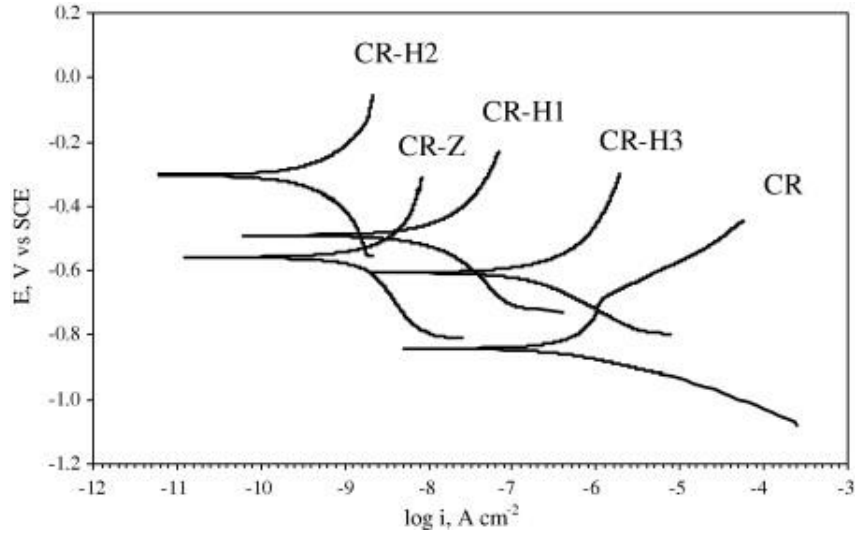


**Figure 2.20.** Potentiodynamic polarization curves of the CR paint without and with anticorrosion pigments after 40 days of immersion in 3.5% NaCl solution [71].

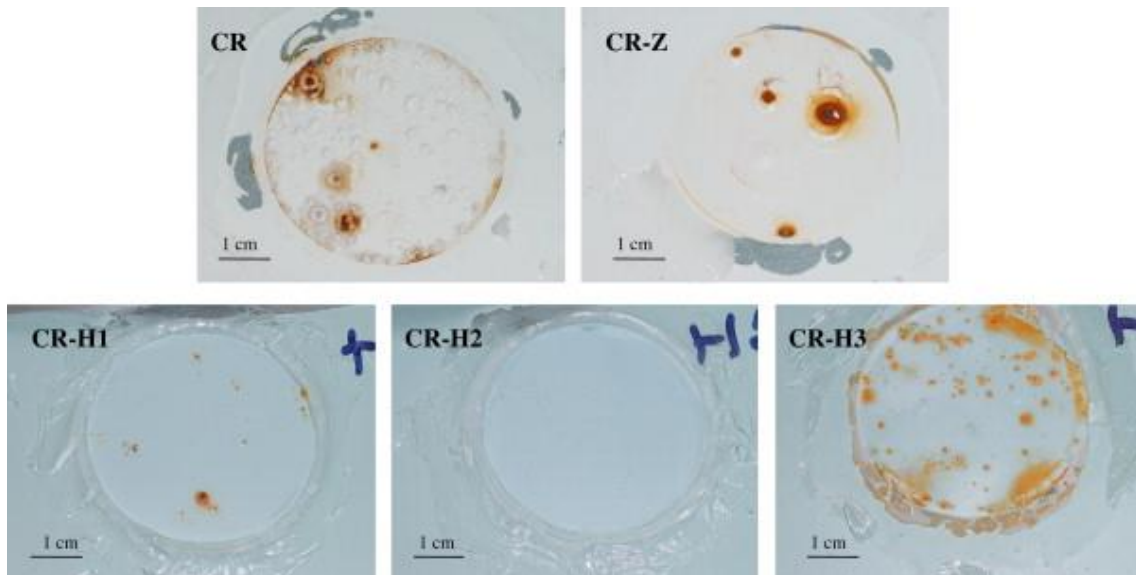


**Figure 2.21.** Photograph of the painted steel panels after 80 days of exposure in 3.5% NaCl solution (scale bar: 1 cm) [71].

### **2.3. Possible mechanisms of the mild steel corrosion protection with polyaniline composite coatings**

Because of the doubt about the role of the electroactive forms of polyaniline in the corrosion protection, different mechanisms of protection has been proposed [32, 33, 72]. Anticorrosion mechanisms for PANI-based coatings are considered to be quite complex. The morphology and composition of PANI, type of matrix resin, local pH, humidity, galvanic activity, corrosive environment, and test method affect the rate of corrosion; all of these factors are regarded as important parameters [73].

The main problem arises due to the fact that many studies have been carried out using a wide variation of experimental procedures, causing difficulties in trying to compare the results. In particular, the surface preparation, the coating deposition method, the corrosion environment and the test method, can be very different from one study to another study. However, an effort has been made in this study to classify the corrosion protection mechanism. The possible mechanisms of corrosion protection of PANI on steel are essentially of following types [32]:

- **Barrier properties** (involving a *physical action*)
- **Corrosion inhibition** (involving a *chemical action*)
- **Anodic protection** (involving an *electrochemical action*)
- **Complex formation effect** (involving an *electrochemical action*)

#### **2.3.1. Barrier properties**

Organic coatings in general (including coatings with ICP's as PANI) can protect metal substrates against corrosion following a general mechanism [74, 75]. It is well established that most of the organic coatings with barrier effect permits the oxygen and water diffusion in quantities lower than the necessary amount for the corrosion rate measured on bare metal. By the additions of polyaniline in the coatings, the diffusion length of the water and oxygen are increased, as schematically shown in Fig. 2.22, so prolonged anticorrosion protection is expected.

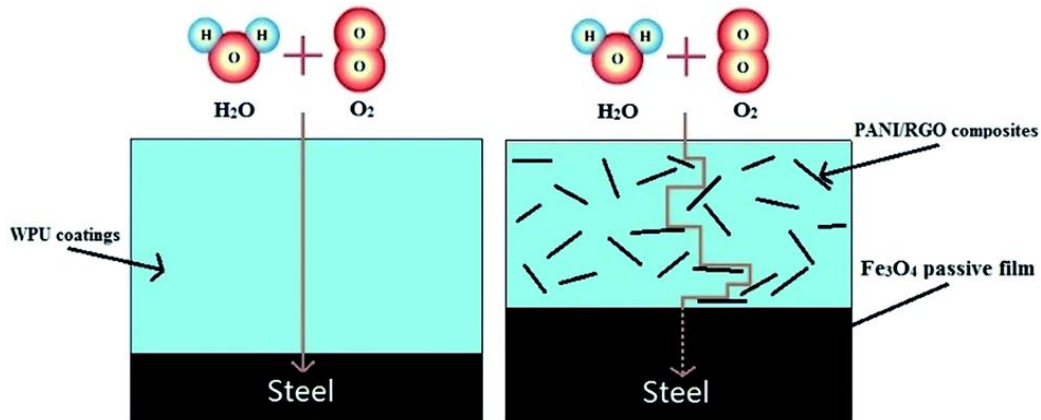


**Figure 2.22.** Schematic representation of corrosion medium following paths through a classical coating and a composite coating [76].

### 2.3.2. Corrosion inhibition

The presence of organic compounds close to the metal surface in principle could affect both anodic and cathodic corrosion reactions [74]. In this case, the organic compound is called inhibitor. Organic inhibitors are usually designated to act as film forming, protect the metal by forming a hydrophobic film on the metal surface. In this way, the corrosion rate is influenced. Their effectiveness depends on the chemical composition, their molecular structures, and their affinities to the metal surface. However, this behavior is not expected for PANI, because after polymerization the mobility of the molecular chains is strongly reduced. The only possible inhibition effect is indirect and it is related to the released counter ions in doped PANI.

### 2.3.3. Anodic protection

Anodic protection is a corrosion protection strategy based on an anodic polarization by controlling the potential in a zone where the metal tends to be passive. In other words, it is an approach favoring passivity and stabilization. For this reason, it can be used only for materials having passivation possibility. Iron (steel) can passivate, as shown in Pourbaix diagram, Fig 2.23 [77].

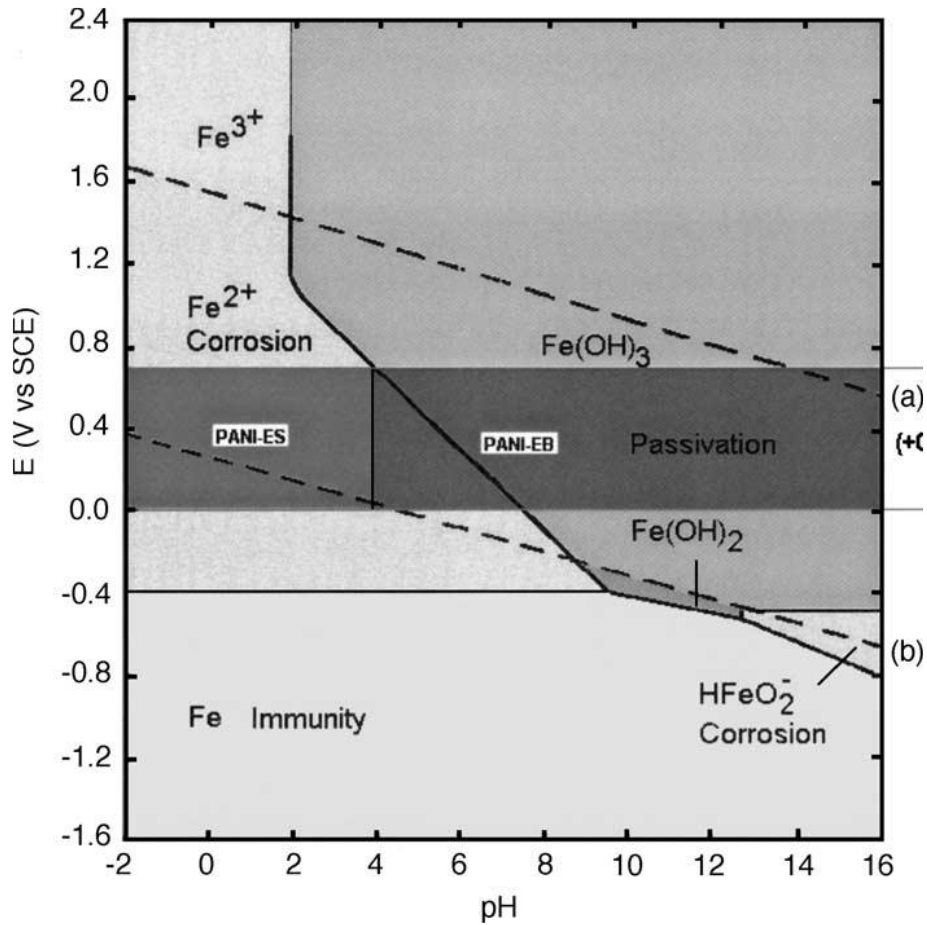
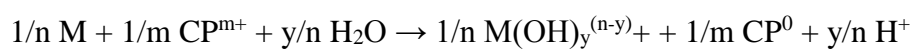


**Figure 2.23.** Pourbaix diagram for steel in water. The stable regions for PANi–ES and EB are superimposed on the stable regions for iron. Dashed lines (a) and (b) represent the reduction potential for oxygen (in water) and hydrogen ions, respectively [77].

From Fig. 2.23 it can be deduced that near neutral or alkaline pH is necessary to promote passivation. This aspect must be considered carefully because it can be in conflict with PANI's pH stability. In other terms, to have an anodic protection action it is necessary to have a system in which both the passivation layer and the ICP based coating (PANI) are stable. The general anodic protection mechanism of ICP is the following:



(where M is the metal (steel) and CP any electroactive conductive polymer), and



Many authors have tried to prove this mechanism by using different experimental approaches: open circuit potential measurements, metal surface analysis to identify the oxide layer and surface analysis of ICP's to identify its oxidation state. Some authors reported an increase of the OCP (moving to anodic direction) of steel coated with CP in comparison with bare steel (ennobling). Considering that the passivation potential of steel is expected to be between 0.5 and 1 V SCE, the observed ennobling can be an indication of passivation. However, it is important to keep in mind that the passivation potential is in general dependent on the local environment (pH, oxygen concentration, chlorides, etc.) normally unknown close to the corroding area.

Ennobling is a necessary condition for anodic protection, but it is not sufficient since the OCP of coated steel is often increased also for barrier coatings because of the different corrosion conditions (concentration polarization and ohmic drop). In addition, it has been proven that PANI can modify the steel surface conditions (electrochemical studies of bare steel and bare steel obtained after removal of the PANI layer exposed to the electrolyte). These results have been obtained using different techniques, as impedance measurements (charge transfer resistance), visual observation (change of color), XPS analysis (formation of  $\text{Fe}_2\text{O}_3$ ,  $\text{Fe}_3\text{O}_4$ ), mass spectroscopy, etc. It is important to remember that surface conditions depend on the PANI form, EB (emeraldine base) or ES (emeraldine salt). Wessling [78] considered that the formation of the passive film is due to catalytic oxide-redox reactions. He reported the catalytic passivation mechanism of PANI to iron, as shown in Fig. 2.24. ES was an intermediate in the oxidation of aniline, and LS (leucoemeraldine state) was the reduction state of polyaniline. The theory pointed out that the dense oxide film kept the metal the passivating region and decreased the corrosion rate of iron. But the existence of  $\text{Fe}^{3+}$  is possible only under highly acidic media, so the first step in the reaction mechanism is disputable.

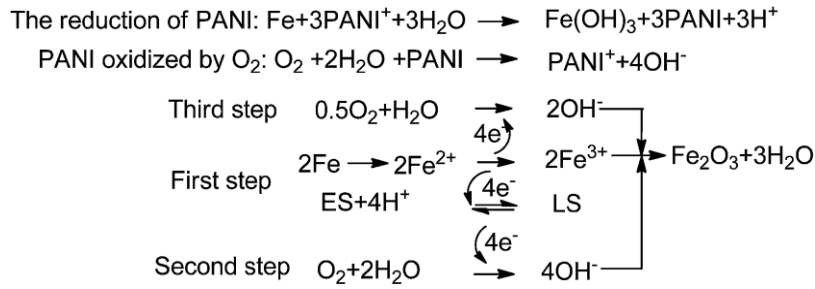
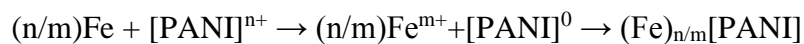


**Figure 2.24.** Description of the catalytic passivation of iron by PANI [78].

Based on all these results and considerations, a conclusion can be drawn: **anodic protection is a possible corrosion protection mechanism for PANi on steel**, under specific restrictive conditions, i.e., the presence of PANI in the ES form and the presence of balancing-counter anions.

#### 2.3.4. Complex formation effect

The main theme of complex formation effect is that the redox reaction, which occurs at the interface between iron and PANI, will generate a complex compound. The oxidation potential of the complex is higher than that of pure PANI, and it promotes the reduction of oxygen, which results in compensating the charge consumed by the dissolution of iron. Complex formation effect can maintain the potential of iron in the passivation region to be stable. Mohammad et al. [79] produced PANI–PS core-shell latex microspheres through the adsorption of suspension polymerization method. They assumed the mechanism was one in which PANI and iron generated a complex at the metal interface. The oxidized PANI–PS can react with a ferrous or ferric ion to yield corrosion-protective Fe–PANI complex, according to the proposed reaction:



where  $m = 2$  or  $3$ .

During this process, the metal is protected and PANI is reduced. By comparing FTIR spectra of the area before and after the corrosion test, Kamaraj and other researchers

[80, 81, 82] considered that the complex film was formed by the interaction between metals and PANI composites.

### 2.3.5. Other mechanisms and factors

A further critical issue in the PANI corrosion protection mechanisms is the role of counter ions [83]. It has been already established that we need the ES form (salty form) to have conductive PANI and in this case, we need negative counter ions. The release of anions during redox processes could affect the corrosion rate, both promoting corrosion if the ions are aggressive (as chlorides) or reducing the corrosion rate by complexation with Fe ions and causing a precipitation of insoluble salts (pseudo-passivation). This possible mechanism is very important in the case of contemporary presence of other ions because of the formation of complex insoluble salts. Additionally, some released ions could act as inorganic or organic corrosion inhibitors.

Recently Grgur et al. [48], suggested that in the composite PANI-benzoate coatings, the PANI might serve as a center for oxygen reduction reactions followed two electron pathway. These processes prevent the penetration of corrosion agents ( $O_2$ ) into the metal surface, as illustrated in Fig. 2.25. Therefore, the polyaniline acts as an active barrier. The polyaniline might be partially reoxidized and doped with chloride ions during oxygen reduction or by the released hydrogen peroxide. Notably, using increased amounts of the PANI powder in a composite provides better contact between the individual particles obtained, increasing the redox ability of the active pigment.

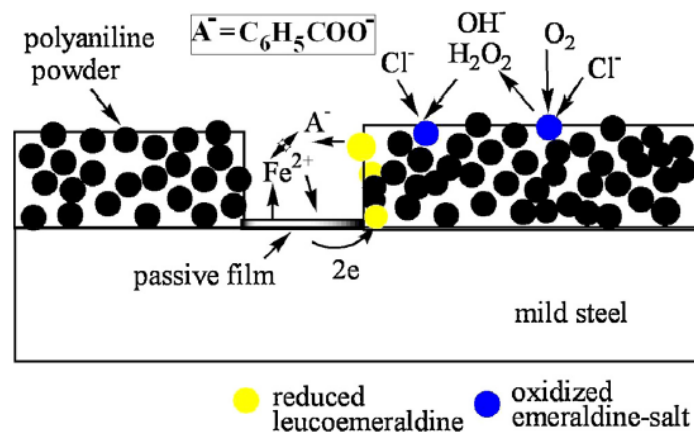


**Figure. 2.25.** Schematic representations of corrosion processes with polyaniline composite coatings [48].



Authors [48] also shows that best protection against corrosion possess, among chemically (C) and electrochemically (EC) formed emeraldine salt (ES) and bases (EB), chemically synthesized polyaniline in emeraldine salt form, as it can be seen from Fig. 2.26.

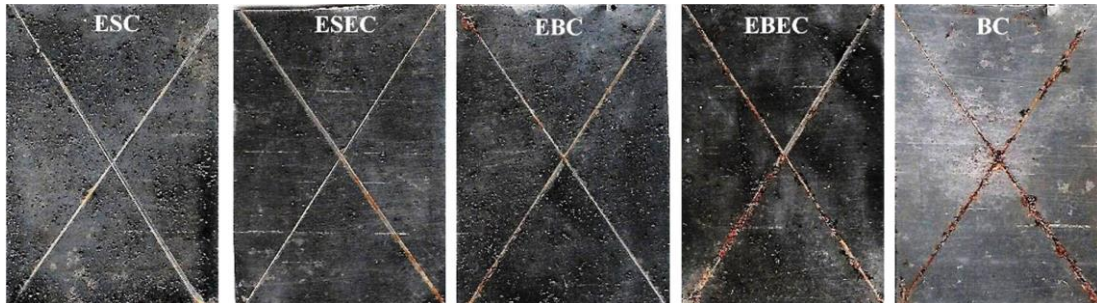


**Figure 2.26.** Comparison of the samples (4 cm × 6 cm) after treatment in a humid chamber for 5 days [48].

## 2.4. Methods for polyaniline characterization and corrosion determination

### 2.4.1. UV visible spectroscopy study of polyaniline

Ultraviolet-Visible absorption spectroscopy is the measurement of the attenuation of the beam of light after it passes through a sample or after reflection from a sample surface. UV-Vis includes transmittance, absorption and reflection measurements in UV, visible and Near Infra-Red region [84]. Schematic presentation of the UV-visible for measuring absorption is shown in Fig. 2.27.

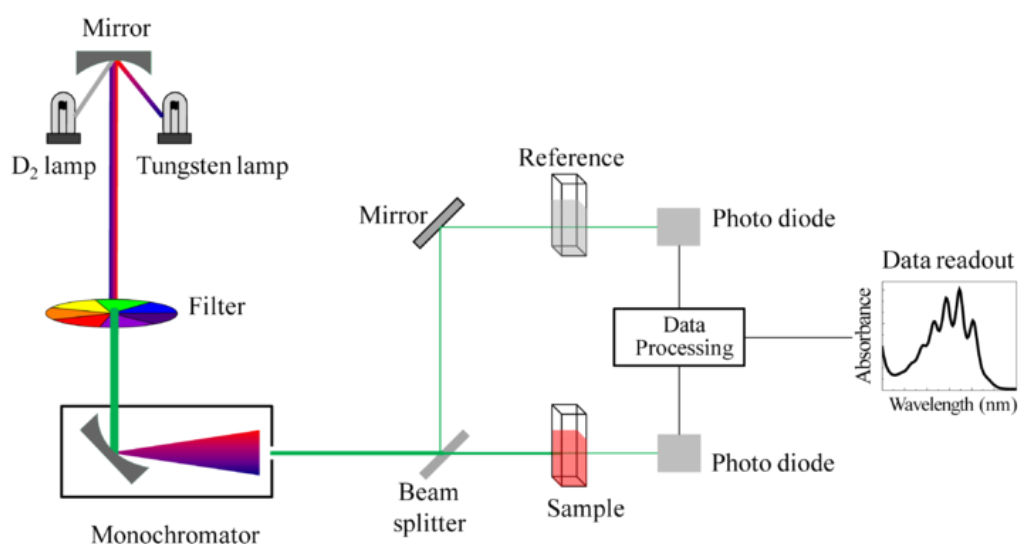


**Figure 2.27.** Schematic of UV- visible spectrophotometer.

The method is most often used in a quantitative way to determine concentrations of an absorbing species in solution, using the Beer-Lambert law:

$$A = \log(I_0/I) = \epsilon cL \quad (2.1)$$

where  $A$  is the measured absorbance (in Absorbance Units (AU)),  $I_0$  is the intensity of the incident light at a given wavelength,  $I$  is the transmitted intensity,  $L$  the path length

through the sample, and  $c$  the concentration of the absorbing species. For each species and wavelength,  $\epsilon$  is a constant known as the molar absorptivity or extinction coefficient. This constant is a fundamental molecular property in a given solvent, at a particular temperature and pressure.

The absorption of UV radiation by organic compounds in the visible and ultraviolet region involves promotion of electrons in  $\sigma$ ,  $\pi$  and  $n$ -orbitals from the ground state to higher energy state. These higher energy states are described by molecular orbitals that are vacant in the ground state and are commonly called anti bonding orbitals. The anti bonding orbitals associated with  $\sigma$  bond is called the  $\sigma^*$  orbital and that associated with  $\pi$  bond is called the  $\pi^*$  orbital. As the  $n$  electrons do not form bonds, their antibonding orbitals are not associated with them. The electronic transitions that are involved in the UV and visible regions are of various types viz;  $\sigma \rightarrow \sigma^*$ ,  $n \rightarrow \pi^*$ ,  $\pi \rightarrow \pi^*$ . Transitions to antibonding  $\pi^*$  orbitals are associated only with unsaturated centers in the molecule. Compounds containing isolated double bond absorb in the range 162 nm to 190 nm, whilst conjugated molecules (those containing single and double bonds) absorb above 210 nm. Extension of conjugated systems intensifies the absorption peaks and shifts it further to the higher wavelengths, towards the visible spectrum. This technique not only provides information about the different bonding but also is an excellent tool for determining the band energy, which is an important parameter used in investigating the conduction mechanism in the organic conductors.

The UV-vis spectroscopy is very useful tools for characterization of the polyaniline. For examples Flavel et al. [85], investigated UV-Vis spectra of both adsorbed emeraldine salt and emeraldine base, shown in Fig. 2.28. The spectra for the un-protonated emeraldine base (dedoped) shows two absorption peaks at 340 and 602 nm, which are due to the  $\pi - \pi^*$  transition of the benzenoid rings and the exciton absorption of the quinoid rings, respectively. In the case of the protonated emeraldine salt (doped states), three absorption peaks at 360, 430 and 796 nm are distinguishable with the absorption at 602 nm observed for the emeraldine base disappearing, indicating a protonation of the imine sites. The peak at 340 nm for the emeraldine base is red-shifted to 360 nm and the new peaks at 430 and 796 nm are

related to a doping level and the formation of a polaron band transition. Furthermore, the peak at 430 nm is a result of a polaron–bipolaron transition.

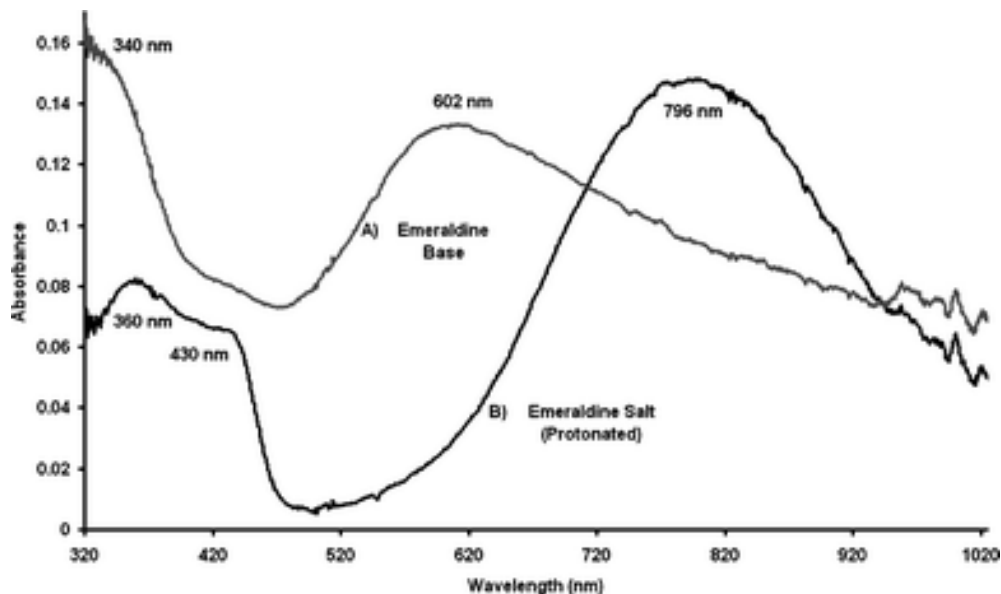


**Figure 2.28.** UV-Vis spectra of polyaniline films deposited for 50 minutes in the a) non-conducting and b) conducting forms [85].

Similar results are presented by Xu et al. [86] showing the UV-vis spectra of PFOS (perfluorooctanesulfonic acid)-doped PANi and dedoped PANi fibers, Fig. 2.29. The doped form of PANi fibers exhibits a peak maximum at 450 nm and a broad band at around 950 nm assigned to the polaron band transitions [87] indicating that the as-prepared PANi is in conducting emeraldine salt form. The dedoped form of PANi fibers has absorbance peak maxima at 335 and 635 nm, which agrees well with those of the emeraldine base form of PANi [88]. It should be mentioned that the exact position of the band maximum depends on the polyaniline structure and used solvents.

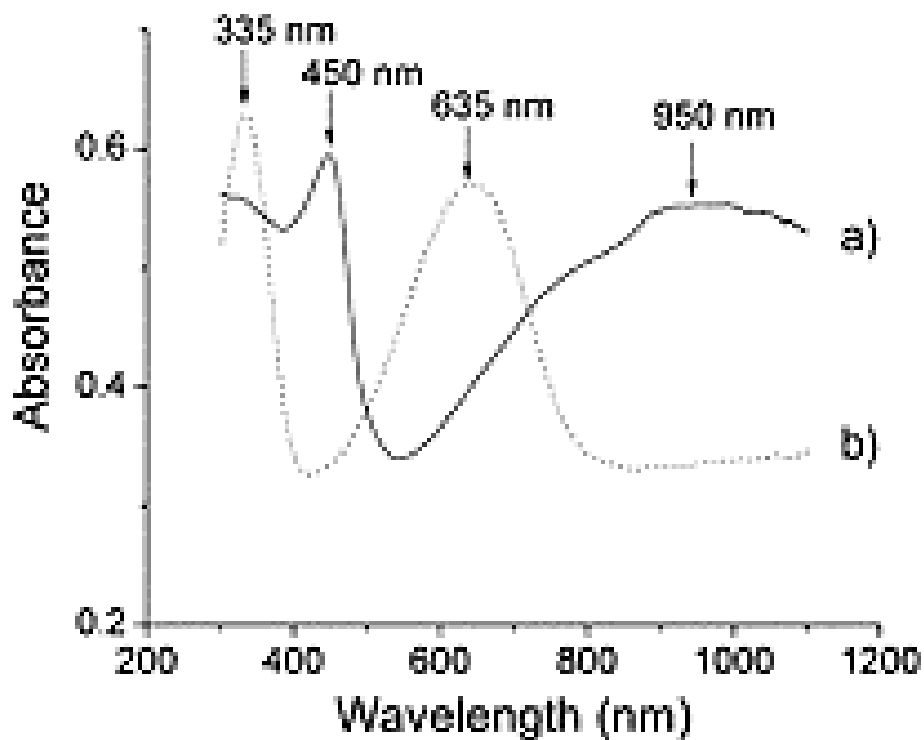


**Figure 2.29.** UV-vis spectra of sub-micron polyaniline fibers dispersed in acetonitrile: a) doped polyaniline (solid line); (b) de-doped polyaniline (dotted line) [86].

Sk and Yue [89] investigated PANI dispersions in the water. The UV-visible spectra of the doped polyaniline nanotubes are recorded by dispersing in a water. The spectra, Fig. 2.30 revealed two main characteristic absorption peaks at approximately 312 nm and 452 nm.

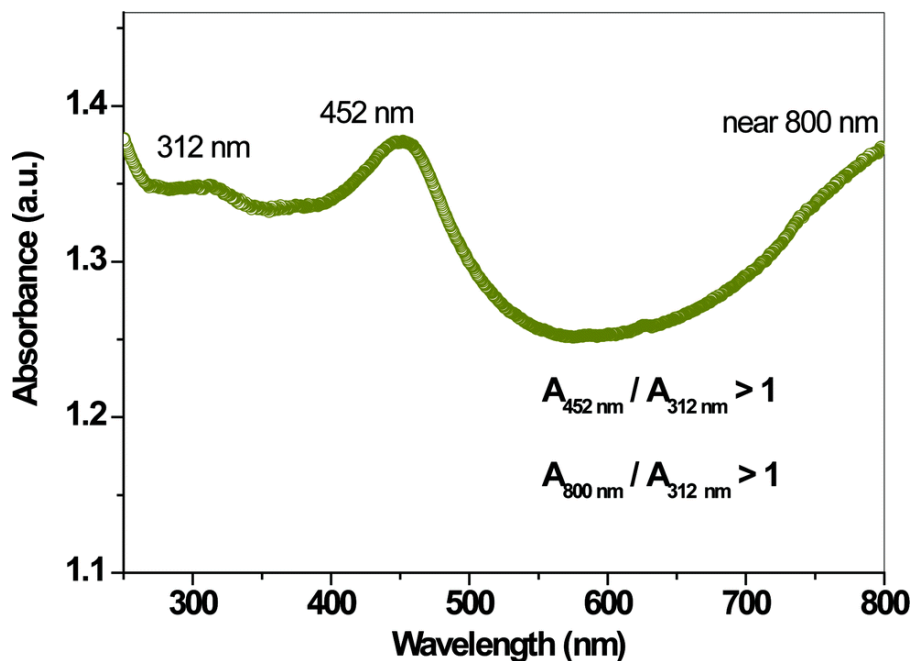


**Figure 2.30.** The UV–vis spectra of the doped PANI dispersed in water [89].

The first one is due to a  $\pi$ – $\pi^*$  transition at 312 nm in the benzenoid rings and the second one is assigned as a polaron band (polaron– $\pi^*$  transition) at 452 nm. A broader peak at a higher wavelength near 800 nm corresponded to the  $\pi$ -polaron transition. It is demonstrated that the PANI chains are in the doped state. The polaronic transitions (polaron– $\pi^*$  and  $\pi$ -polaron) clearly indicate the presence of charge carriers in the polymer chain, the  $\pi$ – $\pi^*$  transition arose from neutral benzenoid segments. Moreover, the proportions of the absorbance of the polaronic band to that of the  $\pi$ – $\pi^*$  band are estimated, which provided a measure of the average oxidation level of the PANI nanostructure. It is apparent from Fig. 2.30 that the absorbance peak intensity ratios of  $A_{452 \text{ nm}}/A_{312 \text{ nm}}$  and  $A_{800 \text{ nm}}/A_{312 \text{ nm}}$  are higher than one, which reveals that the PANI nanotubes appeared to be in the higher oxidation level.

Optical absorption spectra of polyaniline dispersions in aqueous media have been also investigated by Stejskal et al. [90]. They prepared polyaniline dispersions by the oxidative polymerization of aniline in the hydrochloric acid using ammonium persulfate.

From the spectra shown in Fig. 2.31 it can be seen that three absorption maximums at 350, 430 and 810 nm are typical of the protonated form of PANI dispersion in a slightly acidic region (, pH = 4 to 7). The individual bands are separated by isosbestic points where spectra intersect. However, these points are unclear and messy.

From Fig. 2.28, it can be clearly seen that with increasing pH or polyaniline dedoping the adsorption maximum at 350 nm increase, while at 430 nm decrease.

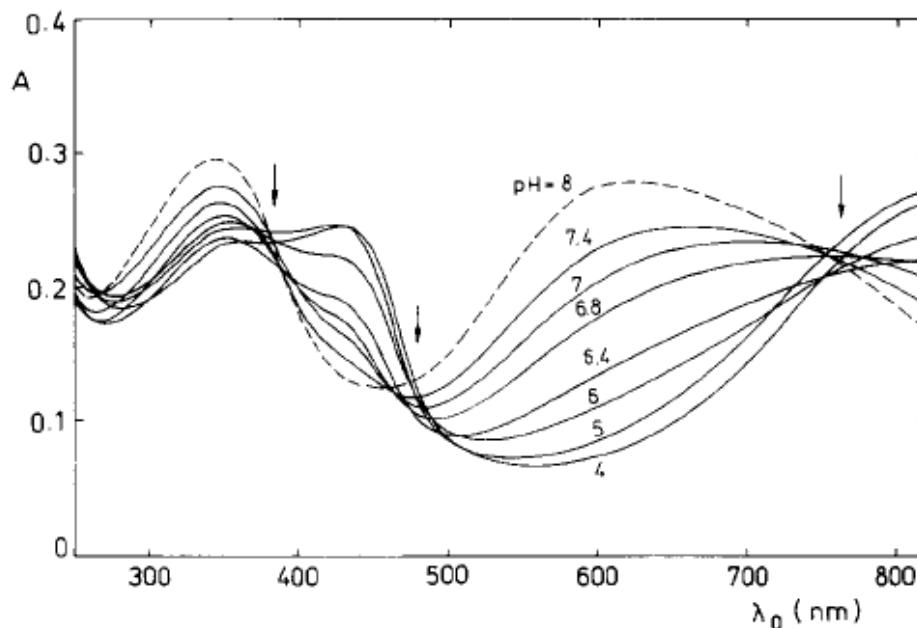


**Figure 2.31.** Absorption spectra of PANI dispersion and their changes in the intermediate range of pH. Isosbestic regions are marked by arrows. The spectrum for pH=8 is the dashed line. Concentration of PANI salt,  $8.5 \times 10^{-5}$  g/ml [90].

Lindfors et al. [91] presented the more detailed study of the optical pH measurements with a water dispersion of polyaniline nanoparticles and their redox sensitivity by the characterization of the emeraldine salt-emeraldine base transition. The UV-visible spectra of the PANI water dispersion, which are measured after an equilibration time of 10 (pH 2-12) and 30 min (pH 7-10), are shown in Figs. 2.32a and b. The spectra are measured with pH intervals of  $\Delta\text{pH} = 0.25$  between pH 6 and 10. Only very small time-dependent changes are observed in the UV-visible spectra between pH 2 and  $\sim 8.5$ , while more pronounced time-dependent changes are observed between pH 8.75 and 9.75. It can be expected that the EB-ES transition mainly takes place in this pH

interval. The UV-visible spectrum recorded at pH 2 is typical for the electrically conducting emeraldine salt form of PANI with characteristic absorbance maximums at  $\sim 415$  and  $757$  nm associated with polaron band transitions (Fig. 2.32a). The somewhat narrow band with a peak at  $757$  nm designates a localized charge distribution in the PANI chains. The nonconducting emeraldine base form has a characteristic absorbance maximum at  $568$  nm (pH 10). The spectra measured between pH 2 and 9 show two rather well-defined isosbestic points at  $\sim 450$  and  $\sim 685$  nm indicating that the emeraldine salt form is transformed directly to the emeraldine base form. Deviations from the isosbestic points are observed at higher pH values. It should also be noted that the color of the PANI solution became dark blue-violet at pH 11 and 12 (dark blue at pH 10), indicating the presence of a small amount of the pernigraniline (PNB) impurities (violet) in the PANI water dispersion. It can be concluded based on the UV-visible measurements that the ES-EB transition of the PANI water dispersion takes place between pH 6 and 10 and the most pronounced changes in the absorbance spectra are observed at  $\sim 400$ - $420$ ,  $\sim 530$ - $600$ , and  $\sim 750$ - $840$  nm

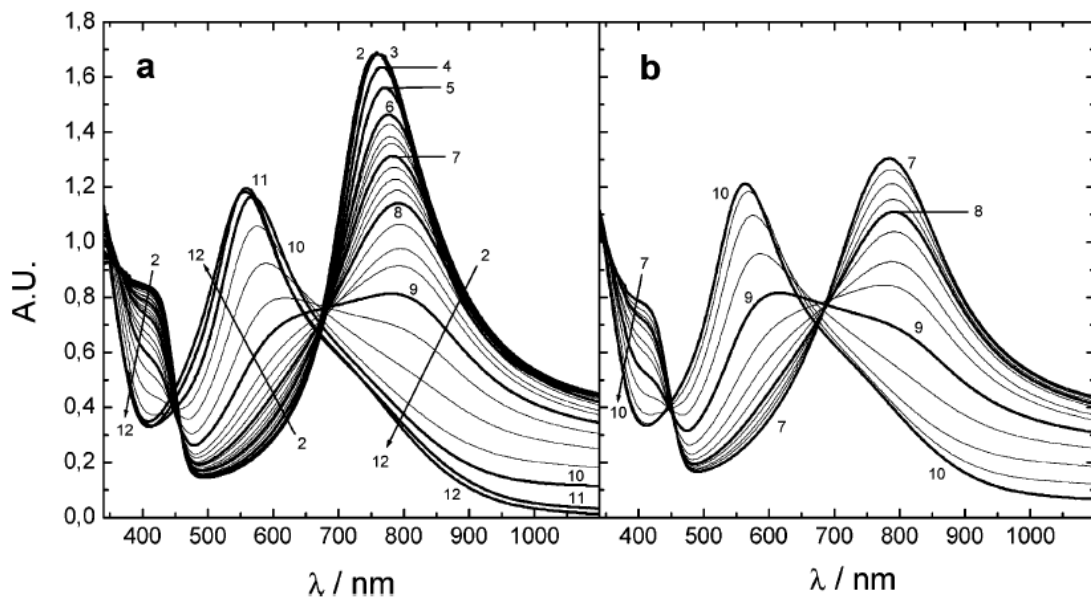


**Figure 2.32.** UV-visible spectra of the PANI water dispersion in pH buffer solutions. (a) pH 2-12, equilibration time: 10 min. (b) pH 7-10, equilibration time: 30 min. The UV-visible spectra were measured with  $\Delta\text{pH} = 0.25$  between pH 6 and 10 [91].



### 2.4.2. The determination of the corrosion current densities by the electrochemical measurements

In contrast, with pure electrochemical reaction which consists only of one oxidation-reduction reaction on the same place [92]:



in the corrosion reaction participated minimum two reactants:



with different electrochemical behavior.

From that reasons, the corrosion is treated on the basis of mixed potential theory, where minimum two reactions simultaneously occur, but the total net current equal to zero. The net current density can be given as differences of anodic and cathodic current densities:

$$j = j_a - |j_c| = j_0 \exp\left[\frac{\alpha_a F(E - E_{r,a})}{RT}\right] - j_{0,c} \exp\left[-\frac{\alpha_c F(E - E_{r,c})}{RT}\right] \quad (2.6)$$

where symbol “a” denotes anodic half reaction and “c” cathodic half-reaction.

When the actual potential is equal to the corrosion potential,  $E = E_{cor}$ , it follows that  $j_a = j_c = j_{cor}$

$$j_{kor} = j_{0,a} \exp\left[\frac{\alpha_a F(E_{kor} - E_{r,a})}{RT}\right] = j_{0,c} \exp\left[-\frac{\alpha_k F(E_{kor} - E_{r,c})}{RT}\right] \quad (2.7)$$

or:

$$\alpha_a E_{cor} - \alpha_a E_{r,a} + \alpha_k E_{cor} - \alpha_k E_{r,c} = \frac{2.3RT}{F} \log \frac{j_{0,c}}{j_{0,a}} \quad (2.8)$$

and it follows that:

$$E_{cor} = \frac{\alpha_a}{\alpha_a + \alpha_c} E_{r,a} + \frac{\alpha_c}{\alpha_a + \alpha_c} E_{r,c} + \frac{2.3RT}{(\alpha_a + \alpha_c)F} \log \frac{j_{0,c}}{j_{0,a}} \quad (2.9)$$

The expression for total corrosion current density is given as:

$$j = j_{cor} \left[ \exp\left(\frac{\alpha_a F(E - E_{cor})}{RT}\right) - \exp\left(-\frac{\alpha_c F(E - E_{cor})}{RT}\right) \right] \quad (2.10)$$

or as:

$$j = j_{cor} \left[ \exp\left(\frac{2.3F(E - E_{cor})}{b_a}\right) - \exp\left(-\frac{2.3F(E - E_{cor})}{b_c}\right) \right] \quad (2.11)$$

In the Fig. 2.33 situation explained above is graphically presented.

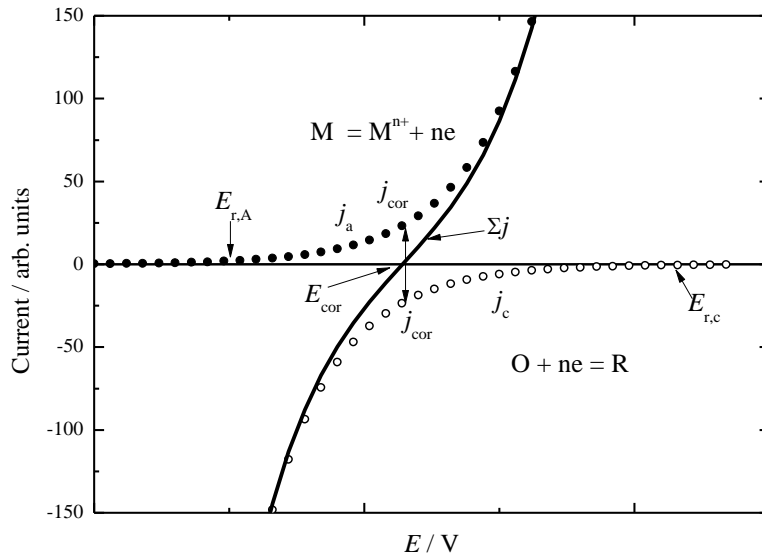


**Figure. 2.33.** Graphical presentations of the polarization curves of the corrosion processes [92].

The corrosion current density can be obtained from the Tafel diagrams of real polarization curves, shown in Fig. 2.34. as the intercepts of anodic and cathodic lines with corrosion potentials.

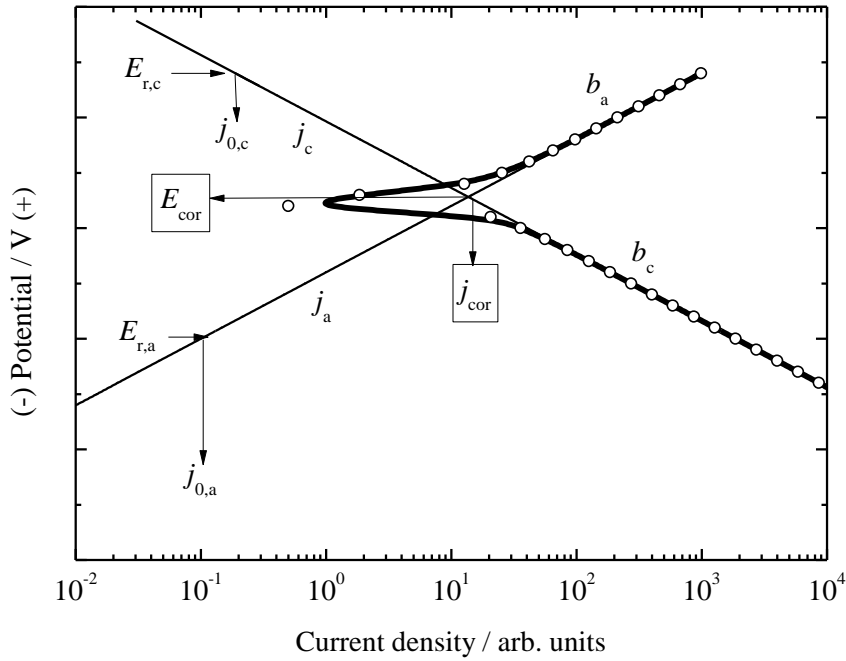


**Figure 2.34.** The determination of corrosion current density from the Tafel diagram [92].

If the Eq. 2.11:

$$j = j_{kor} \left[ \exp\left(\frac{2.3F\eta}{b_A}\right) - \exp\left(-\frac{2.3F\eta}{b_K}\right) \right]$$

develop in the Taylor series, it can be shown that near the corrosion potential (linear polarization region) the following approximating exist:

$$\frac{\partial \eta}{\partial j} = \frac{\partial E}{\partial j} = R_p = \frac{b_a \times b_k}{2.3(b_a + b_k) j_{kor}} \quad (2.12)$$

from which corrosion current density can be obtained:

$$j_{kor} = \frac{b_a \times |b_k|}{2.3(b_a + |b_k|)R_p} \quad (2.13)$$

$R_p, \Omega \text{ cm}^2$ , is called **polarization resistance**

As an example, in Fig. 2.35, the Tafel diagram for the corrosion processes, taking that  $E_{cor} = -0,05 \text{ V}$ ,  $j_{cor} = 1 \times 10^{-5} \text{ A cm}^{-2}$ , a  $b_a = b_c = 0,120 \text{ V dek}^{-1}$ . In the inset of the figure the linear polarization region is shown, from which the value of the polarization resistance of  $R_p = 2150 \Omega \text{ cm}^2$  is determined. From Eq. 2.13 the corrosion current density of  $1.2 \times 10^{-5} \text{ A cm}^{-2}$ , is calculated which is practically identical value as determined from the Tafel diagram. Therefore, the polarization resistance is a direct measure of the corrosion rate.

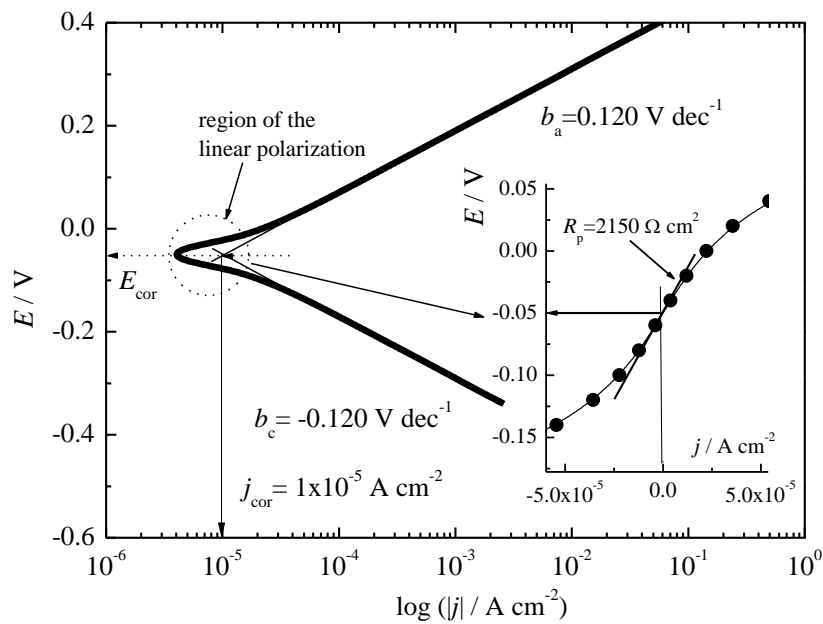


**Figure 2.35.** The determination of the corrosion current density from the linear polarization region [92].

In the case when the cathodic reaction is under diffusion limitation, cathodic current is equal to the limiting diffusion current density,  $j_L$ , and Eq. 2.13 can be divided into:

$$j_{kor} = \frac{b_a \times b_k}{2.3(b_a + b_k)R_p} = \left( \frac{b_a \times \frac{b_k}{b_k}}{2.3\left(\frac{b_a}{b_k} + \frac{b_k}{b_k}\right)R_p} \right)_{b_k \rightarrow \infty} = \frac{b_a}{2.3R_p} \quad (2.14)$$

The procedures of the linear polarization measurement are well elaborated in the ASTM standard ASTM Designation: G 59 – 97 [93].

#### 2.4.3. The 1,10-phenanthroline spectroscopic determination of the iron

The best way for the corrosion determination is a quantitative determination of the corroded iron in the solution. One of the methods is based on the standard test method for iron in trace quantities using the 1,10-phenanthroline method, defined by the ASTM, Designation: E 394 – 00 standards [94].

In this procedure, the amount of iron present in a sample is quantitated by first reacting the iron with 1,10-phenanthroline to form a colored complex and then measuring the amount of light absorbed by this complex. The iron reacts with 1,10-phenanthroline and forms colored complex according to the reaction shown in Fig. 2.36.

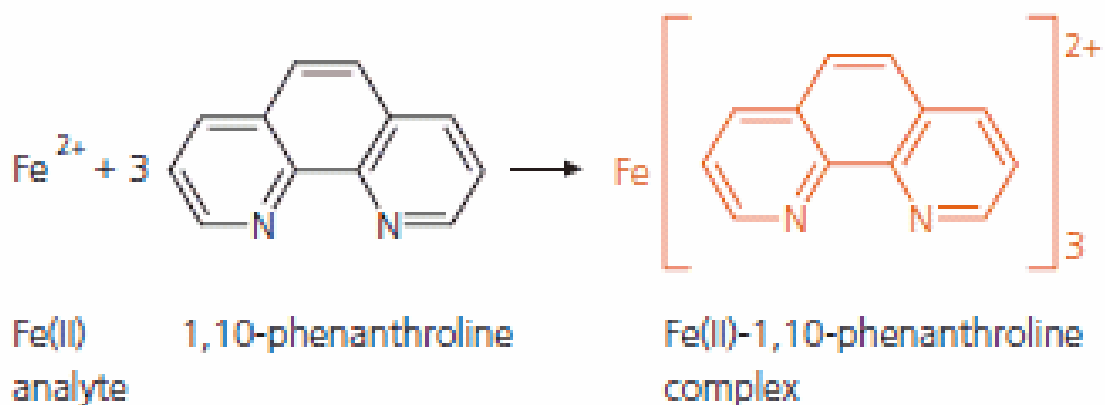
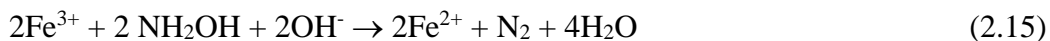


**Figure 2.36.** Reaction of  $\text{Fe}^{2+}$  with 1,10-phenanthroline.

To form a complex, the iron must be first reduced to its ferrous ( $\text{Fe}^{2+}$ ) state, because  $\text{Fe}^{3+}$  does not form a colored complex. This is usually done by reacting the iron with hydroxylamine hydrochloride ( $\text{NH}_2\text{OH HCl}$ ) by the following reaction [95]:



The pH is adjusted to a value between 6 and 9 by addition of an ammonia or sodium acetate buffers. Once a colored complex is formed, the wavelength of light which is most strongly absorbed is found by measuring the absorbance at various wavelengths between 400 - 600 nm. The maximum usually lies at 508 nm as can be seen from Fig. 2.37 [96].

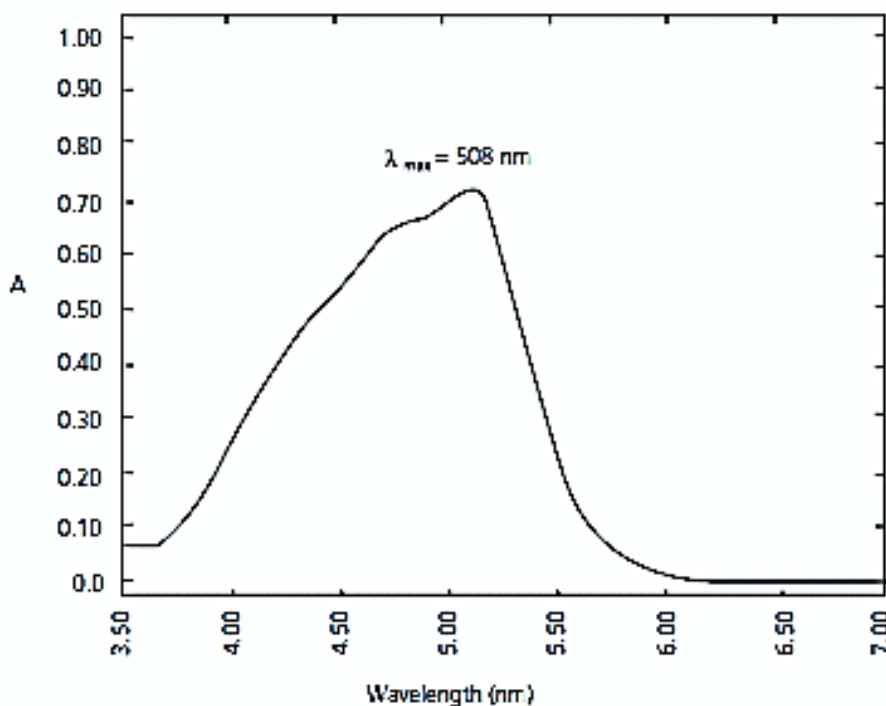


**Figure 2.37.** Absorption spectra of Fe(II)-1,10-phenanthroline complex [96].

After the most suitable wavelength is determined, a series of iron standards is measured at this wavelength and a calibration plot of absorbance vs. concentration is prepared. The absorbance of the unknown sample is measured and the calibration curve is used to calculate the concentration of iron in the sample. As an example, Fig. 2.38 shows the absorption maximum of the iron samples in the concentration range between 1 and 4 mg dm<sup>-3</sup> [96].

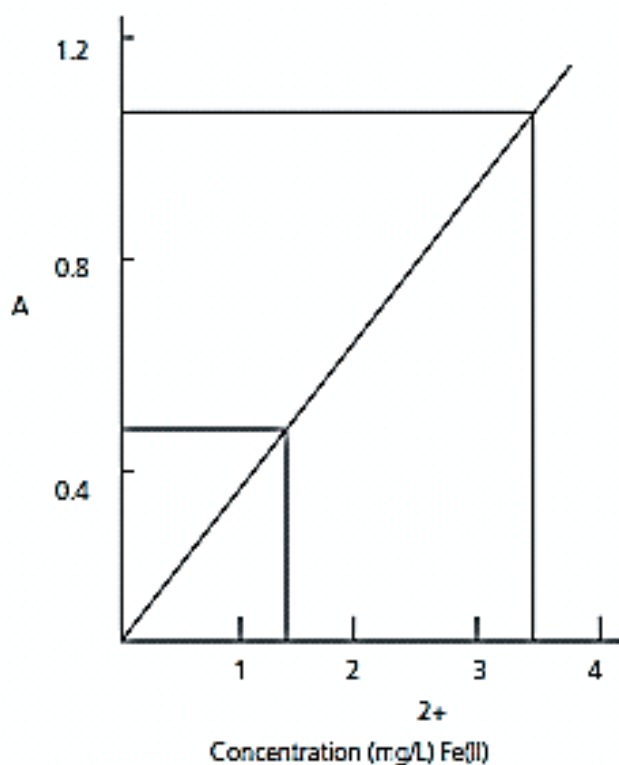


**Figure 2.38.** Standard calibration curve of Fe(II) following derivatization with 1,10-phenanthroline [96].

For the proper unknown iron concentration determination, the calibration curve must be prepared with care. As an example of properly prepared calibration curve, Fig 2.39 shows results obtained by Ülker and Kavano [97] for the iron concentration range from 0.1 ppm to 10 ppm.

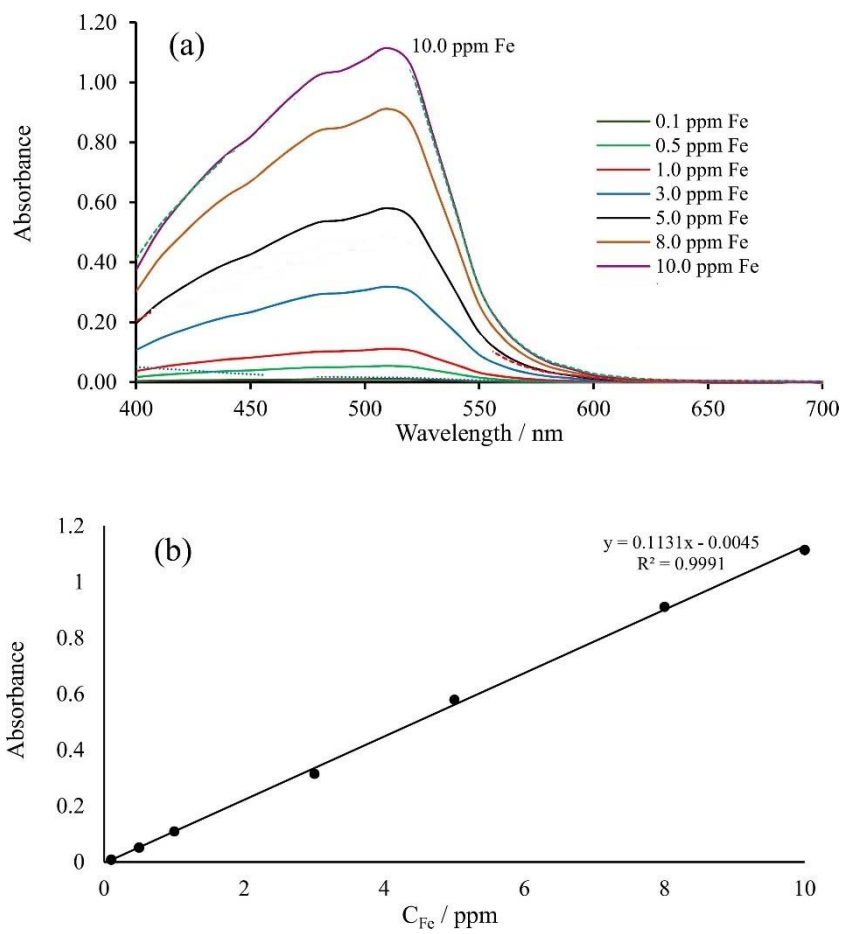


**Figure 2.39.** (a) UV-Vis spectra of standard  $\text{Fe}^{2+}$  solution (b) calibration curve of standard  $\text{Fe}^{2+}$  solution [adopted from Ref. 97].



### 3. EXPERIMENTAL

#### 3.1. Preparation and characterization of the polyaniline powders

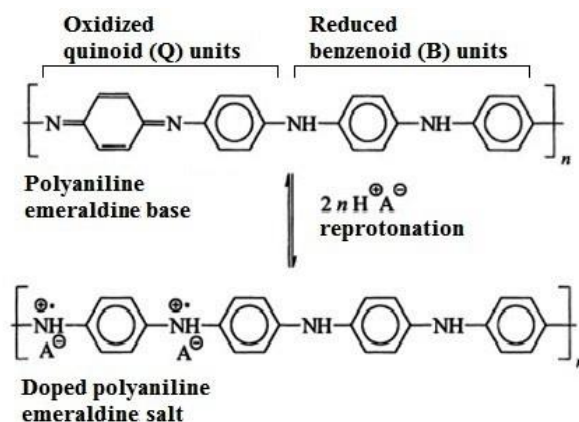
The chemical synthesis of polyaniline is conducted according to the standard IUPAC procedures, recommended by Stejskal et al. [36].

Aniline hydrochloride is prepared by mixing of 0.22 mol HCl (8 g or 26 cm<sup>3</sup> of 37 wt.% HCl, p.a. Merck) with 0.22 mol aniline monomer (20.46 g or 20.8 cm<sup>3</sup>, p.a. Sigma Aldrich, previously distilled under reduced pressure) at room temperature in 500 ml of distilled water. After stirring, 500 ml of 0.22 mol HCl contained 0.275 mol (62.81 g) of (NH<sub>4</sub>)<sub>2</sub>S<sub>2</sub>O<sub>7</sub> is slowly added dropwise. After 24 h of stirring, the green powder is filtered, washed several times with 0.1 M HCl, distilled water, and acetone, and dried overnight. Part of the obtained as synthesized polyaniline powder (ES-IUPAC) is treated with 1 M NH<sub>4</sub>OH for 24 hours to obtain the emeraldine base. The reported electrical conductivity of polyaniline hydrochloride thus prepared is  $4.4 \pm 1.7 \text{ S cm}^{-1}$  (average of 59 samples) and polyaniline base  $3 \times 10^{-9} \text{ S cm}^{-1}$  [57].

For the preparation of previously well characterized polyaniline-benzoate powder [48], the obtained emeraldine base powder (3 g) is treated with 150 cm<sup>3</sup> of 0.1 M benzoic acid ( $pK_a=4.202$ ,  $pH \sim 2.6$ ) for 24 hours at 70°C due to its low solubility at room temperature to produce the polyaniline-benzoate doped emeraldine salt.

For the preparation of composite coatings with polyaniline doped with sulfamic, succinic, citric and acetic acids the following procedure is applied. The obtained emeraldine base (EB-IUPAC) powder is separately treated 24 h with 0.8 M of sulfamic, succinic, citric and acetic acid solutions, to produce the polyaniline in the form of emeraldine salt. In a typical procedure, 2 g of the polyaniline base is added to 100 cm<sup>3</sup>

solutions of corresponding acids. The process of the reprotonation of the polyaniline emeraldine base in salt form is shown in Scheme 3.1.



**Scheme 3.1.** Representation of polyaniline base reprotonation with corresponding acids (HA).

The UV-vis spectra of the polyaniline samples in a powdered form dispersed in the water ( $\sim 15 \text{ mg}/20 \text{ cm}^3$ ) is recorded using a LLG uniSPEC 2 spectrophotometers. The water dispersion of polyaniline is prepared by vigorous sonication during 30 minutes, and precipitation of a larger particle during one hour.

### 3.2. Sample preparations and corrosion investigations

In order to establish the corrosion investigation procedure, as a base coating the commercial TESSAROL<sup>®</sup>-Helios, Slovenia, a primer paint for iron, based on an alkyd binder, with red pigments in the mixture of organic solvents (CAS No: 1174522-20-3, hydrocarbons, C9-C11, n-alkanes, isoalkanes, cyclics, < 2% aromatics, up to 30 wt.%), is used [98]. The composite coating is prepared by the mechanical mixing 10 g of base paint with 5 wt.% of well grinded polyaniline-benzoate powder, 0.335 g based on dry paint, with the particle size between 5 to 10  $\mu\text{m}$ , determined by an optical microscope. The base primer paint and composite coating are applied using a doctor-blade method on the properly cleaned mild steel (ANSI 1212) in the shape of cylinders inserted in a plastic holder (to avoid edge effect) on the free circle side ( $2 \text{ cm}^2$ ) of the sample. The image of

the sample holder, which is made to simultaneously measure two samples, is shown in Fig. 3.1.

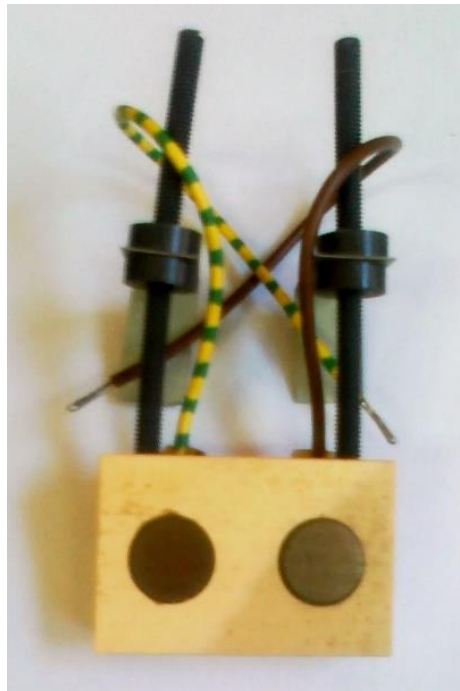


**Figure 3.1.** Image of the samples holder used in the polarization investigations.

After drying in the air for 24 h, the thickness of the coating are  $60 \pm 5 \mu\text{m}$ , measured using Byko-test 4500 FE/NFe (Germany) coating thickness tester, Fig. 3.2.



**Figure 3.2.** Byko-tester 4500 FE/NFe.

The same procedure is applied on two 4 cm × 5 cm mild steel coupons, which backsides and the edges are protected with thick, ~200 μm, an epoxy coating that is separately immersed in 200 cm<sup>3</sup> of 3% NaCl for 10 days.

For the further investigations composite coatings are prepared using the commercial finishing paint for iron, “*Professional emajl lak*”, Nevena Color Xemmax, Serbia, based on an alkyd binder and white pigments in organic solvents, containing 67% of solids (determine by a measure of wet and dry paint). The base paint and base paint modified with 5 wt.% polyaniline emeraldine salts (based on dry paint), after proper mechanical mixing, is applied using a scalpel-blade based method on the properly cleaned AISI 1212 mild steel, in the shape of cylinders inserted in plastic holder to avoid edge effects on the free circle side ( $A = 2 \text{ cm}^2$ ) of the sample. Sample holders, shown in Fig. 3.3, is constructed to simultaneously measure five samples.

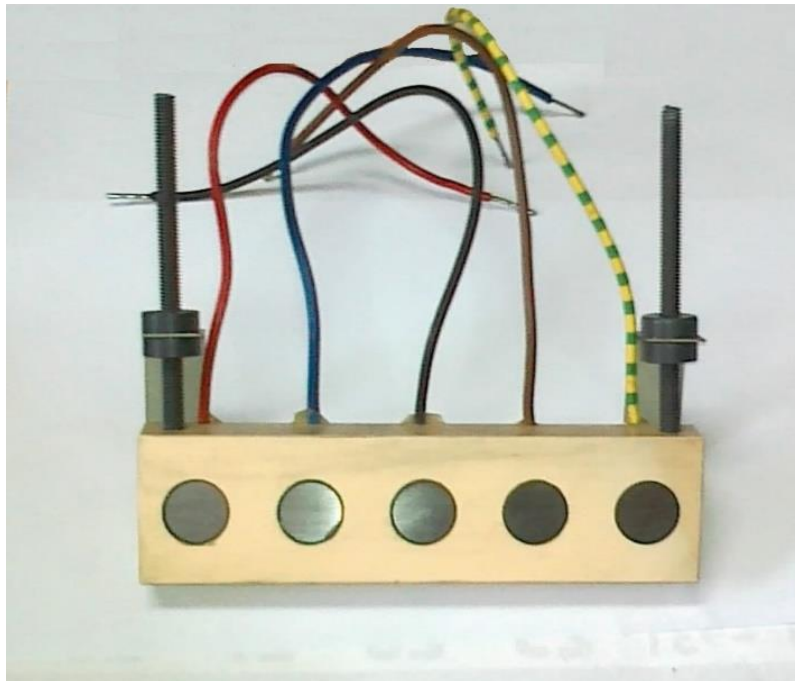


**Figure 3.3.** Image of the sample holder used for the corrosion investigations.

After drying in the air for 24 h, the average coating thickness is  $40 \pm 2 \text{ μm}$ , measured using Byko-test 4500 FE/NFe (Germany) coating thickness tester. Qualitative investigations of the coatings are also performed. In that manner the base and composite coatings are painted on well-cleaned mild steel samples, 5 cm × 4.5 cm, using roller brushes, which back side and the edges are protected with thick ~200 μm epoxy based

paint. The average coating thickness of  $d \sim 25 \pm 5 \mu\text{m}$  is measured. The samples are separately dipped in a  $200 \text{ cm}^3$  of 3% NaCl solution. The quality of the coatings is visually compared after 150 h of immersion, and the images are taken with a digital camera. Optical micrographs are obtained with an optical microscope Olympus CX41 connected to the personal computer.

The corrosion of the samples, using sample holders shown in Figs. 3.1 and 3.2, are investigated in 3% NaCl over time applying the ASTM International recommended linear polarization method for determination of the polarization resistance,  $R_p$  [93] from the polarization measurements, using Gamry PC3 potentiostat controlled by a computer. The rectangular glass cell with volume  $1 \text{ dm}^3$  is used. The stainless steel series 304 counter electrode ( $4 \text{ cm} \times 16 \text{ cm}$ ) and saturated calomel electrode as reference are used.

The corrosion of mild steel is investigated using the similar holder, but with one electrode.

### **3.3. 1,10-phenanthroline standard method for iron concentration determination**

The rate of the corrosion of  $4 \text{ cm} \times 5 \text{ cm}$  mild steel samples with base and composite coatings, as a concentration of iron in  $200 \text{ cm}^3$  of 3% NaCl solution, are determined after 10 days of corrosion using the slightly modified ASTM International 1,10-phenanthroline standard method [94]. In a typical procedure, after 10 days of corrosion, samples are taken from corrosion media (and if indicated transferred to the pure 3% NaCl solution for the extended corrosion testing), and  $10 \text{ cm}^3$  concentrated HCl acid is added to dissolve eventually present insoluble corrosion products. The  $10 \text{ cm}^3$  of stack solutions is transferred to  $100 \text{ cm}^3$  volumetric flask. Then  $1 \text{ cm}^3$  of the hydroxylamine solution ( $100 \text{ g dm}^{-3}$ ),  $10 \text{ cm}^3$  of the 1,10-phenanthroline solution ( $1 \text{ g dm}^{-3}$ ) and  $8 \text{ cm}^3$  of the sodium acetate solution (1.2 M) is added, respectively. For the preparation of the iron standard solutions, the ferrous ammonium sulfate hexahydrate,  $(\text{NH}_4)_2(\text{SO}_4)_2 \times 6\text{H}_2\text{O}$  (Aldrich, p.a.) is used. The concentrations are determined measuring the UV-visible absorbance at 508 nm of standard and investigated solutions, using a LLG uniSPEC 2 spectrophotometers, Fig. 3.4.



**Figure 3.4.** Photograph of the LLG uniSPEC 2 spectrophotometer.

The quality of the coatings after corrosion are investigated using optical microscopy, and optical micrographs are obtained with an optical microscope Olympus CX41 connected to a personal computer, Fig. 3.5.

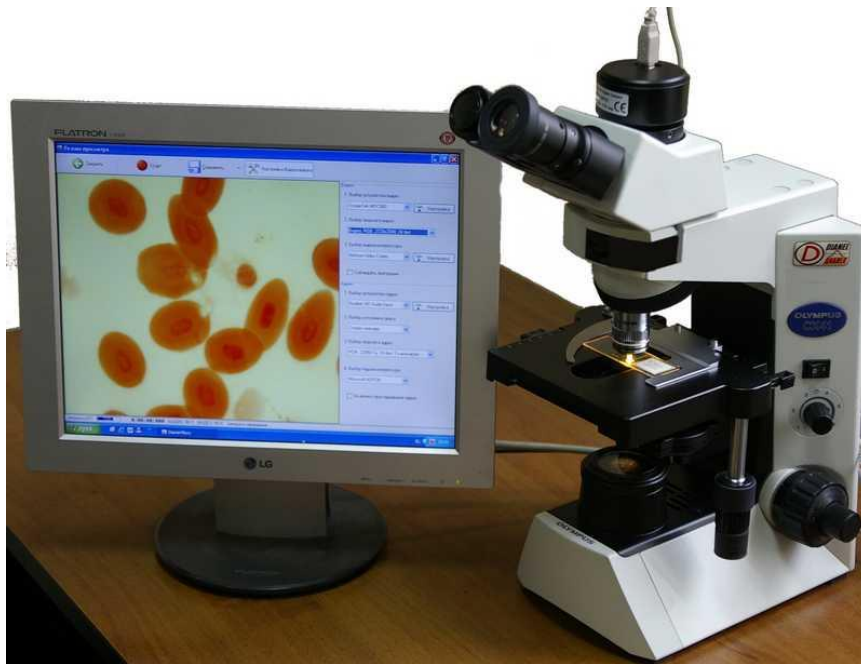


**Figure 3.5.** Olympus CX41 microscope connected to a personal computer

## 4. RESULTS AND DISCUSSION

### 4.1. Characterization of the polyaniline-benzoate powder

The UV-visible spectra of different PANI samples dispersed in water from 190 to 1100 nm are shown in Fig. 4.1. For as synthesized polyaniline in the emeraldine salt form (ES-IUPAC; doping degree:  $y = 0.5$ ) the absorption peak at  $\sim 350$  nm is assigned to the  $\pi-\pi^*$  transition within the benzenoid ring (B), peak at  $\sim 462$  nm could be assigned to polaron -  $\pi^*$  transition within doped quinoid (Q) structure [99], followed by broad tail associated with polaronic structures. The spectra of the polyaniline in emeraldine base form (EB-IUPAC) among peak at 350 nm, has a strong peak at  $\sim 700$  nm, which is attributed to the molecular excitation associated with the quinoid-imine structure [100]. The ratio of the absorption at 350 nm and at 700 nm, is equal to one, suggesting the same numbers of Q and B repeated units in the polymer chain, or pure half oxidized emeraldine structure.

The strong sharp peak at 273 nm of the chemically doped (reprotonated) sample corresponds to the absorption of benzoic acid, which absorption spectra are also shown in Fig. 4.1, and is ascribed to the  $\pi-\pi^*$  transition in the benzoates, suggesting successful doping of emeraldine base. The strong peak at 350 nm is generated by the  $\pi-\pi^*$  transition in the PANI chains. Broadtail above  $\sim 500$  nm is associated with polaronic structures in the polyaniline [99, 100]. The appearance of the absorption at 462 nm, is associated with the doping of the quinoid (Q) structures with benzoate anions.

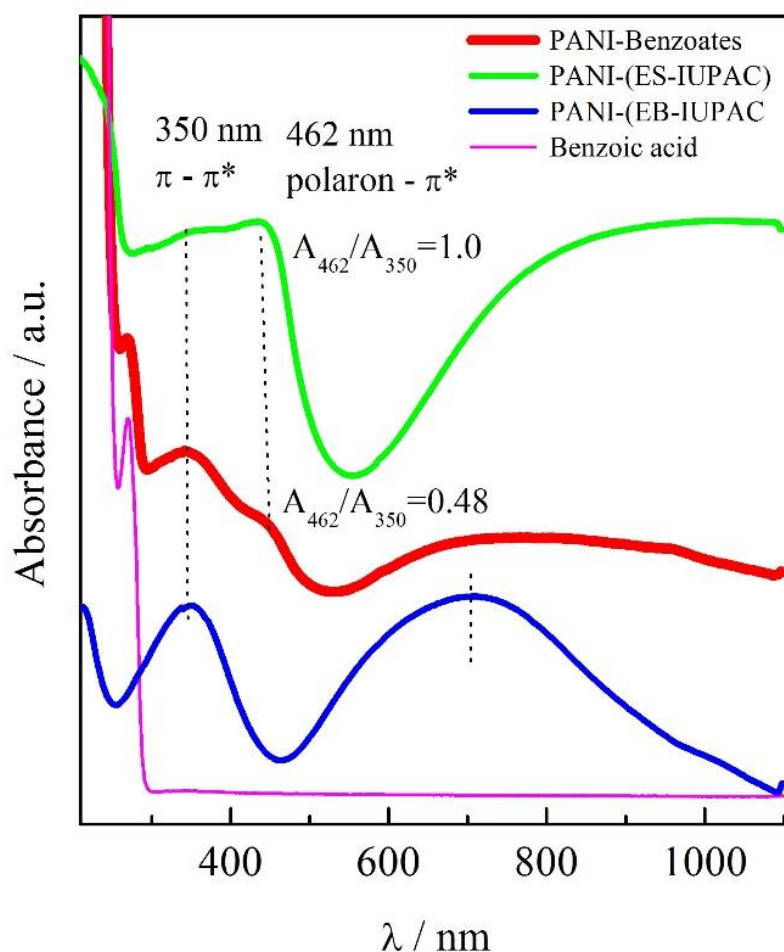


**Figure 4.1.** The UV-vis spectra of the PANI samples ultrasonically dispersed in distilled water ( $15 \text{ mg}/20 \text{ cm}^3$ ).

According to the UV-visible spectra, shown in Fig. 4.1, it can be concluded that interconversion of polyaniline emeraldine base to emeraldine salt according to the scheme shown in Fig. 4.2 is successful. However, from the ratio of  $A_{462}/A_{350}$  peaks, marked in Fig. 4.1, which for the as synthesized sample is equal to one, it could be also concluded that benzoate doped polymer has a lower oxidation state than as synthesized polyaniline. Assuming that doping degree (number of anions per polymer units) of as synthesized sample is  $y = 0.5$ , two anions per four monomer units, the doping degree of benzoate doped polyaniline is estimated to  $\sim 0.24$  or only one anions per four monomer units.



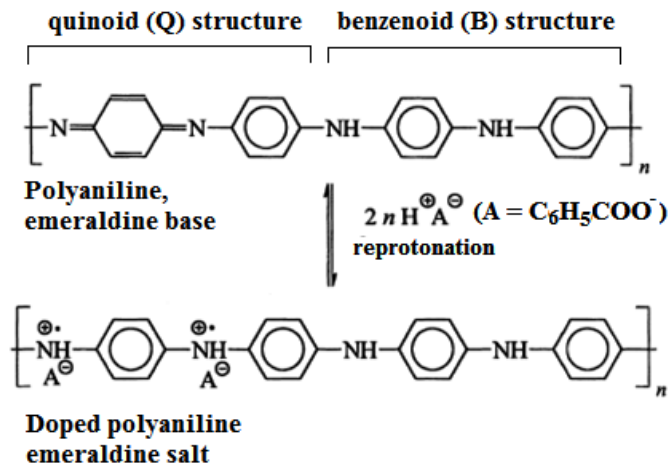


**Figure 4.2.** Schematic presentation of the reprotoation of the polyaniline emeraldine base to emeraldine salt with a benzoic acid.

#### 4.1.1. Corrosion investigations

Mild steel corrode in the saline solutions under the diffusion controlled oxygen reduction reaction, as can be seen in Fig. 4.3, according to the equation:



as the cathodic reaction, while the anodic reaction is dissolution of the iron:



From Fig. 4.3, can be also seen that anodic part of the polarization curve is characterized with two Tafel slopes,  $b$ , of  $78 \text{ mV dec}^{-1}$  at low current density region, and  $135 \text{ mV dec}^{-1}$  at high current density region. From intercept of Tafel slope from low current density region on the corrosion potential of  $-0.642 \text{ V}$ , the corrosion current density of  $12 \mu\text{A cm}^{-2}$  is obtained. Inset of Fig. 4.3 shows the polarization in the linear region, where slopes of  $E = f(j)$  represents polarization resistance:

$$R_p = \left( \frac{\partial E}{\partial j} \right)_{\eta < \pm 20 \text{ mV}} \quad (4.3)$$

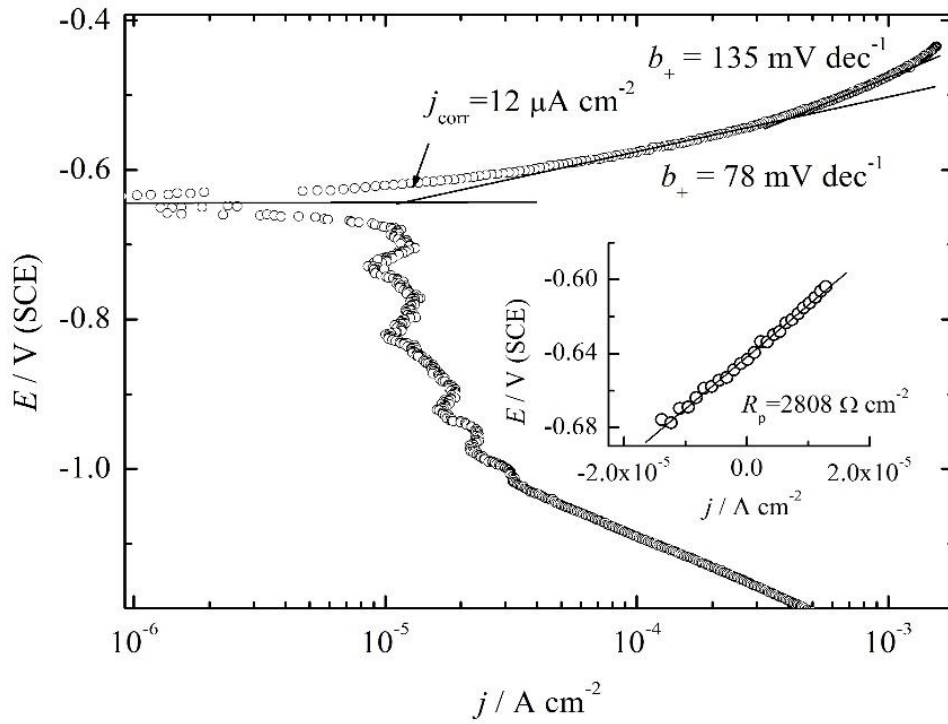


**Figure 4.3.** Polarization curve ( $\nu = 1 \text{ mV s}^{-1}$ ) of mild steel in the aerated 3% NaCl. Inset: the linear polarization region and determination of the polarization resistance  $R_p$ .

The corrosion current density can be obtained from determined  $R_p$  using the Stern-Geary equation:

$$j_{corr} = \frac{b_+ b_-}{2.3(b_+ + b_-)R_p} \quad (4.4)$$

or in the case of diffusion limitations when  $b_- \rightarrow \infty$ , of the cathodic reaction:

$$j_{corr} = \frac{b_+}{2.3R_p} \quad (4.5)$$

For the determined  $R_p$  of  $2808 \Omega \text{ cm}^2$ , inset in Fig. 4.3, corresponding calculated current density, Eq. 4.5, is  $12.1 \mu\text{A cm}^{-2}$ , which is an identical value as obtained from the Tafel extrapolation.

Using the same approach, the polarization measurements over the immersion times in 3% NaCl are performed on the samples covered with base and composite coating. In Fig. 4.4a some of the measured polarization curves of the investigated samples in the form of Tafel plots for better visibility,  $\sim \pm 50 \text{ mV}$  around the corrosion potential during few characteristics times are shown. Fig. 4.4b shows as an example, linear polarization lines from which the polarization resistance is determined after 24 h of immersion in 3% NaCl. The same analysis is applied for all measured polarization curves over the times. From Fig. 4.4a, can be seen that composite coating possess more positive corrosion potential and lower ranges of corrosion current densities than a base coating. The deterioration of the base coating characteristic is observed after ten days, while the composite coating last for twenty-five days.

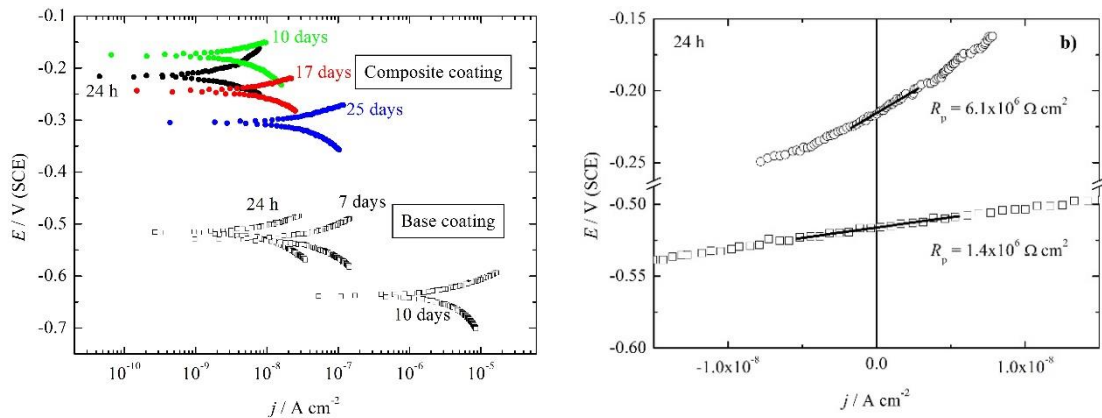


**Figure 4.4.** a) Representative polarization curves ( $v = 1 \text{ mV s}^{-1}$ ) of investigated samples over time in 3% NaCl. b) Examples of the polarization resistance,  $R_p$ , determination from the linear polarization lines after 24 h of immersion in 3% NaCl; ( $\square$ ) base coating, and ( $\circ$ ) composite coating with 5 wt.% of polyaniline-benzoate powder.

In Fig. 4.5 the dependence of the determined polarization resistance for all measured times of the investigated samples are shown. For the comparison the determined polarization resistance ( $\sim 3 \times 10^3 \Omega \text{ cm}^2$ ) of mild steel during five days are also shown.

During first two days of immersion base coatings show a decrease of the polarization resistance from  $3 \times 10^6 \Omega \text{ cm}^2$  to  $\sim 3 \times 10^5 \Omega \text{ cm}^2$  as a consequence of the electrolyte uptake, followed by a plateau over next eight days. This period can be assigned to the macropores development and penetration of the electrolyte in the coating connected with good protection performances [101]. After ten days, the electrolyte is in contact with the metal surface in the pores that lead to the loss of adhesion and to delamination of the coating. This is caused by the accumulations of the hydroxyl ions into pores, increases of the pH to the very high values and degradations of the polymer to metal bonds and loss of the adhesion [102]. The composite coatings show much better polarization characteristics. Initially, a small increase of the polarization resistance is observed, followed by a plateau with an order of magnitude higher value than base coating, and retain the value over  $4 \times 10^5 \Omega \text{ cm}^2$  even after 25 days of immersion. In comparison with mild steel, it can be seen that the polarization resistance is more than three order of magnitude higher.

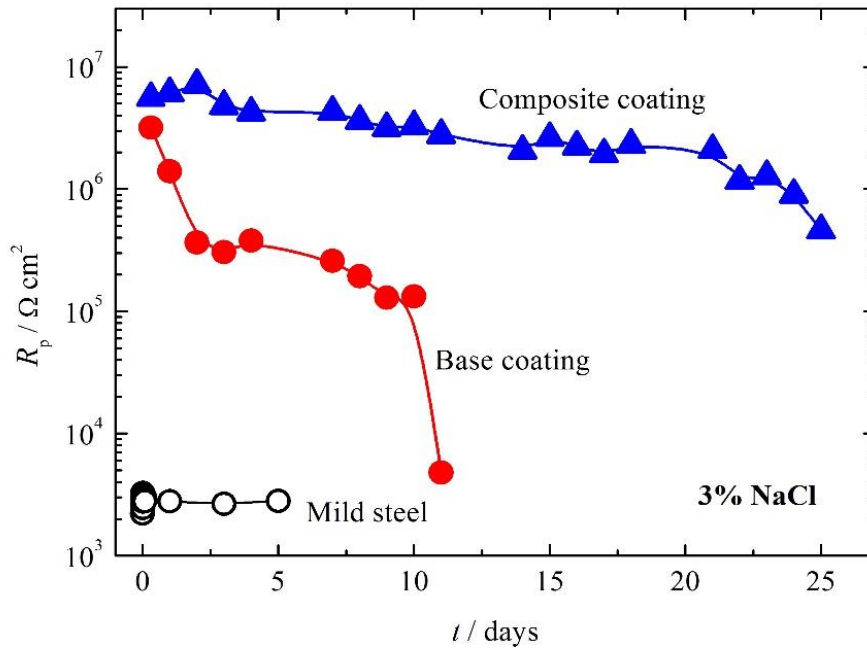


**Figure 4.5.** The dependence of the determined polarization resistance,  $R_p$ , from the polarization measurements over time of the investigated samples.

From the determined values of the polarization resistances, presented in Fig. 4.5, assuming that anodic and cathodic reaction through pores of the coated mild steel are the

same as for the uncoated mild steel sample, the corrosion current density can be estimated using the Eq. 4.5 and the value of the anodic Tafel slope of  $78 \text{ mV dec}^{-1}$ . The calculated values of the corrosion current densities are shown in Fig. 4.6. It is obvious that composite coating has superior characteristics than base coating, and a three order of magnitude lower corrosion current densities than pure mild steel, which is shown for comparisons.

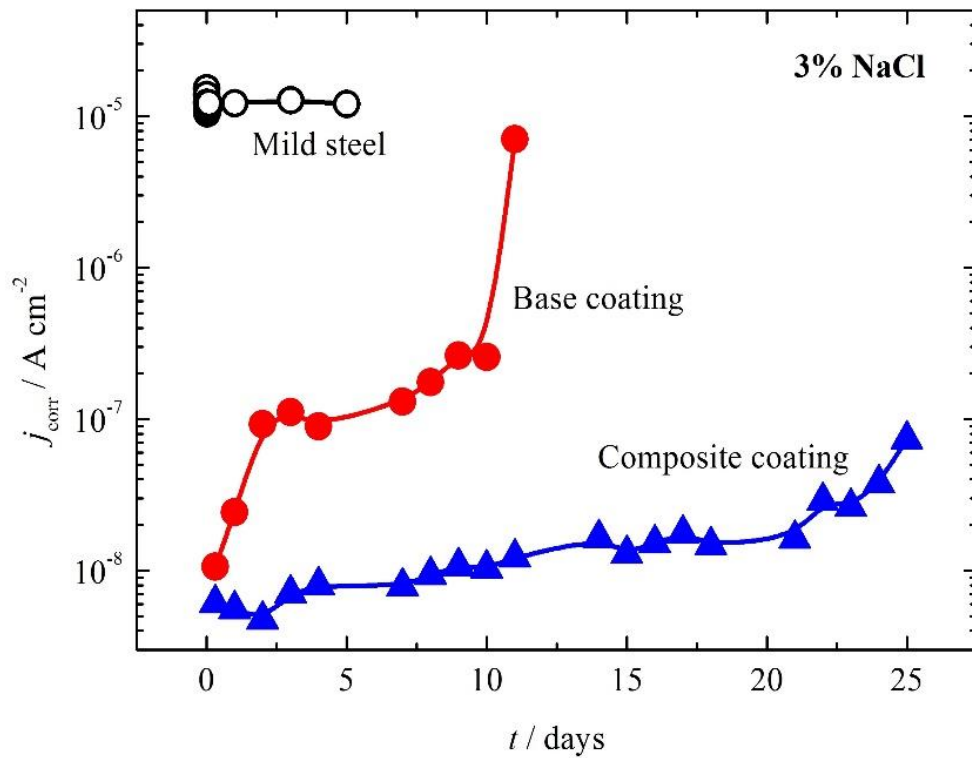


**Figure 4.6.** Estimated corrosion current densities using data from Fig. 4.5 and Eq. 4.5 in 3% NaCl for the investigated samples over time.

The corrosion rate of the higher area samples after ten days of immersion in 3% NaCl is determined using the 1,10-phenanthroline method.

In the inset of Fig. 4.7, the dependence of the absorption on standard iron solutions with different concentrations is shown. The linear dependence of the absorption of standard solutions at 508 nm is in accordance with Lambert–Beer law. The absorption can be given as  $A = 1.68 c(\text{Fe}^{2+})$ , so the iron concentration is  $c(\text{Fe}^{2+}) = A/1.68$ . The absorption maximum for the solution in which base coating corroded is 0.0855, Fig. 4.7, which correspond to 0.051 mg per  $10 \text{ cm}^3$  of the investigated samples or 1.02 mg of iron in  $200 \text{ cm}^3$ . For the solution in which composite coating corroded the absorption

maximum is 0.014, corresponding to 0.167 mg per 200 cm<sup>3</sup> of the solution. Using the Faraday law in the form:

$$j_{\text{corr}} = \frac{I_{\text{corr}}}{A} = \frac{c(\text{Fe}^{2+}) \times n \times F}{t \times M(\text{Fe})} \quad (4.6)$$

where,  $A$  is the surface area of the samples, 20 cm<sup>2</sup>,  $c(\text{Fe}^{2+})$  is mass of iron in grams (per 200 cm<sup>3</sup>),  $F$  is Faraday constant (26.8 Ah mol<sup>-1</sup>) and  $t$  immersion time in hours, the corrosion current density of  $2 \times 10^{-7}$  A cm<sup>-2</sup> for the base coating, and  $3.3 \times 10^{-8}$  A cm<sup>-2</sup> for the composite coating are determined. Very similar value of  $2.7 \times 10^{-7}$  A cm<sup>-2</sup> for the base coating, and  $1.1 \times 10^{-8}$  A cm<sup>-2</sup> for the composite coating are obtained using the linear polarization method (compare the data in Fig. 4.6, after ten days).

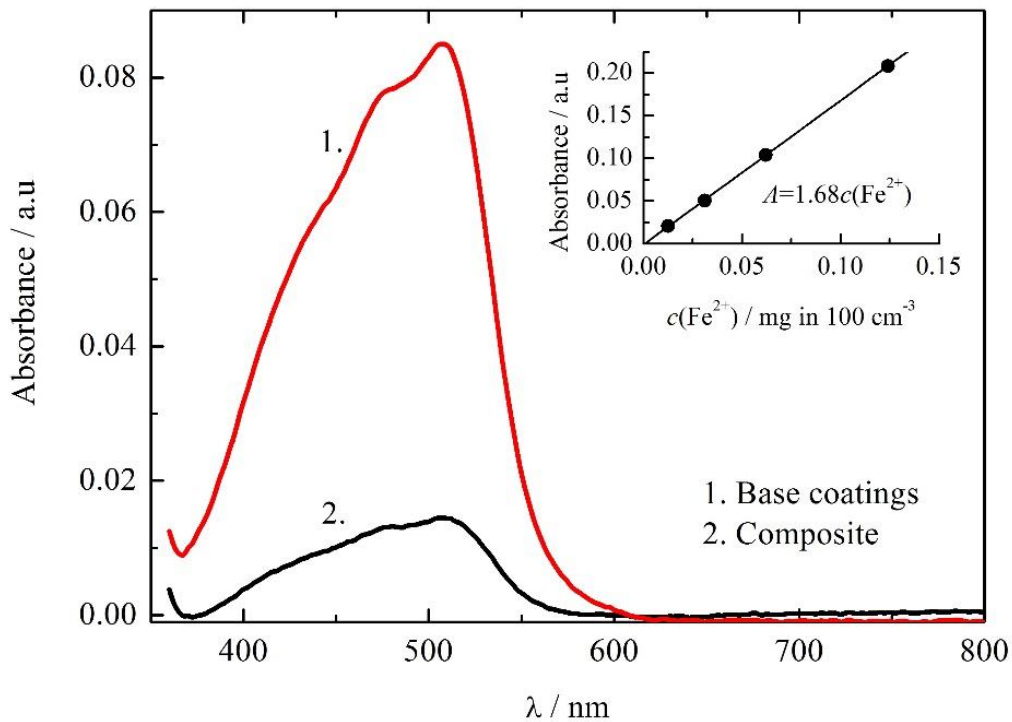


**Figure 4.7.** UV-visible spectra of the corrosion media samples after ten days of corrosion. Inset: Absorption at 508 nm of standard iron solutions.

The base and composite coating containing 5 wt.% of polyaniline benzoate are also investigated with an optical microscope after ten days of immersion in a 3% NaCl solution. A micrograph image of the samples after the corrosion test is shown in Fig. 9. The base coating corroded and forms blisters and large delamination areas. However, the base coating with 5 wt.% of polyaniline-benzoate remained practically unchanged, showing the superior anticorrosion characteristics.

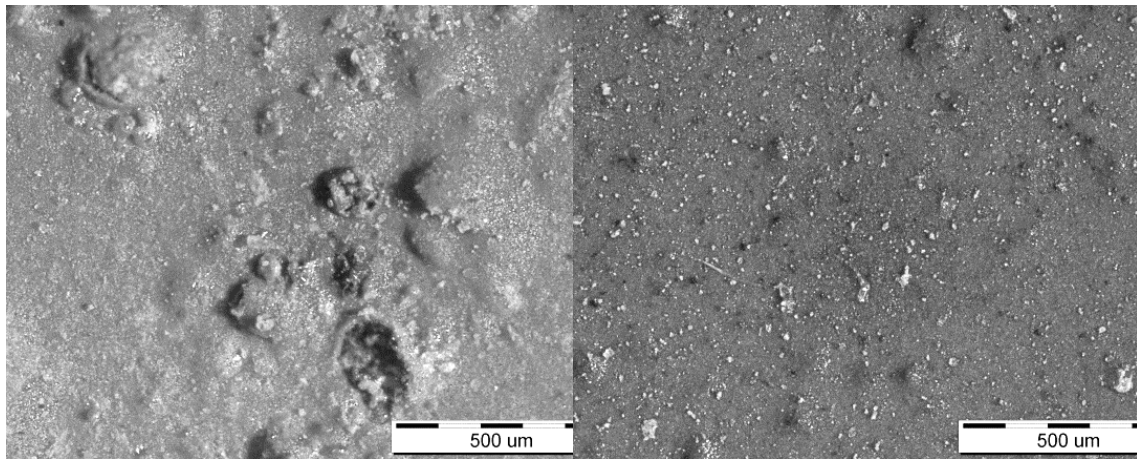


**Figure 4.8.** The micrographs of the samples after ten days of immersion in 3% NaCl. Left: base coating; right: base coating with + 5 wt% PANI-benzoate.

Similar results of the base coatings corrosion stability improvement are obtained by different authors [25, 31, 32, 33, 103, 104, 105, 106, 107], and explained mainly by the ennobling of the mild steel in contacts and interactions with polyaniline [108]. However, as previously explained, delamination of the base coating is initiated by the accumulations of the hydroxyl ions into pores *via* reaction given by Eq. 4.1, and increases of the pH to the very high values. Therefore, we would like to propose an alternative view that the main differences in the improved corrosion performance of the composite coating are in the oxygen reduction reaction mechanism. In comparisons with a base coating, it is possible that in the pores of composite coating oxygen reduction could be mainly via hydrogen peroxide path (two-electron path), on the exposed polyaniline particles, as shown by few authors for some conducting polymers [109, 110, 111, 112]:



Therefore, during this reaction only one hydroxyl ions are released, instead of four, which suppress a high increase in pH into the pores, and prolong delamination effect. This could be an additional effect among well-elaborated ennobling effect [108] in the role of the polyaniline in the corrosion protection of steel.

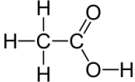
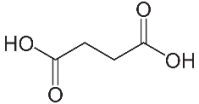
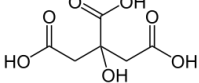
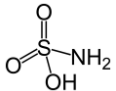


## 4.2. The influence of the initial oxidation state of polyaniline on the corrosion of steel with composite coatings

### 4.2.1. Characterization of the polyaniline powder

In order to investigate does the initial doping degree of the polyaniline have some effect on corrosion of steel with composite coatings, the polyaniline base is doped with acetic, succinic, citric and sulfamic acid. Those acids are chosen due to a high range of doped polyaniline conductivity (which is an indicator of doping degree as reported by Stejskal et al. [57]). Some characteristics data of used acids are summarized in Table 4.1.

**Table 4.1.** The characteristics data of used acids for the reprotonation of the polyaniline.

Acid	Structure	$M_w$ g mol <sup>-1</sup>	pK	$c_{AC}$ mol dm <sup>-3</sup>	pH	$\sigma / S\ cm^{-1}$ [57]
Acetic		60.05	4.76	1	2.6	$7.1 \times 10^{-9}$
Succinic		118.09	$pK_{a1} = 4.2$ $pK_{a2} = 5.6$	0.87 (sat)	2.5	$5.9 \times 10^{-6}$
Citric		192.12	$pK_{a1} = 3.13$ $pK_{a2} = 4.76$	1	1.51	$4.4 \times 10^{-3}$
Sulfamic		97.1	1	1	0.6	0.11

The UV-visible spectra of the different polyaniline samples dispersed in distilled water from 190 to 1100 nm are shown in Fig. 4.9. For as synthesized polyaniline in the emeraldine salt form (ES-IUPAC) the absorption peak at 365 nm is assigned to the  $\pi-\pi^*$  transition within the benzenoid ring (B). The peak at 440 nm could be assigned to polaron -  $\pi^*$  transition within the quinoid structure (Q), followed by a broad tail associated with polaronic structures [99, 100]. The spectra of the deprotonated polyaniline in the

emeraldine base form (EB-IUPAC) among red shifted B peak to ~340 nm, had a strong broad peak centered at ~700 nm, which is attributed to the molecular excitation associated with the quinoid-imine structure [100]. The ratio of absorbance of benzenoid, 365 nm ( $\pi - \pi^*$  transition) to quinoid, 440 nm (polaron-  $\pi^*$  transition) bands can be taken as a measure of the oxidation state in the polyaniline type conducting polymer [89, 113, 114, 115, 116].

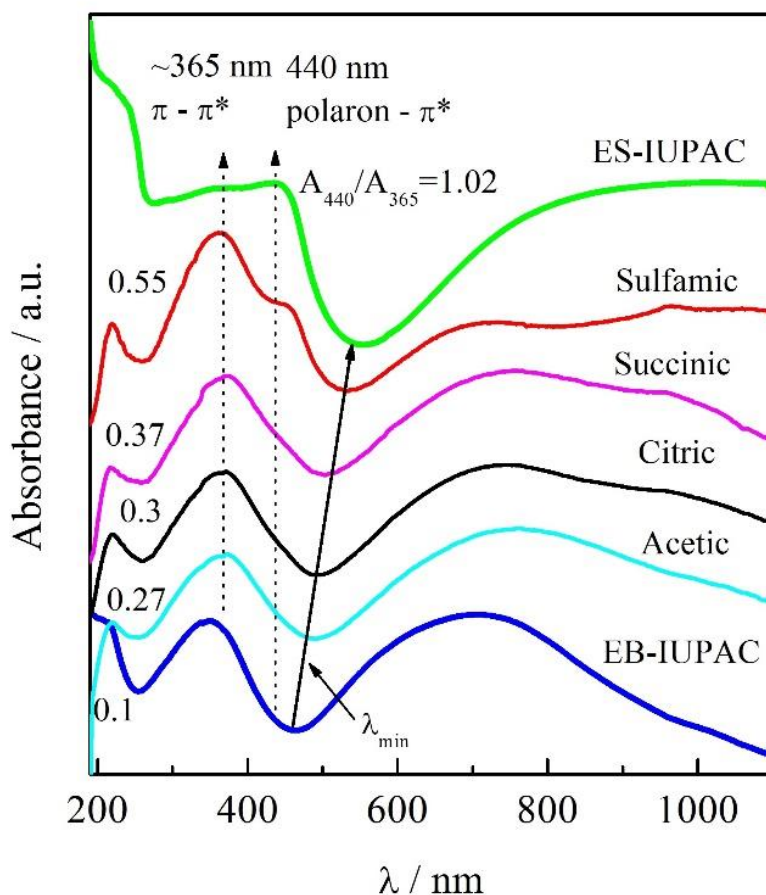


**Figure 4.9.** UV-vis absorption spectra of the polyaniline samples dispersed in distilled water.

For the chemically doped (reprotonated) samples, Fig. 4.9, broad tail above ~500 nm is associated with polaronic structures in the polyaniline [99, 100]. The peaks at ~200-240 nm can be assigned to the absorption of corresponding acids (Fig. 4.10).

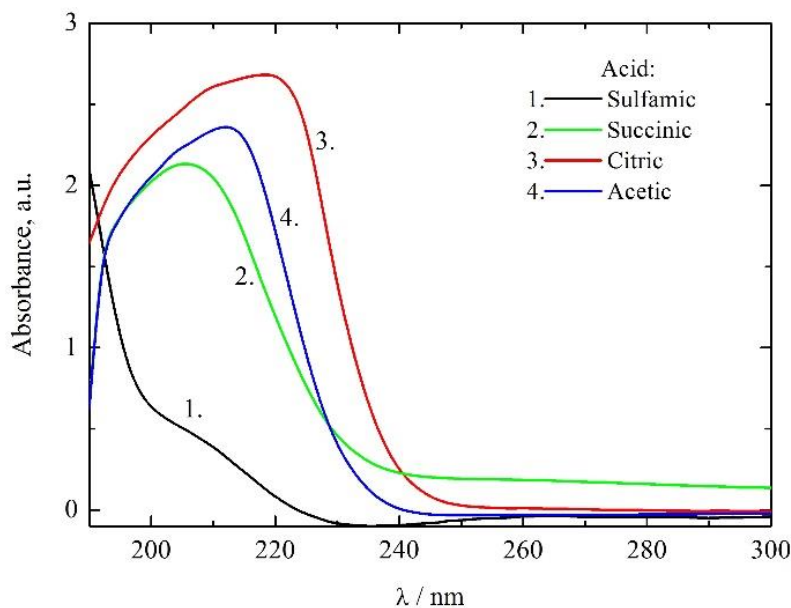


**Figure 4.10.** UV-visible spectra of the acids water solution used for reprotonation of the polyaniline base.

All the reprotonated samples have a peak at 365 nm from  $\pi$ - $\pi^*$  transition, and more or less pronounced absorption at 440 nm from the polaron- $\pi^*$  transition. From Fig. 4.9 can be seen that sulfamic acid doped polyaniline have a peak at 440 nm, polyaniline doped with succinic acid have a shoulder, while samples doped with citric and acetic acids has increased absorption in comparison with emeraldine base form. So, the ration of  $A_{365}/A_{440}$  absorptions could be used as an indicator of the reprotonated polyaniline oxidation level. The absorption  $A_{365}/A_{440}$  ratio of as-synthesized polyaniline emeraldine salt form (ES-IUPAC) sample is 1.02, for sulfamic acid 0.55, for succinic acid 0.37, for citric acid 0.30 and for acetic acid 0.27, as shown in Fig. 4.11. Hereafter, if we assume that as-synthesized sample of the polyaniline (ES-IUPAC) is fully oxidized emeraldine salt with doping degree,  $y$  equal to 0.5, the doping degree of the reprotonated polyaniline could be estimated as  $0.5 \times A_{365}/A_{440}$ . Accordingly, the doping degree, of the polyaniline doped with sulfamic acid is 0.28, with succinic acid 0.18, with citric acid 0.15 and with acetic acid 0.13. It should be also mentioned that minimum absorption,  $\lambda_{\min}$ , in the range of 450 to 500 nm, is shifted to the higher wavelengths by increasing the  $A_{365}/A_{440}$  ratios, as showed by an arrow in Fig 4.9, indicating increased of the polyaniline oxidation level.

The value of  $A_{365}/A_{440}$  ratio practically linearly depends on the minimum absorption as can be seen from the inset in Fig. 4.11.

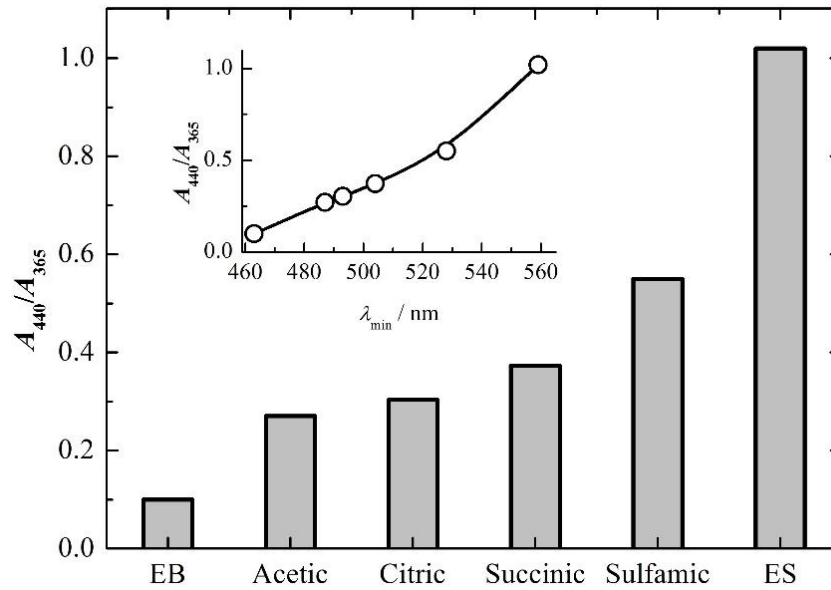


**Figure 4.11.** The ratio of the absorption at 440 nm and 365 nm of the investigated samples. Inset: the dependence of the ratio of absorption,  $A_{440}/A_{365}$ , on the spectra minimum wavelength.

#### 4.2.2. Corrosion behavior

Figures 4.12 a - f. shows the polarization curves  $\pm 50$  mV near the corrosion potential of the investigated samples, obtained in the 3% NaCl solution after 22 h, 44 h, 166 h, 190 h, 324 h and 348 h of exposure. After 22 h of immersion the base coating and composite with acetic acid doped polyaniline, displays similar polarization curves with practically the same corrosion potential of  $\sim -0.48$  V. Samples with sulfamic, succinic and citric acid doped polyaniline establish more positive corrosion potentials, between  $-0.4$  V and  $-0.34$  V. After 166 h, the base coatings practically completely lose the protection characteristics, while all composite coatings samples still possess good protection ability. From Figs. 4.12 it can be seen that corrosion potential of the base coating decrease and for the composite coatings mainly increase from its initial values. In order to determine polarization resistance ( $R_p$ ) of the samples, the polarization curves are analyzed in the region of linear polarization, e.g.  $\sim \pm 10$  mV vs.  $E_{corr}$ . The polarization

resistances are determined as a slope of the linear potential-current density part of the polarization curve, as shown in Fig. 4.13 as an example for  $t = 144$  h. The dependence of the corrosion potentials for all the investigated times of examined samples are shown in Fig. 4.14a.

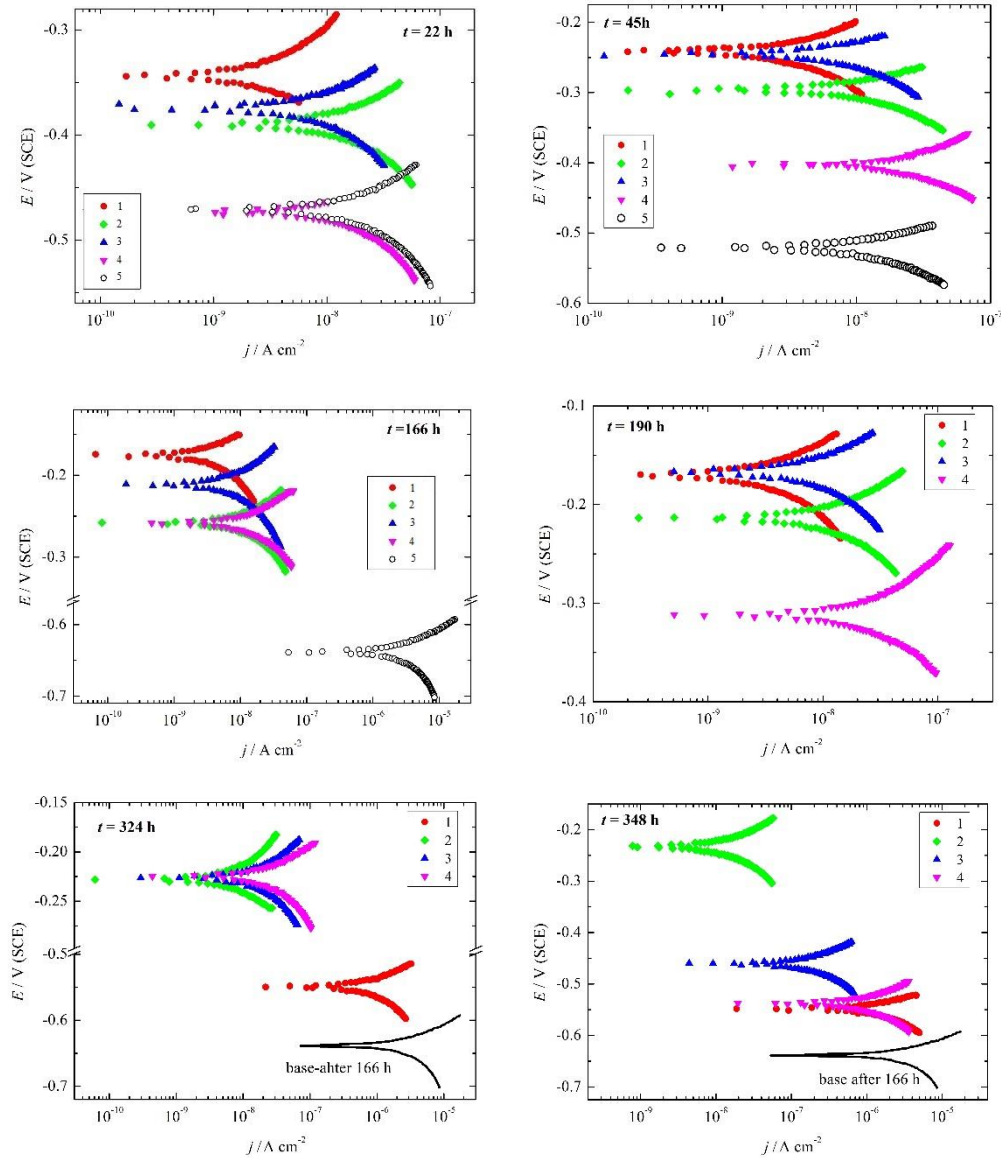


**Figure. 4.12.** Polarization curves,  $v = 1\text{ mV s}^{-1}$ ,  $\pm 50\text{ mV vs. }E_{\text{corr}}$ , of the investigated samples after different times of immersion (marked in the figure) in 3% NaCl. Composite coatings with: 1-sulfamic acid; 2-citric acid; 3-succinic acid and 4-acetic acid doped polyaniline; 5-base coating.

From Fig. 4.14a, can be seen that during the first 50 h of immersion, corrosion potential of the base coating decrease from,  $-0.4\text{ V}$  to  $-0.55\text{ V}$ , followed by a plateau at

-0.55 V over 100 h, and again decrease to -0.65 V after 166 h. On the contrary, samples with composite coatings show the increase of the corrosion potentials during ~70 h, after which remains relatively stable up to 150 h. After that time, some instability of the corrosion potentials is observed, which could be connected with base coating behavior. At 300 h of immersion practically for all the samples, similar values of corrosion potentials of -0.2 V to -0.25 V are observed. After 300 h of immersion, samples gradually decrease in corrosion potentials to the value of ~ -0.55 to -0.6 V. Accordingly, four stages of the corrosion potential values could be separated, as marked in Fig. 4.14a.

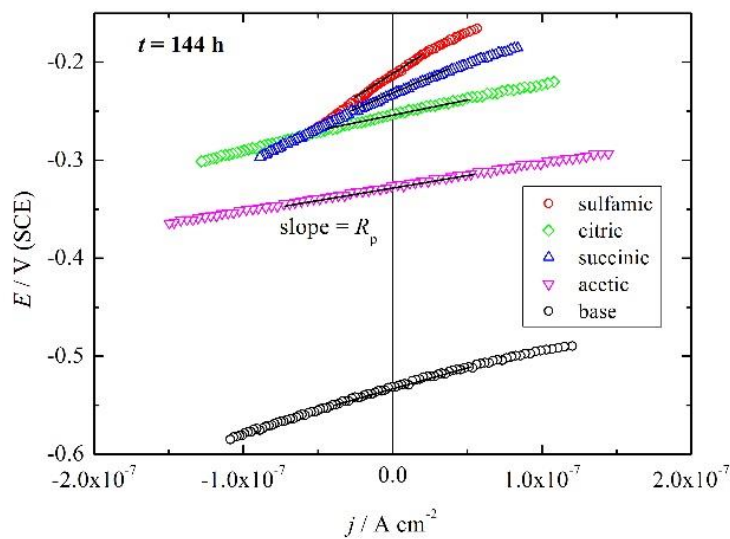


**Figure 4.13.** The dependence of the potential on the current density of the investigated samples in the linear polarization region for  $t = 144$  h.

From the results shown in Fig. 4.14b it can be seen that initially all the samples, after ~4 h of immersion, possess relatively high  $R_p$  values between  $3 \times 10^6 \Omega \text{ cm}^2$  to  $8 \times 10^6 \Omega \text{ cm}^2$ . After 24 h of immersion, except for the sulfamic acid doped polyaniline,  $R_p$  values fall to the relatively stable plateaus over the next ~150 h. Samples with composite coatings with sulfamic acid doped polyaniline initially show the increase of the  $R_p$  values from  $3 \times 10^6 \Omega \text{ cm}^2$  to  $6 \times 10^6 \Omega \text{ cm}^2$ . After 166 h the  $R_p$  of the base coating rapidly falls to the value of  $\sim 3 \times 10^3 \Omega \text{ cm}^2$ , indicating delamination of the coating from the metal base. After the same period of time, the composite coatings show some fluctuations of the  $R_p$ , with the order of values,  $R_p(\text{sulfamic}) 4 \times 10^6 \Omega \text{ cm}^2 > R_p(\text{succinic}) 2 \times 10^6 \Omega \text{ cm}^2 > R_p(\text{citric}) 1 \times 10^6 \Omega \text{ cm}^2 > R_p(\text{acetic}) 0.7 \times 10^6 \Omega \text{ cm}^2$ . The gradual decreases of  $R_p$  values

are observed only after ~300 h. From the Fig. 4.14b can be also seen that samples with acetic acid doped polyaniline, shows similar  $R_p$  values as base coating, but the higher value of  $R_p$  last more than double.

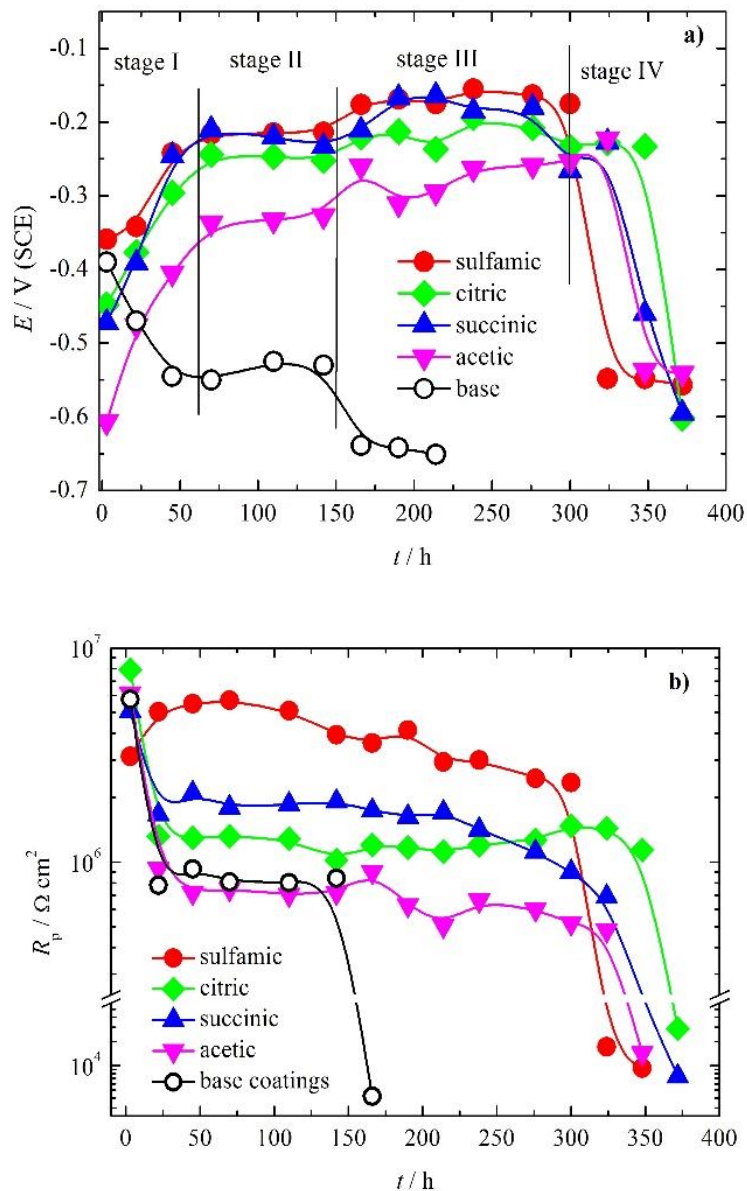


**Figure 4.14.** a) The dependence of the corrosion potentials over time; b) the dependence of the determined polarization resistance over time, for the investigated samples.

Considering the corrosion behavior of the composite coatings, it is obvious that  $R_p$  values can be connected with UV-vis  $A_{365}/A_{440}$  absorption ratios, or with the doping

degree of the polyaniline. Figure 4.15 shows that the sample with sulfamic acid doped polyaniline, possessing the highest doping degree of 0.27, demonstrate the highest  $R_p$  values among investigated samples. The order of the  $R_p$  values are:  $R_p(\text{sulfamic}, y = 0.27) > R_p(\text{succinic}, y = 0.18) > R_p(\text{citric}, y = 0.15) > R_p(\text{acetic}, y = 0.13)$ , and can be connected with the doping degree of the polyaniline given in the brackets.

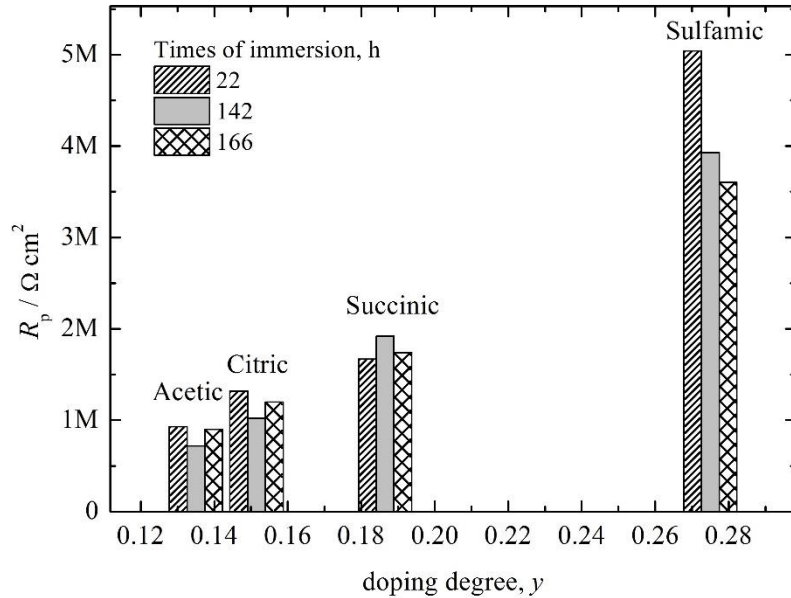


**Figure 4.15.** The dependence of the polarization resistance of the investigated samples on estimated doping degree for different times of immersion.

The order of  $R_p$  values can also be clearly connected with the corrosion product appearance of the investigated samples taken after 238 h of immersion in 3% NaCl, shown in Fig. 4.16. Composite coating with sulfamic acid doped polyaniline practically do not have visible corrosion products, succinic acid doped polyaniline sample shows some traces of corrosion products, while the composite samples with citric and acetic acid doped polyaniline show visible corrosion products. However, in comparison with a base coating, which is practically completely delaminated and covered with corrosion products, it is obvious that all the composite coatings show only traces of the corrosion products, suggesting in principle lower tendency of delamination.



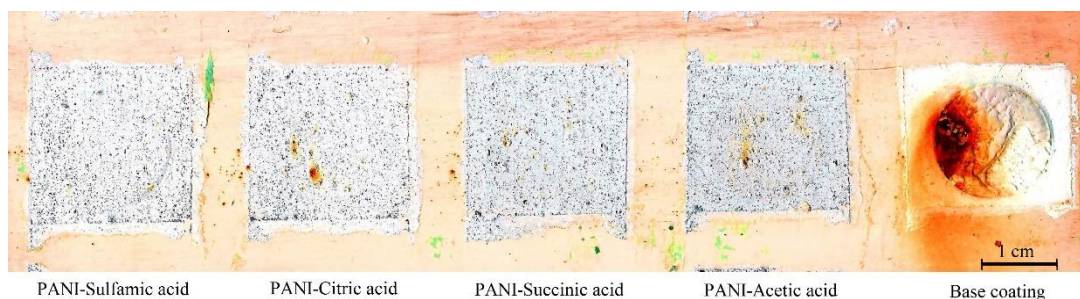


**Figure 4.16.** The images of the investigated samples after 238 h of immersion in 3% NaCl.

Similar observations are made for the higher surface area samples after exposure to 3% NaCl for 150 h, as can be seen from Fig. 4.17.

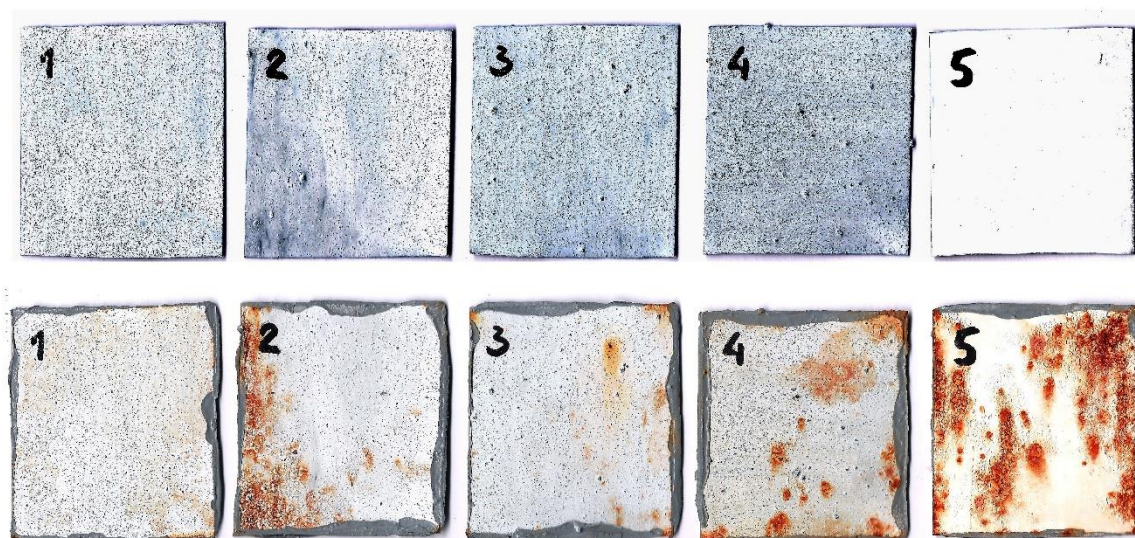


**Figure 4.17.** The images of the samples before (top) and after 150 h of immersion in 3% NaCl (bottom). Composite coatings with: 1-sulfamic acid; 2-citric acid; 3-succinic acid and 4-acetic acid doped polyaniline; 5-base coating.

The composite coating with sulfamic acid doped polyaniline shows some existence of the uniformly distributed corrosion product on the surface, while the appearance of the corrosion products follows the orders; PANI-succinic < PANI-citric < PANI-acetic << base coating. Visual observation clearly demonstrates that appearance of the corrosion products of the composite coatings can be connected with the initial doping

degree of the polyaniline filler. For the comparison, in Fig. 4.18, the images and micrographs of the composite coating with sulfamic acid doped polyaniline and a base coating are shown. The micrograph of composite coating shows the existence of some localized corrosion attack present as cracks of the coating with dimensions up to  $50\ \mu\text{m}$ , while the surface of the base coating, among delaminated parts visible in the image, is practically completely covered with blisters, with average dimensions from  $50\ \mu\text{m}$  to  $200\ \mu\text{m}$ .

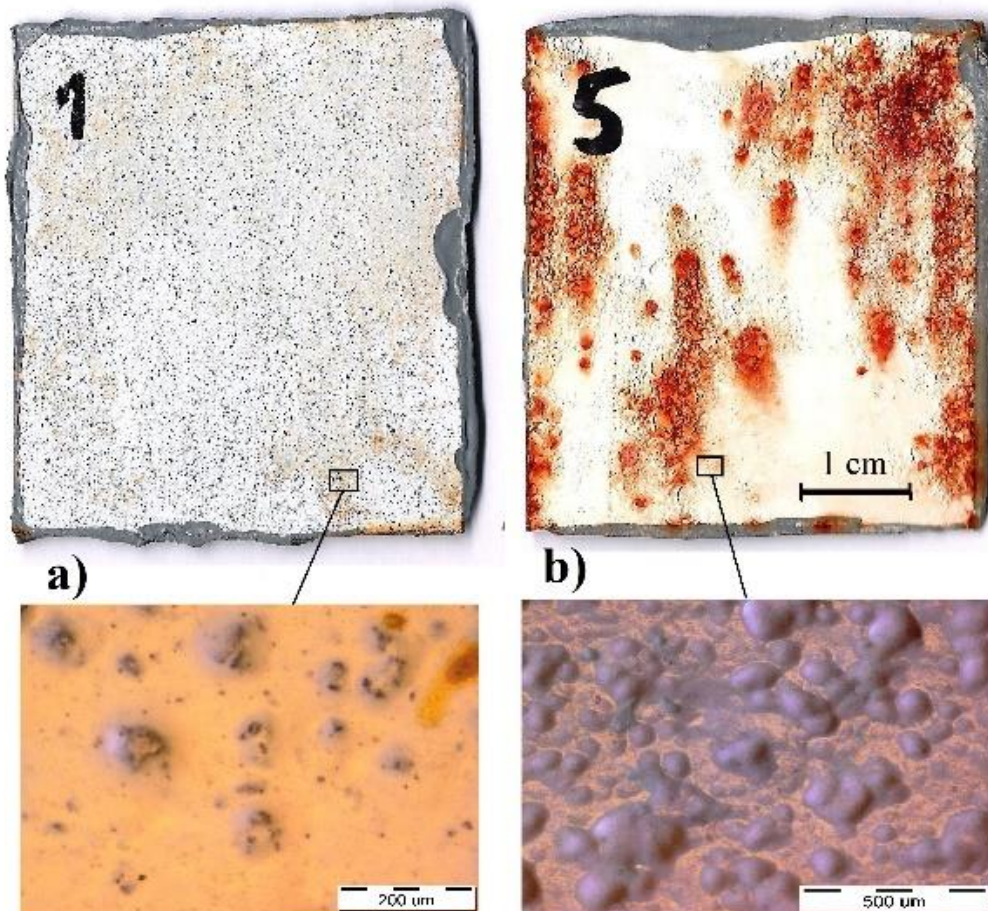


**Figure 4.18.** The images (top) and optical micrographs (bottom) of the a) composite coating with sulfamic acid doped polyaniline and b) base coating after 150 h of immersion in 3% NaCl.

Microphotographs of all investigated samples are shown in Fig.4.19. It is notable that polyaniline particles conglomerates probably due to solvophobicity. For the composite coatings of PANI-doped with sulfamic and succinic only the traces of the corrosion product is visible onto the surface. For the citric and acetic acid doped polyaniline more corrosion product is formed, but in all cases, the blister formations are practically suppressed.

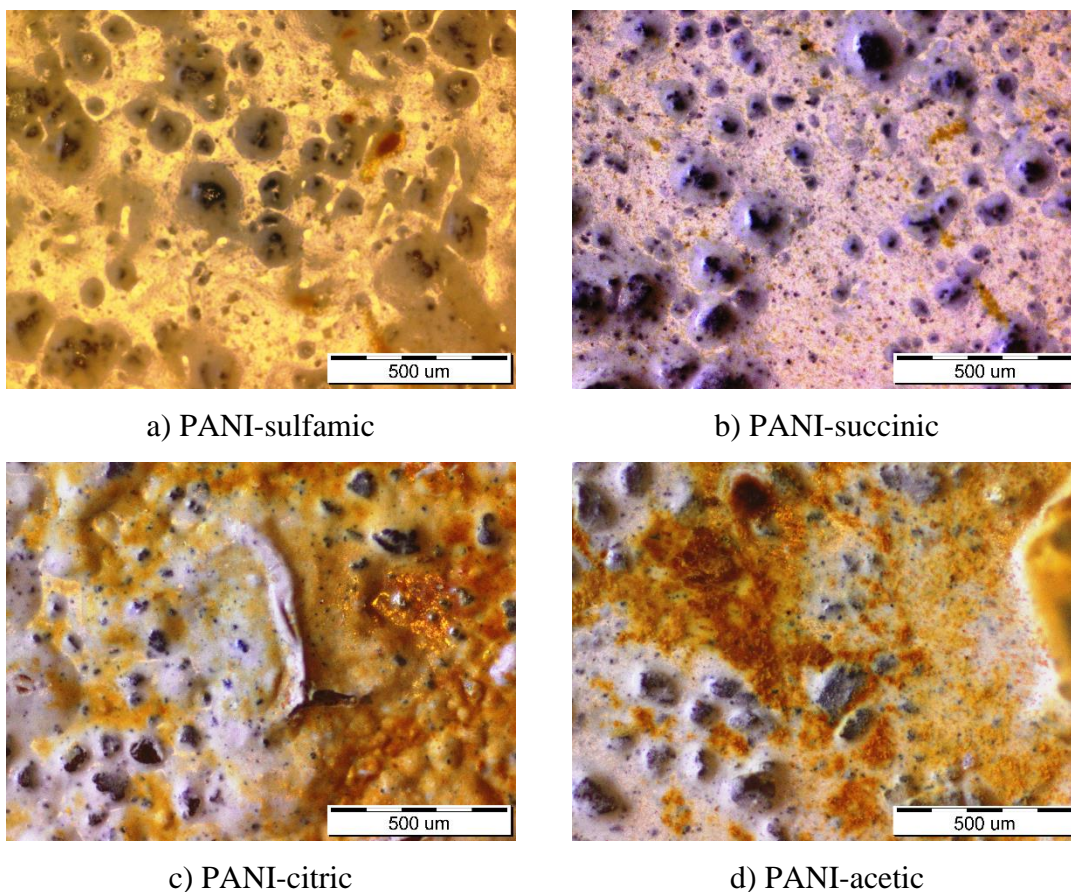


**Figure 4.19.** Microphotographs of the investigated samples after 150 h of the immersion in 3% NaCl.

#### ***4.2.3. The 1,10-phenanthroline spectroscopic determination of the iron corrosion***

In order to quantitatively determine the rate of the samples corrosion, the solution after 96 h of the samples immersion is analyzed by UV-visible spectroscopy using the 1,10-phenanthroline method. as previously described (see pgs. 58-59.). Figure 4.20 shows

the UV-visible spectra of the corresponding solutions. From the inset of Fig. 4.20 it is obvious, that absorption decrease with the same manner as the polarization resistance.

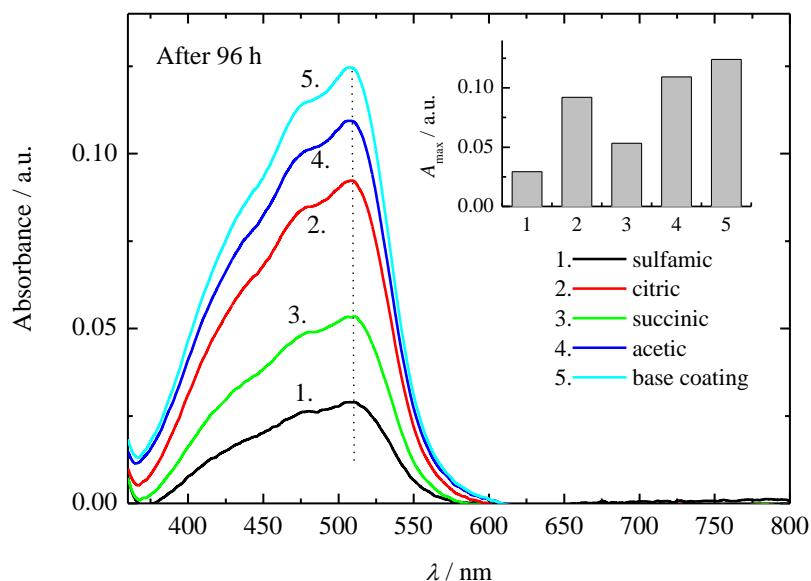


**Figure 4.20.** The UV-visible spectra of the corresponding solutions after 96 h of the samples corrosion. Inset: The maximum absorption maximums of the corresponding samples.

The UV-vis spectra of the standard iron solutions are shown in Fig. 4.21, and calibration curve in the inset of the figure.

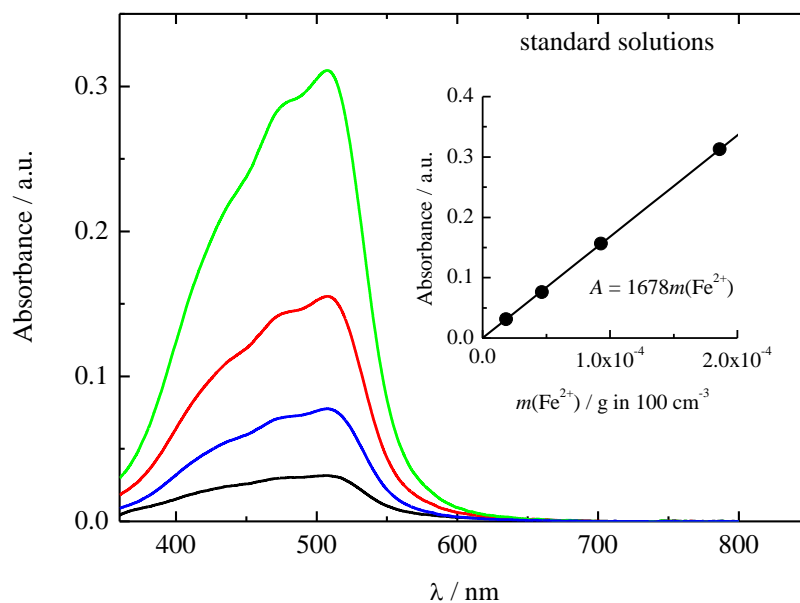


**Figure 4.21.** The UV-vis spectra of the standard iron solutions. Inset: calibration curve.

Using the Eq. 4.6, the corrosion current densities are calculated and shown in Fig. 4.22. It is obvious that average corrosion current density closely follows the initial doping degree of the polyaniline.

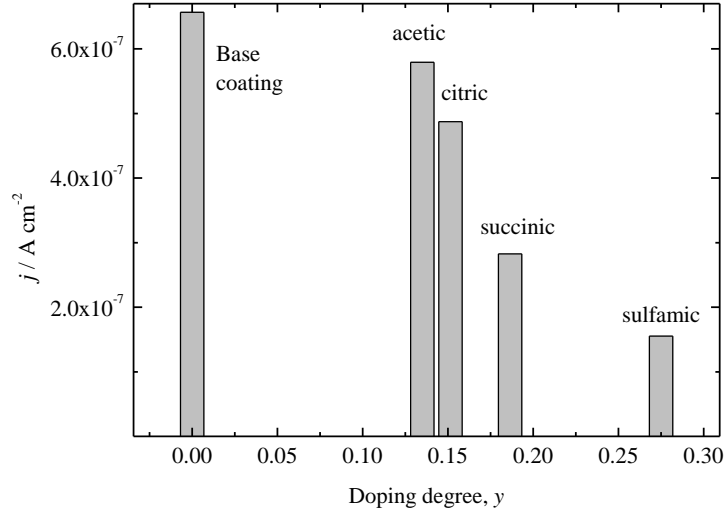


**Figure 4.22.** The calculated corrosion current densities of the samples using the Eq. 4.6.

In the Fig. 4.23 the calculated corrosion protection efficiency (CE) are shown. It can be seen that acetic acid doped polyaniline offers only slight protection, while citric 20%, succinic doped PANI 55%, while sulfamic acid doped PANI 75%.

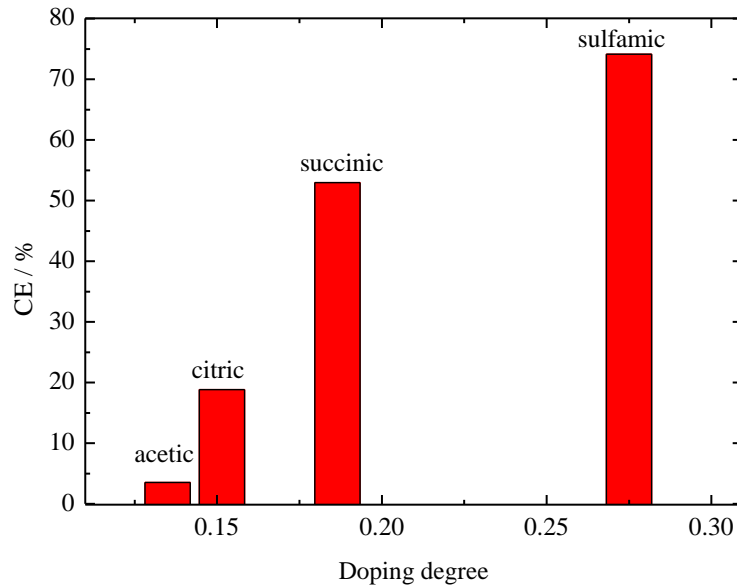


**Figure 4.23.** The calculated corrosion protection efficiency (CE) of the composite coatings in comparisons with the base coating.

To compare results of the in-situ determined corrosion current densities with reciprocal values of the polarization resistance (see Fig. 4.13b,  $R_p$  are estimated from the figure for 96 h). The comparison is shown in Fig. 4.24, from which can be seen that same trend exist, confirming that both methods can be successfully applied in order to investigate corrosion of the composite coatings.

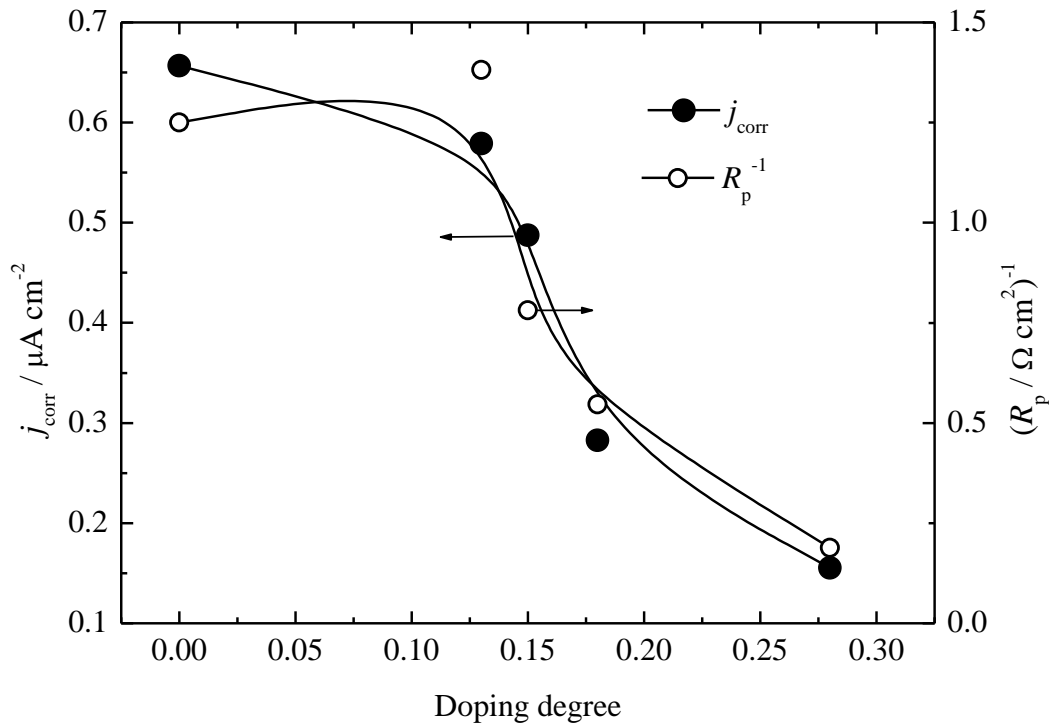


**Figure 4.24.** Comparisons of the results of the in-situ determined corrosion current densities with reciprocal values of the polarization resistance estimated from Fig. 4.13b

Using the ImageJ software [117], the area of the corrosion product of all samples are determined, as shown in Fig. 4.25, and the values are presented in Fig. 4.26. From Fig. 4.26 it is obvious that formation of the rust on the samples surfaces and corrosion current density has the same tendency and closely follows the initial doping degree of used polyaniline.

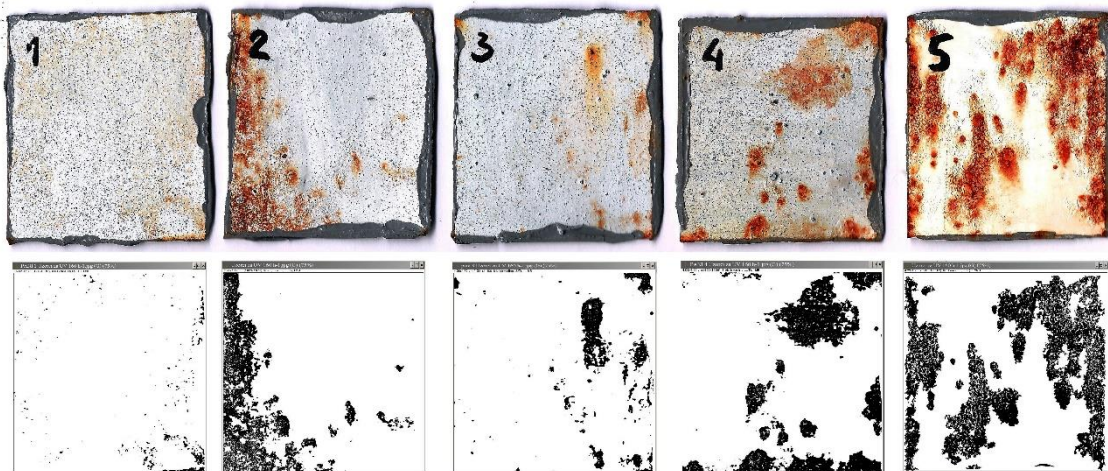


**Figure 4.25.** The estimated corroded area of the samples using ImageJ software.

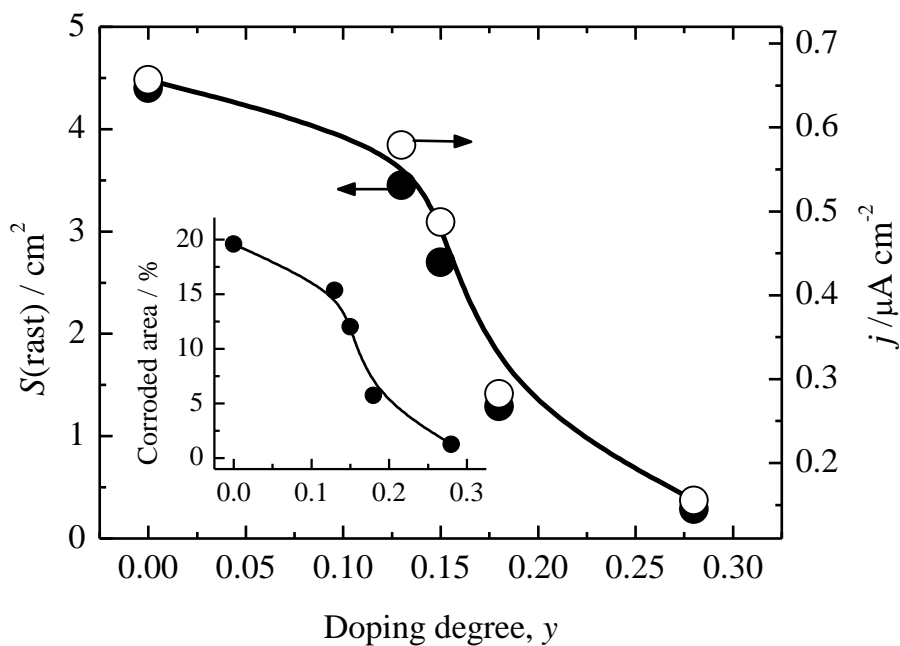


**Figure 4.26.** The dependence of the surface area covered with rust for the sample area of  $20 \text{ cm}^2$ , on doping degree (left), in comparisons with UV-visible determined corrosion current densities (right). Inset: The percentage of rust on the investigated samples.

### 4.3. Possible mechanism of the corrosion behavior

The main mechanisms of the organic coating characteristic deterioration are delamination and blistering [118, 119, 120]. The mechanism of the delamination (as schematically shown in Fig. 4.26a) consists of separated reactions in the coating pores, which develops over time [121], where in the one pore the oxidation of iron, occur:



Released electrons are transferred via metal to the neighboring pore, where the oxygen reduction reaction takes place:



During this reaction four  $\text{OH}^-$  anions are formed, which leads to the increases of pH into the pores to very high values, causing the losses of coating adhesion from a metal base and consequently delamination. During the blister formation, Fig. 4.27b, the oxygen, as well as water and anion, penetrate through the coating, reduce to the hydroxyl anions which with  $\text{Fe}^{2+}$  forms rust (porous iron oxy-hydroxide). The growth of the rust mechanically lifted of coating, producing blisters.

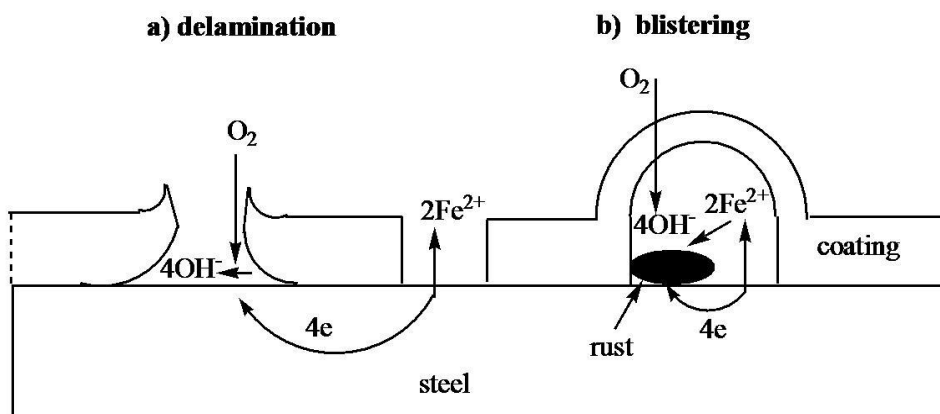


**Figure 4.27.** Schematic representations of the coating delamination (a) and the blister formation (b) in the organic coating.



Among well-elaborated increase of the barrier properties of the composite coatings [25], in which polyaniline particles physically decrease the rate of oxygen and water molecules diffusion through the coatings, we would like to suggest some additional effect that could be involved in corrosion reactions of the composite coatings.

For the composite coatings in the initial period of ~70 h, during the pore development, more polyaniline particles into the pore walls are exposed to the electrolyte. Initially, the anodic reactions can be described by the following equations, and schematically shown in Fig. 4.27:

iron dissolution:



and partial oxidation of some of the polyaniline particles with chloride anions from the electrolyte:



accompanied by the oxygen reduction as cathodic reaction. It should be also mentioned that the possibility of the polyaniline doping with  $\text{OH}^-$  anions could occur as well [122, 123].

That auto-doping reaction of the polyaniline in the interaction with molecular oxygen is possible can be seen in Fig. 4.28, where UV-visible spectra of the polyaniline dispersion doped with acetic acid in 3% NaCl solution open to the air, of the as-synthesized sample and after 24 h are shown. It is noticeable that initial  $A_{440}/A_{365}$  value from 0.26 increase to 0.32, as well an increased absorption of the polaronic tail above 500 nm.

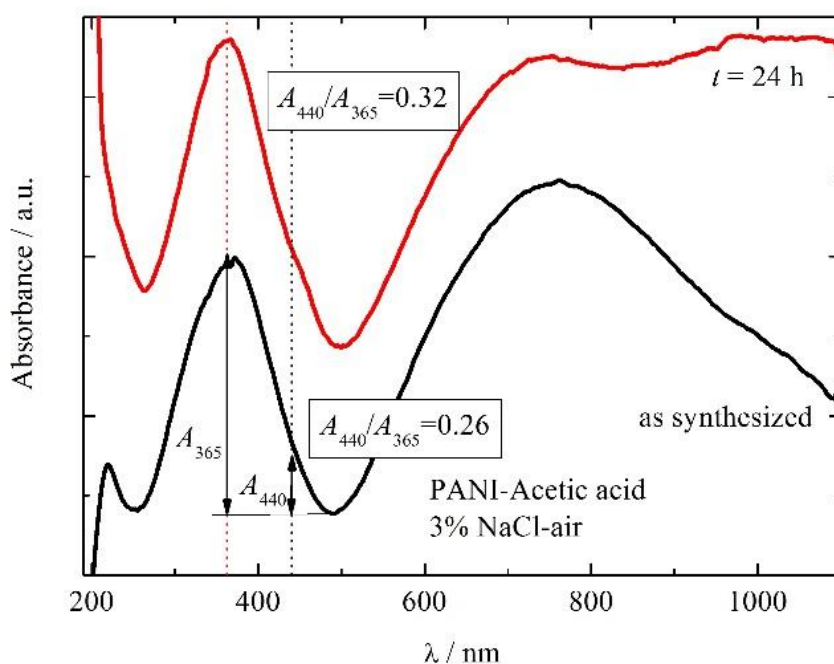
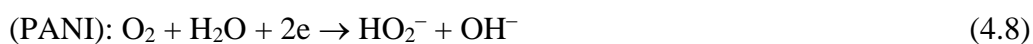


**Figure 4.28.** UV-visible spectra of the polyaniline dispersion doped with acetic acid in 3% NaCl solution open to the air, of the as-synthesized sample and after 24 h of immersion.

Partial oxidation of the polyaniline can explain the increase of the corrosion potentials during initial 70 h of immersion in 3% NaCl, termed “stage I” in Fig. 13a. Consequently, the released electrons are transferred through some of the partially doped conducting polyaniline particles, and involved in the oxygen reduction reaction as a cathodic site, as shown in Fig. 4.29. The main differences in the oxygen reduction reaction in comparisons with a classical coating could be that the product is mainly hydrogen peroxide anions (two-electron path), as mentioned above and shown by few authors for some conducting polymers [109, 110, 111, 112]:



Formed hydrogen peroxide anions could oxidize initially formed  $\text{Fe}^{2+}$  to Fe(III)-species, like:



which precipitates as compact insoluble  $\text{Fe}_2\text{O}_3$  in the form of the passive layer in the coating pores. Released hydronium ions react with hydroxyl ions forming water and additionally reduce the possibilities of the coating delamination. By the reaction given with Eq. 4.9, the precipitation of porous non-protective  $\text{Fe}(\text{OH})_2$  with solubility constants  $L_s[\text{Fe}(\text{OH})_2] = 4.87 \times 10^{-17}$  [111] is suppressed. The formed passive layer reduces the iron dissolution reaction, reducing the overall corrosion rate. The rate of the oxygen reduction reaction could be governed by the oxidation states-doping degree, of the used polyaniline. Therefore, more doped polyaniline is better electron conductor and more hydrogen peroxide ions could be formed. It should be also mentioned that during the four-electron path, four  $\text{OH}^-$  is released, while during the two-electron path only one  $\text{OH}^-$ , inducing much smaller pH increase in the pores lowering the possibility of coating delamination. Lesser-doped polyaniline is practically insulator and oxygen reduction reaction could proceed mainly via four-electron path to  $\text{OH}^-$  into the bottom of the pore on exposed iron surfaces. Thus, the initial doping degree of the used polyaniline determines the oxygen reduction reaction mechanism, properties of the formed iron passive layer, and quality of the composite coatings against corrosion.

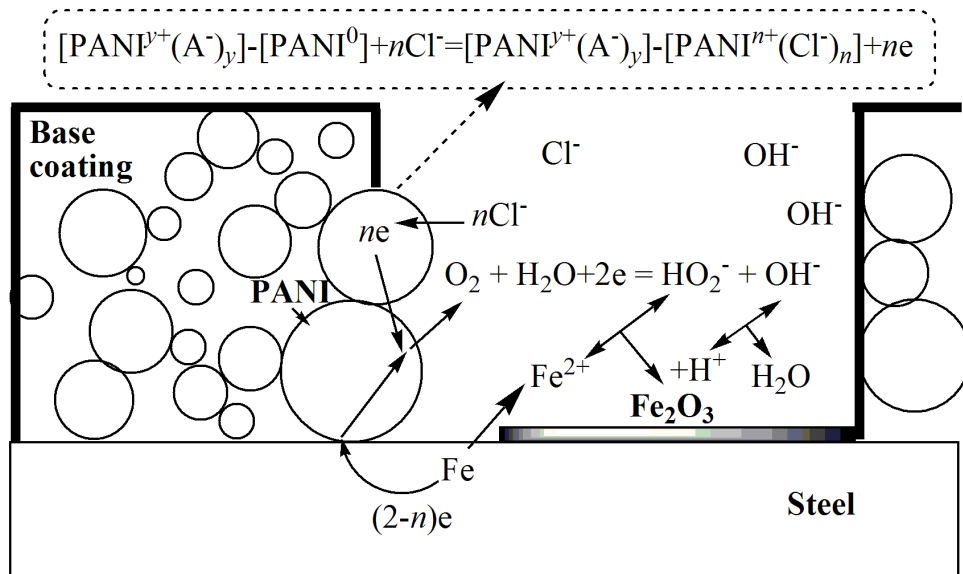


**Figure 4.29.** Simplified, nonstoichiometric, schematic representation of the possible reactions during the corrosion of the mild steel with composite polyaniline based coatings.

Further corrosion protection mechanism with relatively stable corrosion potentials and polarization resistance, stage II in Fig. 13a, could be connected with the stability of formed passive layer, where the corrosion rate is connected with the balanced iron dissolution through passive layer and oxygen reduction reaction. In stage III in Fig. 4.13a after ~150 h, practically oscillatory behavior of the corrosion potentials and some instability of the polarization resistance values could be connected with the finishing of the pore development in the base coating, but without delamination. In that stage, the delicate balance between partial polyaniline particles doping, oxygen reduction, and iron dissolution reactions exist. After ~300 h, the corrosion potentials of all investigated samples are practically the same indicating that equilibrium states of doping are achieved, stage IV in Fig. 4.13a. It is interesting to note that composite coating with an initially lower doping degree polyaniline offers high value of the polarization resistance for a longer time, see in Fig. 4.13a. Hence, on the fully doped polyaniline particles, now formed hydrogen peroxide ions, which concentration in the pores could be significant, can react with polyaniline chains producing different degradation products, such as p-benzoquinone, hydroquinone, p-aminophenol or quinoeimine [124]. Breakdown of the polyaniline chain conjugations leads to the loss of the conductivity and subsequent changes in the oxygen reduction mechanism from two to four-electron path. Similarly, as in the case of the classical organic coating, deterioration of the coating characteristics and delamination occurred due increased hydroxyl anions production.

## 5. CONCLUSIONS

The reprotonation of the polyaniline base obtained following the standard IUPAC procedure is successfully demonstrated. UV-visible techniques can be applied to determine the oxidation states of the reprotonated samples. Commercial paint is modified as a composite paint by addition of 5 wt.% benzoic acid reprotonated polyaniline powder. The linear polarization measurements are effectively performed in the polarization resistance and corrosion current density determination over time, suggesting that such investigations will be a good indication of corrosion behavior of the systems, and can be used in the further study. Using the UV-visible studies of the corrosion products, based on ASTM 1,10-phenanthroline method, the corrosion current density practically identical to obtained ones by linear polarization method is determined. Based on the performed corrosion experiments and microscopic observations, it is concluded that composite coatings based on commercial paint with the addition of the polyaniline-doped with benzoate anions show much better protection of the mild steel than base commercial coating, preventing the blister formation and coating delamination after prolonged periods.

The chemically synthesized polyaniline is deprotonated with the ammonium hydroxide and also reprotonated with sulfamic, succinic, citric and acetic acid. Using the UV-visible absorption spectroscopy from the ratio of absorbance at 365 nm and 440 nm the polyaniline oxidation level is estimated. Based on the polyaniline absorption rate  $A_{440}/A_{365}$  in the emeraldine state form ( $y = 0.5$ ) obtained by IUPAC procedure, the doping degree of the investigated samples are determined: 0.27 for sulfamic acid; 0.18 for succinic acid; 0.15 for citric acid and 0.13 for acetic acid doped polyaniline. Composite coatings are prepared by mixing of the 5 wt.% of polyaniline powder with commercial alkyd based paint. The corrosion behavior is examined in 3% NaCl using the linear

polarization measurements and visual observations. It is concluded that value of the polarization resistance and appearance of the corrosion products depends on the initial doping degree of the polyaniline. It is observed that composite coatings with more doped polyaniline possess higher value of the polarization resistance in order  $R_p(\text{sulfamic}) > R_p(\text{succinic}) > R_p(\text{citric}) > R_p(\text{acetic}) \sim R_p(\text{base})$ . After ~150 h base coating shows high decrease of the polarization resistance value and the corrosion potential, connected with the partial coating delamination, while for the composite coatings gradual decreases of the polarization resistance values are observed after ~300 h. For the higher area painted steel samples the UV-visible quantitative determination of the current densities and qualitative visual and microscopic investigations of the coatings are also performed after being immersed in 3% NaCl for 100 and 150 h respectively. It is shown that composite coatings reduce the possibility of blister formations and delamination in comparison with base coating. The appearance of the corrosion products on the coatings surfaces closely follow the initial oxidation state of the polyaniline.

## REFERENCES

---

- [1] A.A. Syed, M.K. Dinesan, Review: Polyaniline, A novel polymeric material, *Talanta* 38 (1991) 815-837.
- [2] E.T. Kang, K.L. Neoh, Polyaniline: A polymer with many interesting intrinsic redox states, *Prog. Polym. Sci.*, 23 (1998) 277-324.
- [3] N. Gospodinova, L. Terlemezyan, Conducting polymers prepared by oxidative polymerization: polyaniline, *Prog. Polym. Sci.*, 23 (1998) 1443-1484.
- [4] Trivedi DC, in *Handbook of Organic Conductive Molecules and Polymers*, 2, ed. by Nalwa HS. Wiley, Chichester, 1997, pp. 505–572.
- [5] Stejskal J., in *Dendrimers, Assemblies, Nanocomposites*, MMLSeries, 5, ed. by Arshady R and Guyot A. Citus Books, London, 2002, pp. 195–281.
- [6] A. G. MacDiarmid, Nobel Lecture: “Synthetic metals”: A novel role for organic polymers, *Rev. Mod. Phys.*, 73(3) (2001) 701-712.
- [7] A. J. Heeger, Nobel Lecture: Semiconducting and metallic polymers: The fourth generation of polymeric materials, *Rev. Mod. Phys.*, 73(3) (2001) 681-700.
- [8] H. Shirakawa, Nobel Lecture: The discovery of polyacetylene film—the dawning of an era of conducting polymers, *Rev. Mod. Phys.*, 73(3) (2001) 713-718.
- [9] A. Malinauskas, Chemical deposition of conducting polymers, *Polymer*, 42 (2001) 3957-3972.
- [10] A. Battacharya, A. De., Conducting polymers in solution—progress toward processibility, *J Macromol Sci. Rev Macromol Chem Phys.*, C39 (1999) 17-56.
- [11] J. Mort, G. Pfister, S. Grammatica., Charge transport and photogeneration in molecularly doped polymers, *Solid State Commun.* 18 (1976) 693-696.

- 
- [12] R. Wilson, A.P.F. Turner, Glucose oxidase: an ideal enzyme, *Biosensors Bioelectronics*, 7 (1992) 165-185.
- [13] H. Bai, G. Shi, Gas Sensors Based on Conducting Polymers, *Sensor*, 7 (2007) 267-307.
- [14] M. H. Ram, N. S. Sunaresan, B. D. Malhotra, Performance of electrochromic cells of polyaniline in polymeric electrolytes, *J. Mat. Sci. Lett.*, 13 (1994) 1490-1493.
- [15] D.C. Trivedi, S.K. Dhawan, Shielding of electromagnetic interference using polyaniline, *Synth. Met.*, 59 (1993) 267-272.
- [16] N.C. Greeham., S.C. Moratti, D.D.C. Bradley, R.H. Friend, A.B. Holmes, Efficient light-emitting diodes based on polymers with high electron affinities, *Nature*, 365 (1993) 628-630.
- [17] Nalwa, H. S., Ed., *Handbook of Organic Conductive Materials and Polymers*, Wiley, New York, 1997.
- [18] R. Holze, Y.P. Wu, Intrinsically conducting polymers in electrochemical energy technology: Trends and progress, *Electrochim. Acta*, 122 (2014) 93– 107.
- [19] G.Tourillon, F. Garnier, New electrochemically generated organic conducting polymers, *J. Electroanal. Chem.*, 135 (1982) 173-178.
- [20] P. Burgmayer, R.W. Murray, Faster ion gate membranes, *J. Electroanal. Chem.*, 147 (1983) 339-344.
- [21] D.M. Ivory, G. G. Miller, J.M. Sowa, L.W Shackleton, R. R. Chance., R. H. Baughman, Highly conducting charge-transfer complexes of poly(p-phenylene), *J. Chem. Phys.*, 71 (1997) 1506-1507.
- [22] B.D. Malhotra, N.Kumar, S. Chandra, Recent studies of heterocyclic and aromatic conducting polymers, *Prog. Polym. Sci.* 12 (1986) 189-218.
- [23] Kuan, Sun Shupeng Zhang, Pengcheng Li, Yijie Xia, Xiang Zhang, Donghe Du, Furkan Halis Isikgor, Jianyong Ouyang, Review on application of PEDOTs and PEDOT:PSS in energy conversion and storage devices, *J. Mat. Sci.: Materials in Electronics*, 26 (7) (2015) 4438–4462.



- 
- [24] G. Ćirić-Marjanović, Recent advances in polyaniline research: Polymerization mechanisms, structural aspects, properties and applications, *Synth. Met.*, 177 (2013) 1-47.
- [25] Pravin P. Deshpande, Niteen G. Jadhav, Victoria J. Gelling, Dimitra Sazou, Conducting polymers for corrosion protection: a review, *J. Coat. Technol. Res.*, 11 (4) (2014) 473–494.
- [26] D.W. DeBerry, Modification of the electrochemical and corrosion behavior of stainless steels with an electroactive coating. *J. Electrochem. Soc.*, 132 (5) (1985) 1022–1026.
- [27] B. Wessling, Passivation of metals by coating with polyaniline: Corrosion potential shift and morphological changes, *Adv. Mater.*, 6 (3) (1994) 226–228.
- [28] N. Ahmad, A.G. MacDiarmid, Inhibition of corrosion of steels with the exploitation of conducting polymers, *Synth. Met.*, 78 (2) (1996) 103–110.
- [29] D. Sazou, C. Georgolios, Formation of conducting polyaniline coatings on iron surfaces by electropolymerization of aniline in aqueous solutions, *J. Electroanal. Chem.*, 429 (1–2) (1997) 81–93.
- [30] S.P. Sitaram, J.O. Stoffer, T.J. O’Keefe, Application of conducting polymers in corrosion protection, *J. Coat. Technol. Res.*, 69 (866) (1997) 65–69.
- [31] M. Rohwerder, Conducting polymers for corrosion protection: A Review, *Int. J. Mater. Res.*, 100 (10) (2009) 1331–1342.
- [32] M. Khan, A.U. Chaudhry, S. Hashim, M.K. Zahoor, M.Z. Iqbal, Recent developments in intrinsically conductive polymers, *J. Coat. Technol. Res.*, 11 (4) (2014) 473–494.
- [33] T. Ohtsuka, Corrosion protection of steels by conducting polymer coating, *Int. J. Corros.*, 2012 (2012) 7-13.
- [34] S. Biallozor, A. Kupniewska, Conducting polymers electrodeposited on active metals, *Synth. Met.*, 155 (3) (2005) 443–449.
- [35] E.W Brooman, Modifying organic coatings to provide corrosion resistance. Part III: Organic additives and conducting polymers, *Met. Finish.*, 100 (6) (2002) 104–110.

- 
- [36] J. Stejskal, R. G. Gilbert, Polyaniline. Preparation of a conducting polymer (IUPAC Technical Report), *Pure Appl. Chem.*, 74 (5) (2002) 857–867.
- [37] H.D. Tran, J.M. D’Arcy, Y. Wang, P. J. Beltramo, V.A. Strong, R.B. Kaner, The oxidation of aniline to produce “polyaniline”: A process yielding many different nanoscale structures, *J. Mater. Chem.*, 21 (2011) 3534–3550.
- [38] E. Smela, W. Lu, B.R. Mattes, Polyaniline actuators: Part 1. PANI(AMPS) in HCl, *Synthetic Met.* 151 (2005) 25–42.
- [39] A.D. MacDiarmid, Nobel Prize 2001 Lecture: “Synthetic metals” a novel role for organic polymers, *Curr. Appl. Phys.*, 1 (2001) 269–279.
- [40] J. Stejskal I. Sapurina, M. Trchová, Polyaniline nanostructures and the role of aniline oligomers in their formation, *Prog. Polymer Sci.*, 35 (2010) 1420–1481.
- [41] M. Kohl, A. Kalendová, Effect of polyaniline salts on the mechanical and corrosion properties of organic protective coatings, *Prog. Org. Coat.*, 86 (2015) 96–107.
- [42] T. Li, Z. Qin, B. Liang, F. Tian, J. Zhao, N. Liu, M. Zhu, Morphology-dependent capacitive properties of three nanostructured polyanilines through interfacial polymerization in various acidic media, *Electrochim. Acta*, 177 (2015) 343–351.
- [43] S. Pour-Ali, C. Dehghanian, A. Kosari, In situ synthesis of polyaniline–camphorsulfonate particles in an epoxy matrix for corrosion protection of mild steel in NaCl solution, *Corr. Sci.*, 85 (2014) 204–214.
- [44] M.V. Kulkarni, A.K. Viswanath, R. Marimuthu, T. Seth, Synthesis and characterization of polyaniline doped with organic acids, *J. Polym. Sci. A Polym. Chem.*, 42 (8) (2004) 2043–2049.
- [45] Y. Wei, X. Tang, Y. Sun, W.W. Focke, A study of the mechanism of aniline polymerization, *J. Polym. Sci.*, 27 (1989) 2385–2396.
- [46] Y. Wei, G-W Jang, Ch-Ch. Chan, K.F. Hsuen, R. Hariharan, S,A. Patel, C.K. Whitecar, Polymerization of aniline and alkyl ring-substituted anilines in the presence of aromatic additives, *J. Phys. Chem.*, 94 (1990) 7716–7721.
- [47] I. Sapurina, J. Stejskal, The mechanism of the oxidative polymerization of aniline and the formation of supramolecular polyaniline structures, *Polym Int.*, 57 (2008) 1295–1325.

- 
- [48] B.N. Grgur, A.R. Elkaisa, M.M. Gvozdenović, S.Ž. Drmanić, T.Lj. Trišović, B.Z. Jugović, Corrosion of mild steel with composite polyaniline coatings using different formulations, *Prog. Org. Coat.*, 79 (2015) 17–24.
- [49] A.M. Fenelon, C.B. Breslin, Polyaniline-coated iron: studies on the dissolution and electrochemical activity as a function of pH, *Surf. Coat. Technol.*, 190 (2005)264–270.
- [50] W.S. Araujo, I.C.P. Margarit, M. Ferreira, O.R. Mattos, P.L. Neto, Undoped polyaniline anticorrosive properties, *Electrochim. Acta*, 46 (9) (2001)1307–1312.
- [51] G.M. Spinks, A. Dominis, G.G. Wallace, Comparison of emeraldine salt, emeraldine base, and epoxy coatings for corrosion protection of steel during immersion in a saline solution, *Corrosion*, 59 (2003) 22–31.
- [52] A. Talo, P. Passiniemi, O. Forsen, S. Ylasaari, Polyaniline/epoxy coatings with good anti-corrosion properties, *Synth. Met.*, 85 (1997) 1333–1334.
- [53] A.J. Dominis, G.M. Spinks, G.G. Wallace, Comparison of polyaniline primers prepared with different dopants for corrosion protection of steel, *Prog. Org. Coat.*, 48 (2003) 43–49.
- [54] R. Gasparac, C.R. Martin, The effect of protic doping level on the anticorrosion characteristics of polyaniline in sulfuric acid solutions, *J. Electrochem. Soc.* 149 (2002) B409–B413.
- [55] E. Armelin, R. Pla, F. Liesa, X. Ramis, J.I. Iribarren, C. Alemán, Corrosion protection with polyaniline and polypyrrole as anticorrosive additives for epoxy paint, *Corr. Sci.*, 50 (2008) 721–728.
- [56] E. Armelin, C. Alemán, J.I. Iribarren, Anticorrosion performances of epoxy coatings modified with polyaniline: a comparison between the emeraldine base and salt forms, *Prog. Org. Coat.*, 65 (2009) 88–93.
- [57] J. Stejskal, J. Prokeš, M. Trchová, Reprotonation of polyaniline: A route to various conducting polymer materials, *React. Funct. Polym.*, 68 (2008) 1355–1361.
- [58] J. Anand, S. Palaniappan, D. N Sathyanarayana, Conducting polyaniline blends and composites, *Prog. Polym. Sci.*, 23 (1998) 993–1018.
- [59] A.B. Samui, A.S. Patankar, J. Rangarajan, P.C. Deb, *Prog. Org. Coat.*, 47 (2003) 1–7.

- 
- [60] Y. Chen, X.H. Wang, J. Li, J.L. Lu, F.S. Wang, Long-term anticorrosion behaviour of polyaniline on mild steel, *Corr. Sci.*, 49 (2007) 3052–3063.
- [61] S. Radhakrishnan, Narendra Sonawane, C.R. Siju, Epoxy powder coatings containing polyaniline for enhanced corrosion protection, *Prog. Org. Coat.* 64 (2009) 383–386.
- [62] S. Sathiyarayanan, S. Muthkrishnan, G. Venkatachari, Corrosion protection of steel by polyaniline blended coating, *Electrochim. Acta*, 51 (2006) 6313–6319.
- [63] F.B. Diniz, G.F. De Andrade, C.R. Martins, W.M. De Azevedo, A comparative study of epoxy and polyurethane based coatings containing polyaniline-DBSA pigments for corrosion protection on mild steel, *Prog. Org. Coat.*, 76 (2013) 912–916.
- [64] A. Sakhri, F.X. Perrin, A. Benaboura, E. Aragon, S. Lamouri, Corrosion protection of steel by sulfo-doped polyaniline-pigmented coating, *Prog. Org. Coat.* 72 (2011) 473–479.
- [65] C. Y. Ge, X. G. Yang, B. R. Hou, Synthesis of polyaniline nanofiber and anticorrosion property of polyaniline–epoxy composite coating for Q235 steel, *J. Coat. Technol. Res.*, 1 (2012) 59-69.
- [66] P. A. Sørensen, S. Kiil, K. Dam-Johansen and C. E. Weinell, Anticorrosive coatings: a review, *J. Coat. Technol. Res.*, 6 (2009) 135-176.
- [67] J. Alam, U. Riaz, S. Ahmad, High performance corrosion resistant polyaniline/alkyd ecofriendly coatings, *Curr. Appl. Phys.*, 9 (2009) 80-86.
- [68] B. A. Bhanvase, S. H. Sonawane, New approach for simultaneous enhancement of anticorrosive and mechanical properties of coatings: Application of water repellent nano CaCO<sub>3</sub>–PANI emulsion nanocomposite in alkyd resin, *Chem. Eng. J.*, 156 (2010) 177-183.
- [69] M. Marti, G. Fabregat, D. S. Azambuja, C. Aleman, E. Armelin, Evaluation of an environmentally friendly anticorrosive pigment for alkyd primer, *Prog. Org. Coat.*, 73 (2012) 321-329.
- [70] M. R. Bagherzadeh, F. Mahdavi, M. Ghasemi, H. Shariatpanahi, H. R. Faridi, Using nanoemeraldine salt-polyaniline for preparation of a new anticorrosive water-based epoxy coating, *Prog. Org. Coat.*, 68 (2010) 319-322.

- 
- [71] A. Sakhri, F. X. Perrin, E. Aragon, S. Lamouric, A. Benaboura, Chlorinated rubber paints for corrosion prevention of mild steel: A comparison between zinc phosphate and polyaniline pigments, *Corros. Sci.*, 52 (2010) 901-909.
- [72] G.G. Wallace, G.M. Spinks, L. P. Kane-Maguire, P.R. Teasdale, *Conductive Electroactive Polymers, Intelligent Polymer Systems*, Third edition, CRC Press, Taylor & Francis Group, NY, 2009.
- [73] Z. Tian, H. Yu, L. Wang, M. Saleem, F. Ren, P. Ren, Y. Chen, R. Sun, Y. Sun, L. Huang, Recent progress in the preparation of polyaniline nanostructures and their applications in anticorrosive coatings, *RSC Adv.*, 4 (2014) 28195-28208.
- [74] D. E. Tallman, G. Spinks, A. Dominis, G. G. Wallace, Electroactive conducting polymers for corrosion control: Part 1. General introduction and a review of non-ferrous metals, *J. Solid State Electrochem.*, 6 (2002) 73-84.
- [75] B. N. Grgur, M. M. Gvozdenović, V. B. Mišković-Stanković, Z. Kačarević-Popović, Corrosion behavior and thermal stability of electrodeposited PANI/epoxy coating system on mild steel in sodium chloride solution, *Prog. Org. Coat.*, 56(2-3) (2006) 214-219.
- [76] K. Cai, S. Zuo, S. Luo, C. Yao, W. Liu, J. Ma, H. Mao, Z. Li, Preparation of polyaniline/graphene composites with excellent anti-corrosion properties and their application in waterborne polyurethane anticorrosive coatings, *RSC Adv.*, 6 (2016) 95965-95972.
- [77] A.J. Dominis, G.M. Spinks, G.G.Wallace, Comparison of polyaniline primers prepared with different dopants for corrosion protection of steel, *Prog. Org. Coat.* 48 (2003) 43-49.
- [78] B. Wessling, Scientific and commercial breakthrough for organic metals, *Synth. Met.*, 85 (1997) 1313-1318.
- [79] Y. M. Abu, K. Aoki, Corrosion protection by polyaniline-coated latex microspheres, *J. Electroanal. Chem.*, 583 (2005) 133-139.
- [80] K. Kamaraj, S. Sathiyarayanan, S. Muthukrishnan, G. Venkatachari, Corrosion protection of iron by benzoate doped polyaniline containing coatings, *Prog. Org. Coat.*, 64 (2009) 460-465.

- 
- [81] K. Kamaraj, T. Siva, S. Sathiyarayanan, S. Muthukrishnan, G. Venkatachari, Synthesis of oxalate doped polyaniline and its corrosion protection performance, *J. Solid State Electrochem.*, 16 (2012) 465-471.
- [82] S. de Souza, J. E. Pereira Da Silva, S. I. Córdoba De Torresi, M. L. A. Temperini, R. M. Torresi, Polyaniline based acrylic blends for iron corrosion protection, *Electrochem. Solid-State Lett.*, 4 (2001) B27-B30.
- [83] A.A. Pud, G.S. Shapoval, P. Kamarchik, N.A. Ogurtsov, V.F. Gromovaya, I.E. Myronyuk, Yu.V. Kotsur, Electrochemical behavior of mild steel coated by polyaniline doped with organic sulfonic acids, *Synth. Met.*, 107 (1999) 111–115.
- [84] Skoog, Douglas A.; Holler, F. James; Crouch, Stanley R.. *Principles of Instrumental Analysis* (6th ed.). Belmont, CA: Thomson Brooks/Cole, 2007, pp. 169–173.
- [85] B. S. Flavel , J. Yu , J. G. Shapter, J. S. Quinton, Patterned polyaniline & carbon nanotube–polyaniline composites on silicon, *Soft Matter*, 5 (2009) 164-172.
- [86] L. Xu, Z. Chen, W. Chen, A. Mulchandani, Y. Yan, Electrochemical synthesis of perfluorinated ion doped conducting polyaniline films consisting of helical fibers and their reversible switching between superhydrophobicity and superhydrophilicity, *Macromol. Rapid Commun.*, 29 (2008) 832–838.
- [87] J. Yue, A. J. Epstein, Synthesis of self-doped conducting polyaniline, *J. Am. Chem. Soc.* 1990, 112, 2800-2801.
- [88] J. G. Masters, Y. Sun, A. G. MacDiarmid, Polyaniline: Allowed oxidation states, *Synth. Met.*, 41–43 (1991) 715-718.
- [89] M.M. Sk, C.Y. Yue, Synthesis of polyaniline nanotubes using the self-assembly behavior of vitamin C: a mechanistic study and application in electrochemical supercapacitors, *J. Mater. Chem. A*, 2 (2014) 2830-2838.
- [90] J. Stejskal, P. Kratochví, N. Radhakrishnan, Polyaniline dispersions 2. UV—Vis absorption spectra, *Synth. Met.*, 61 (1993) 225-231.
- [91] T. Lindfors, L. Harju, A. Ivaska, Optical pH measurements with water dispersion of polyaniline nanoparticles and their redox sensitivity, *Anal. Chem.*, 78 (2006) 3019-3026
- [92] B.N. Grgur, *Corrosion and protection of the materials*, TMF, 2017.

- 
- [93] ASTM Designation: G 59 – 97, Standard test method for conducting potentiodynamic polarization resistance measurements, 2014.
- [94] ASTM, Designation: E 394 – 00, Standard test method for iron in trace quantities using the 1,10-phenanthroline method, 2000.
- [95] Molecular Absorption Spectroscopy: Determination of Iron with 1,10-Phenanthroline [http://www.chem.uky.edu/courses/che226/labs/05-Fe\\_Absorption-2005Fa.pdf](http://www.chem.uky.edu/courses/che226/labs/05-Fe_Absorption-2005Fa.pdf)
- [96] <http://www.sigmaaldrich.com/technical-documents/articles/analytix/spectroscopic-reagents.html>
- [97] E. Ülker, M. Kavano, Synthesis of poly(vinylferrocene) perchlorate/poly(3,3'-diaminobenzidine) modified electrode in dichloromethane for electroanalysis of hydroquinone, *J. Braz. Chem. Soc.*, 26 (9) (2015) 1947-1955.
- [98] <https://www.helios-deco.com/en/products/metal-coatings/?use=&surface=0>
- [99] E. Jin, N. Liu, X. Lu, W. Zhang, Novel micro/nanostructures of polyaniline in the presence of different amino acids via a self-assembly process, *Chem. Lett.*, 36 (2007) 1288-1289.
- [100] J.E. de Albuquerque L.H.C. Mattoso, R.M. Faria, J.G. Masters, A.G. MacDiarmid, Study of the interconversion of polyaniline oxidation states by optical absorption spectroscopy, *Synth. Met.*, 146 (2004) 1-10.
- [101] J.B. Bajat, V.B. Mišković-Stanković, M.D. Maksimović, D.M. Dražić, S. Zec, Electrochemical deposition and characterization of Zn Co alloys and corrosion protection by electrodeposited epoxy coating on Zn Co alloy, *Electrochim. Acta*, 47 (2002) 4101-4112.
- [102] S.B. Lyon, R. Bingham and D.J. Mills, Advances in corrosion protection by organic coatings: What we know and what we would like to know, *Prog. Org. Coat.*, 102 (2017) 2-7.
- [103] B.A. Abd-El-Nabey, O.A. Abdullatef, G.A. El-Naggar, E.A. Matter and R. M. Salman, Effect of Tween 80 Surfactant on the Electropolymerization and Corrosion Performance of Polyaniline on Mild Steel, *Int. J. Electrochem. Sci.*, 11 (2016) 2721-2733.

- 
- [104] O. Kazum, M.B Kannan, Optimising parameters for galvanostatic polyaniline coating on nanostructured bainitic steel, *Surf. Eng.*, 32 (2016) 607-614.
- [105] S. Qiu, C. Chen, M. Cui, W Li, H. Zhao, L. Wang, Corrosion protection performance of waterborne epoxy coatings containing self-doped polyaniline nanofiber, *App. Surf. Sci.*, 407 (2017) 213-222.
- [106] U.A. Samad, M.A. Alam, El-S.M. Sherif, O. Alothman, A.H. Seikh and S. Al-Zahrani, Manufacturing and characterization of corrosion resistant epoxy/2pack coatings incorporated with polyaniline conductive polymer, *Int. J. Electrochem. Sci.*, 10 (2015) 5599-5613.
- [107] R.M. Bandeira, J. van Drunen, G. Tremiliosi-Filho, J.R. dos Santos, J.M.E. de Matos, Polyaniline/polyvinyl chloride blended coatings for the corrosion protection of carbon steel, *Prog. Org. Coat.*, 106 (2017) 50-59.
- [108] M.P. Sokolova, M.A. Smirnov, I.A. Kasatkin, I.Yu. Dmitriev, N.N. Saprykina, A.M. Toikka, E. Lahderanta and G.K. Elyashevich, Interaction of polyaniline with surface of carbon steel, *Int. J. Poly. Sci.*, 2017 (2017), Article ID 6904862.
- [109] V.G. Khomenko, V.Z. Barsukov, A.S. Katashinskii, The catalytic activity of conducting polymers toward oxygen reduction, *Electrochim. Acta*, 50 (2005) 1675-1683.
- [110] V.G. Khomenko, K.V. Lykhnytskyi, V.Z. Barsukov, Oxygen reduction at the surface of polymer/carbon and polymer/carbon/spinel catalysts in aqueous solutions, *Electrochim. Acta*, 104 (2013) 391-399.
- [111] B.N. Grgur, On the role of aniline oligomers on the corrosion protection of mild steel, *Synth. Met.*, 187 (1) (2014) 57-60.
- [112] B.N. Grgur, Metal | polypyrrole battery with the air regenerated positive electrode, *J. Power Sources*, 272 (2014) 1053-1060.
- [113] Y-G Han, T. Kusunose, T. Sekino, One-step reverse micelle polymerization of organic dispersible polyaniline nanoparticles, *Synth. Met.*, 159 (2009) 123-131.
- [114] X. Wang, Y. Li, Y. Zhao, J. Liu, S. Tang, W. Feng, Synthesis of PANI nanostructures with various morphologies from fibers to micromats to disks doped with salicylic acid, *Synth. Met.*, 160 (2010) 2008-2014.



- 
- [115] V. Prevost, A. Petit, F. Pla, Studies on chemical oxidative copolymerization of aniline and o-alkoxysulfonated anilines: I. Synthesis and characterization of novel self-doped polyanilines, *Synth. Met.*, 104 (1999) 79-87.
- [116] H. Xia, Q. Wang, Synthesis and characterization of conductive polyaniline nanoparticles through ultrasonic assisted inverse microemulsion polymerization, *J. Nanopart. Res.*, 3 (2001) 401–411.
- [117] <https://imagej.nih.gov/ij/docs/guide/user-guide.pdf>
- [118] K. B. Tator, Coating Deterioration, *ASM Handbook, Volume 5B, Protective Organic Coatings*, K.B. Tator, (Ed), ASM International, 2015, pp. 462-473.
- [119] P.A. Sørensen, S. Kiil, K. Dam-Johansen, C. E. Weinell, Anticorrosive coatings: a review, *J. Coat. Technol. Res.*, 6 (2) (2009) 135–176.
- [120] S.B. Lyon, R. Bingham, D.J. Mills, Advances in corrosion protection by organic coatings: What we know and what we would like to know, *Prog. Org. Coat.*, 102 (2017) 2–7.
- [121] V.B. Mišković-Stanković, D.M. Dražić, M.J. Teodorović, Electrolyte penetration through epoxy coatings electrodeposited on steel, *Corr. Sci.*, 37 (2) (1995) 241-252.
- [122] J. Wang, Anion exchange nature of emeraldine base (EB) polyaniline (PAn) and a revisit of the EB formula, *Synth. Met.*, 132 (2002) 49–52.
- [123] J. Wang, Polyaniline coatings: anionic membrane nature and bipolar structures for anticorrosion, *Synth. Met.*, 132 (2002) 53–56.
- [124] J. López-Palacios, E. Munoz, M.A. Heras, A. Colina, V. Ruiz, Study of polyaniline films degradation by thin-layer bidimensional spectroelectrochemistry, *Electrochim. Acta*, 52 (2006) 234–239.

---

## **BIOGRAFIJA**

Ayad Abdelsalam Musa Salem, master inženjer tehnologije, je rođen 01. Januara 1965. u Zaviji, Libija. Osnovne akademske studije završio je 1986. godine, na Alfateh Univerzitetu, Zavija, Libija na odseku za Hemija, a drugu diplomu 2003. je stekao na Alfateh Univerzitetu, Zavija, Libija na odseku za Hemijsko inženjerstvo. Master studije je završio na Šefild Univerzitetu, Šefild, Velika Britanija, 30.10.2006, smer Hemijsko inženjerstvo, a diploma mu je nostifikovana odlukom Univerziteta u Beogradu, broj: 06-61301-5 652/3-15 od 12.01.2016. U periodu 1989-1994. radio je u P.R.C. - Petroleum Research Center kao istraživač. U periodu od 1994-2005. radio je kao činovnik na Zavija Univerzitetu, Libija, a u periodu 2006-2014. bio je zaposlen je kao predavač na Zavija Univerzitetu, Libija, na departmentu za hemijsko inženjerstvo, na predmetima Inženjerstvo korozije, Organske hemija, Termodinamika i Reakciono inženjerstvo. Školske 2014/2015 upisao je doktorske studije na Tehnološko-metalurškom fakultetu, Univerziteta u Beogradu, odsek za Hemijsko inženjerstvo. Do sada je publikovao jedan rad vrhunskom međunarodnom časopisu (M21), jedan rad u međunarodnom časopisu (M23) i saopštio dva rada na međunarodnom skupu štampanim u celini (M33). Oženjen je i ima sedmoro dece. Govori, čita i piše arapski i engleski jezik.

## **BIOGRAPHY**

Ayad Abdelsalam Musa Salem, Master Technology Engineer, was born January 1, 1965 in Al-zawiyah, Libya. He completed his basic academic studies in 1986 at the Alfateh University, Al-zawiyah, Libya at the Chemistry Department, and in 2003 he was awarded the second diploma at the Alfateh University, Al-zawiyah, Libya at the Department of Chemical Engineering. He completed his master's degree at Sheffield University, Sheffield, UK, on October 30, 2006, in the field of Chemical Engineering, and his diploma was not confirmed by the decision of the University of Belgrade, number: 06-61301-5 652 / 3-15 of 12.01.2016. In the period 1989-1994. He worked in P.R.C. - Petroleum Research Center as a researcher. In the period from 1994-2005. He worked as a clerk at Al-zawiyah University, Libya, and in the period from 2006 to 2014. He was employed as a lecturer at Al-zawiyah University, Libya, at the Department of Chemical

---

Engineering, on the subjects of Corrosion Engineering, Organic Chemistry, Thermodynamics and Reaction Engineering.

School year 2014/2015 he enrolled in doctoral studies at the Faculty of Technology and Metallurgy, University of Belgrade, Department of Chemical Engineering. So far, he has published one of the works of the top international journal (M21), one paper in an international journal (M23) and has published two papers at the international conference (M33). He is married and has seven children. Speaks, reads and writes Arabic and English.

**Spisak objavljenih naučnih radova proizašlih iz teze / List of published scientific papers from dissertation**

**M21. Rad u vrhunskom međunarodnom časopisu / Paper published in the top international journal**

1. **A.A. Salem**, B.N. Grgur, *The influence of the polyaniline initial oxidation states on the corrosion of steel with composite coatings*, Progress in Organic Coatings, Vol 119, 2018 pp. 138-144 ISSN 0300-9440 *IF(2016): 2.858*

**M23. Rad u međunarodnom časopisu / Paper in an international journal**

1. **A.A. Salem**, B.N. Grgur, *Corrosion of mild steel with composite alkyd polyaniline-benzoate coating*, International Journal of Electrochemical Science, Vol 12, no. 9, 2017, pp. 8683-8694. ISSN 1452-3981 *IF(2016): 1.469*

**M33. Saopštenje sa međunarodnog skupa štampano u celini / Report from the international meeting printed in its entirety**

1. **Salem Ayad**, Omyen Waleed, Jugović Branimir, Gvozdenović Milica, Grgur Branimir, *Corrosion Of Steel With Composite Polyaniline Coatings*, - Metallurgical & Material Engineering Congress of South-East Europe, Proceedings and Book of Abstract, Ed. Marija Korać, June 3rd -5th, Belgrade, Serbia, 2015, pp. 295-300 ISBN 978-86-87183-27-8.

---

Прилог 1.

## Изјава о ауторству

Потписани-а Ayad Abdelsalam Musa Salem

број индекса 4044/2014

### Изјављујем

да је докторска дисертација под насловом

### **CORROSION OF STEEL WITH POLYANILINE BASED COMPOSITE COATINGS**

- резултат сопственог истраживачког рада,
- да предложена дисертација у целини ни у деловима није била предложена за добијање било које дипломе према студијским програмима других високошколских установа,
- да су резултати коректно наведени и
- да нисам кршио/ла ауторска права и користио интелектуалну својину других лица.

Потпис докторанда

У Београду, \_\_\_\_\_

\_\_\_\_\_

---

Прилог 2.

## **Изјава о истоветности штампане и електронске верзије докторског рада**

Име и презиме аутора Ayad Abdelsalam Musa Salem

Број индекса 4044/2014

Студијски програм Хемијско инжењерство

Наслов рада **CORROSION OF STEEL WITH POLYANILINE BASED  
COMPOSITE COATINGS**

Ментор Др Бранимир Гргур, ред. проф.

Потписани Ayad Abdelsalam Musa Salem

Изјављујем да је штампана верзија мог докторског рада истоветна електронској верзији коју сам предао/ла за објављивање на порталу **Дигиталног репозиторијума Универзитета у Београду**.

Дозвољавам да се објаве моји лични подаци везани за добијање академског звања доктора наука, као што су име и презиме, година и место рођења и датум одбране рада.

Ови лични подаци могу се објавити на мрежним страницама дигиталне библиотеке, у електронском каталогу и у публикацијама Универзитета у Београду.

**Потпис докторанда**

У Београду, \_\_\_\_\_

---

Прилог 3.

## Изјава о коришћењу

Овлашћујем Универзитетску библиотеку „Светозар Марковић“ да у Дигитални репозиторијум Универзитета у Београду унесе моју докторску дисертацију под насловом:

### **CORROSION OF STEEL WITH POLYANILINE BASED COMPOSITE COATINGS**

која је моје ауторско дело.

Дисертацију са свим прилозима предао/ла сам у електронском формату погодном за трајно архивирање.

Моју докторску дисертацију похрањену у Дигитални репозиторијум Универзитета у Београду могу да користе сви који поштују одредбе садржане у одабраном типу лиценце Креативне заједнице (Creative Commons) за коју сам се одлучио/ла.

1. Ауторство
2. Ауторство - некомерцијално
3. Ауторство – некомерцијално – без прераде
4. Ауторство – некомерцијално – делити под истим условима
5. Ауторство – без прераде
6. Ауторство – делити под истим условима

(Молимо да заокружите само једну од шест понуђених лиценци, кратак опис лиценци дат је на полеђини листа).

**Потпис докторанда**

У Београду, \_\_\_\_\_

\_\_\_\_\_

---

1. Ауторство - Дозвољаваате умножавање, дистрибуцију и јавно саопштавање дела, и прераде, ако се наведе име аутора на начин одређен од стране аутора или даваоца лиценце, чак и у комерцијалне сврхе. Ово је најслободнија од свих лиценци.

2. Ауторство – некомерцијално. Дозвољаваате умножавање, дистрибуцију и јавно саопштавање дела, и прераде, ако се наведе име аутора на начин одређен од стране аутора или даваоца лиценце. Ова лиценца не дозвољава комерцијалну употребу дела.

3. Ауторство - некомерцијално – без прераде. Дозвољаваате умножавање, дистрибуцију и јавно саопштавање дела, без промена, преобликовања или употребе дела у свом делу, ако се наведе име аутора на начин одређен од стране аутора или даваоца лиценце. Ова лиценца не дозвољава комерцијалну употребу дела. У односу на све остале лиценце, овом лиценцом се ограничава највећи обим права коришћења дела.

4. Ауторство - некомерцијално – делити под истим условима. Дозвољаваате умножавање, дистрибуцију и јавно саопштавање дела, и прераде, ако се наведе име аутора на начин одређен од стране аутора или даваоца лиценце и ако се прерада дистрибуира под истом или сличном лиценцом. Ова лиценца не дозвољава комерцијалну употребу дела и прерада.

5. Ауторство – без прераде. Дозвољаваате умножавање, дистрибуцију и јавно саопштавање дела, без промена, преобликовања или употребе дела у свом делу, ако се наведе име аутора на начин одређен од стране аутора или даваоца лиценце. Ова лиценца дозвољава комерцијалну употребу дела.

6. Ауторство - делити под истим условима. Дозвољаваате умножавање, дистрибуцију и јавно саопштавање дела, и прераде, ако се наведе име аутора на начин одређен од стране аутора или даваоца лиценце и ако се прерада дистрибуира под истом или сличном лиценцом. Ова лиценца дозвољава комерцијалну употребу дела и прерада. Слична је софтверским лиценцама, односно лиценцама отвореног кода.